ISTANBUL TECHNICAL UNIVERSITY ★ GRADUATE SCHOOL OF SCIENCE ENGINEERING AND TECHNOLOGY

DEVELOPMENT OF MICROFLUIDIC BASED SINGLE CELL CAPTURING SYSTEMS FOR EARLY DETECTION OF DISEASES

Ph.D. THESIS

Emre ALTINAĞAÇ

Department of Nanoscience and Nanoengineering

Nanoscience and Nanoengineering Programme

OCTOBER 2020

ISTANBUL TECHNICAL UNIVERSITY ★ GRADUATE SCHOOL OF SCIENCE ENGINEERING AND TECHNOLOGY

DEVELOPMENT OF MICROFLUIDIC BASED SINGLE CELL CAPTURING SYSTEMS FOR EARLY DETECTION OF DISEASES

Ph.D. THESIS

Emre ALTINAĞAÇ
(513132005)

Department of Nanoscience and Nanoengineering

Nanoscience and Nanoengineering Programme

Thesis Advisor: Prof. Dr. Hüseyin KIZIL

OCTOBER 2020

İSTANBUL TEKNİK ÜNİVERSİTESİ ★ FEN BİLİMLERİ ENSTİTÜSÜ

ERKEN TEŞHİSE YÖNELİK MİKROAKIŞKAN TABANLI TEK HÜCRE YAKALAMA SİSTEMLERİNİN GELİŞTİRİLMESİ

DOKTORA TEZİ

Emre ALTINAĞAÇ
(513132005)

Nanobilim ve Nanomühendislik Anabilimdalı

Nanobilim ve Nanomühendislik Programı

Tez Danışmanı: Prof. Dr. Hüseyin KIZIL

EKİM 2020

Emre ALTINAĞAÇ, a Ph.D. student of ITU Graduate School of Science Engineering and Technology student ID 513132005, successfully defended the thesis/dissertation entitled “DEVELOPMENT OF MICROFLUIDIC BASED SINGLE CELL CAPTURING SYSTEMS FOR EARLY DETECTION OF DISEASES”, which he prepared after fulfilling the requirements specified in the associated legislations, before the jury whose signatures are below.

Thesis Advisor: **Prof. Dr. Hüseyin KIZIL**
Istanbul Technical University

Jury Members: **Prof. Dr. Esra ZAYİM**
Istanbul Technical University

Prof. Dr. Arda Deniz YALÇINKAYA
Bogazici University

Prof. Dr. Gizem Dinler DOĞANAY
Istanbul Technical University

Prof. Dr. Alper KİRAZ
Koc University

Date of Submission: 07 September 2020
Date of Defense: 30 September 2020

to my spouse Duygu
and my son Tuna,

FOREWORD

Prof. Dr. Hüseyin KIZIL has made a great contribution throughout my academic career as well as my personal development since I had the opportunity to start studying under his supervision in 2012. It has been my honor to be advised by his visionary guidance and I am thankful to him being patient as I have been gaining experience in the field. Knowing that there are still a lot to learn, feeling the presence of the support he continuously provides, encourages me to welcome new challenges.

Prof. Dr. Esra ZAYİM has always inspired me with her academic commitment and passion, and I feel fortunate as I attended a few classes she lectured. I would like to thank her for her criticisms during this process.

There have been incentive discussions I had with Prof. Dr. Arda Deniz YALÇINKAYA with his sincere approach to the steps I took. I would like to thank him for being greatly contributor to make this work better with his criticism and suggestions.

I owe Assoc. Prof. Dr. Murat DEMİRBİLEK a gratitude for his unlimited support in experiments with biological cells. I am influenced by his work discipline and academic perspective.

I would like to thank all the people I had the opportunity to meet during my studies. Each of them contributed to this study, perhaps without even realizing it. I would like to thank my friends who made the busy lab environment enjoyable.

I especially thank Mümin BALABAN as our friendship did not start with this journey and I believe it will not end here. I will be enjoying his conversations and listening to his perspective on life.

Ömer EROĞLU, Erçin Çağan DURAN and Kadriye ÖLMEZ are my colleagues that I am very happy to had the opportunity to meet. I would like to thank them very much for the good times we had. I would like to thank Yalın SÖNMEZ for his support during the experimental studies. He was with me during many experimental studies and I will always recall him in a joking, upbeat mood.

It cannot be described in words that how much my wife, my son and my family supported me, and I am thankful to them. Throughout this whole process, I have tried to be worthy of their support and their patience whenever I was with them. Although it is nice to feel the support of the family and cheer up a little when things get worse, there is nothing like having a wonderful celebration with them when things go well. It might be because things are always less likely to go well in academia. However, this increases the value of the final achievement even more, and provides motivation to do more experiments and work harder which leads to more celebrations.

This study was granted by ITU Scientific Research Office (BAP) projects under grant numbers 39065 and MDK-2017-40897 “Development of Microfluidic Based Single Cell Capturing Systems for Early Detection of Diseases”.

Chapters 3, 4-5 and 6 of this study was also supported by The Scientific and Technological Research Council of Turkey (TÜBİTAK) under grant numbers 114M730, 114M802 and 117M296 respectively.

October 2020 Emre ALTINAĞAÇ

TABLE OF CONTENTS

Page

ABBREVIATIONS

CFU	**:** Colony forming unit
CM	**:** Clausius-Mossotti
CTC	**:** Circulating Tumor Cells
DEP	**:** DEP
DMEM	**:** Dulbecco's Modified Eagle Medium
EIS	**:** Electrical Impedance Spectroscopy
FBS	**:** Fetal Bovine Serum
IA	**:** Impedance Analysis
IMCD	**:** Inner medullary collecting duct
LOC	**:** Lab-on-a-chip
nDEP	**:** negative Dielectrophoresis
OOC	**:** Organ-on-a-Chip
PBC	**:** Periodic boundary conditions
pDEP	**:** positive Dielectrophoresis
PDMS	**:** Polydimethylsiloxane
REGM	**:** Renal epithelial growth medium
TEER	**:** Trans Epithelial Electric Resistance

SYMBOLS

C	**:** Capacitance
KOH	**:** Potassium Hydroxide
MTT	**:** 3-(4,5-dimethylthiazol-2-yl)-2,5-diphenyltetrazolium bromide
CdTe	**:** Cadmium telluride
HCT116	**:** Human colorectal carcinoma cell line
HEK-293	**:** Human epithelial embryonic kidney cell line
HeLa 229	**:** Human epithelial adenocarcinoma cell line
MDA-MB-231	**:** Human breast cancer cell line
K-562	**:** Human chronic myelogenic lymphoblast
K-562AR	**:** Drug resistant human chronic myelogenic lymphoblast
HCC1143 BL	**:** Human B lymphoblast

LIST OF TABLES

Page

LIST OF FIGURES

Page

DEVELOPMENT OF MICROFLUIDIC BASED SINGLE CELL CAPTURING SYSTEMS FOR EARLY DETECTION OF DISEASES

SUMMARY

It is known that cancer cells in the bloodstream are quite low compared to other cells in the blood. Microfluidic based systems have been studied for diagnosis, follow-up of the disease and new drug tests to be performed on this disease. A microfluidic based system with two successive regions for separation and analysis has been developed. In the first region, the target cell type is differentiated from a complex mixture containing multiple cells by dielectrophoresis, which allows an insulating particle to be polarized under an electric field. Since different cell types can be polarized at different rates under the same electric field, this method allows the separation of the cells from each other under suitable conditions.

In this study, a microfluidic system consists of two consecutive regions, namely the separation and analysis regions are demonstrated. In the first region, the target cell type is separated by dielectrophoresis from a complex cell mixture. The target cells collected in the first region are continuously transferred to the second region and are captured in a single cell array formation at the hydrodynamic capture stations placed on the measuring electrodes. Impedance analysis was performed to establish a platform for detection and drug screening. While both regions were integrated on a single chip in the final device, each region were examined separately during our study. The results of impedance analysis obtained from different cells based on different medium conductivities with a frequency range of 0.1kHz – 500kHz are presented here.

We recorded impedance measurements at stations where cells were individually captured before and after cell entrapment. Experimental results are divided into cases where the conductivity of the medium is higher and lower than the cell conductance. Overall magnitude of impedance shift is significantly higher when the medium conductivity is lower than the cell conductance. When all results are evaluated, it can be seen that depending on the target cell type, an optimum medium conductivity and frequency range can be selected so as to obtain the measurement result with the highest sensitivity.

A microfluidic cell culture platform, named as organ-on-a-chip in the literature, has been increasingly studied over the last few years to mimic tissue and organ-level physiology, containing a membrane with a continuous and porous structure inhabited by living cells, and with microfluidic channels to mimic the mechanical effects and to supply the necessary nutrients. These platforms create tissue and organ environments that are not possible with traditional 2D or 3D culture systems, and enable real time imaging and analysis of biochemical, genetic and metabolic activities of living cells.

In this project, present fabrication techniques of microfluidic devices are used for the fabrication of organ-on-a-chip platforms. The tissue structure was imitated by coating a single-layer cell on the upper and lower sides of the membrane in the structures of the renal chip tubules and lung alveoli on organ-on-a-chip platforms. The cell viability was characterized by MTT test and the cell viability was maintained by providing

oxygen, carbon dioxide and nutrient exchange under incubation conditions by means of nutrient medium flow provided into the upper and lower channels, and the barrier property of the cell tissue was measured by electrical resistance (TEER) measurements.

The viability of the renal tubules cultured in the microfluidic system between 0-48 hours was recorded by MTT assay. TEER results showed that the tight-junctions of cell tissue were different under static and dynamic conditions in the kidney-on-chip systems. The results obtained by MTT test to measure cell viability were in agreement with TEER and the viability of kidney cells was higher in 48 hours under dynamic conditions compared to static conditions.

With the successful culturing of two different cell types under static conditions in lung-on-chip systems, their viability and cell barrier resistance values were recorded by TEER measurement for 0-48 hours. The results obtained by MTT test and TEER measurements showed that lung cells under shear stress and mechanical stress had higher viability than cells under static conditions.

Key words: microfluidic systems, organ-on-a-chip, kidney-on-a-chip, lung- on-a-chip,

MTT assay, TEER.

ERKEN TEŞHİSE YÖNELİK MİKROAKIŞKAN TABANLI TEK HÜCRE YAKALAMA SİSTEMLERİNİN GELİŞTİRİLMESİ

ÖZET

Kan dolaşımındaki kanser hücrelerinin, kandaki diğer hücrelere göre oldukça düşük sayıda olduğu bilinmektedir. Hastalığın tanılanması, takibi ve bu hastalık üzerinde gerçekleştirilecek yeni ilaç testlerine yönelik mikroakışkan tabanlı sistemler üzerinde çalışılmıştır. Ayrıştırma ve analize yönelik birbirini takip eden iki bölgenin yer aldığı mikroakışkan tabanlı bir sistem geliştirilmiştir. İlk bölgede, hedef hücre tipi, birden fazla hücre tipini barındıran karmaşık bir topluluktan dielektrofrez ile ayrıştırılmaktadır. Dielektrofrez, yalıtkan bir parçacığın elektriksel alan altında kutuplanarak yönlendirilmesine imkân vermektedir. Farklı hücre tipleri aynı şartlar altında farklı oranlarda kutuplanabildiğinden, uygun şartlarda hücrelerin birbirlerinden ayrılması bu yöntemle sağlanabilmektedir.

Bu çalışmada, birinci bölgede (ayrıştırma bölgesi) dielektrofrez ile ayrılan hedef hücreler kesintisiz olarak ikinci bölgeye (analiz bölgesi) iletilerek burada hidrodinamik yakalama istasyonlarında tekil olarak yakalanmakta ve her bir hücre ölçüm elektrotlarının üzerine yerleşmektedir. Analiz bölgesinde, hedef hücrenin tanılanmasına ve ilaç testlerine yönelik olarak bu elektrotlar üzerinden empedans analizi gerçekleştirilmektedir. Araştırmamızda her iki bölge de ayrı olarak ele alınmış, en iyi sonucu veren tasarımlar son üründe bir araya getirilmiştir. Farklı medyum iletkenlikleri ve farklı tipte hücreler ile yapılan deneysel çalışmalar bu tezde sunulmuştur.

Analiz bölgesinde, istasyonlarda yer alan elektrotlar üzerinden, hücre yakalanmadan önce ve sonra empedans verileri kaydedilmiştir. Deneysel çalışmalarımız medyum iletkenliğinin hücre iletkenliğinden daha yüksek ya da düşük olduğu durumlar olarak iki gruba ayrılmaktadır. Medyum iletkenliği hücre iletkenliğinden düşük olduğunda empedans kaymasındaki toplam değişim oldukça yüksek olduğu görülmüştür. Tüm sonuçlar değerlendirildiğinde, hedef hücre tipine bağlı olarak, en yüksek hassasiyette tanılamaya yönelik olarak optimum bir medyum iletkenliği ve frekans aralığının belirlenebileceği görülmektedir.

HCT116 hücreleri için empedans sapması çözelti iletkenliği azaldıkça azalırken, MDA-MB-231 hücreleri için empedans sapması çözelti iletkenliği ile arttığı kaydedilmiştir. HEK293 hücreleri ise incelenen iki çözelti iletkenlik seviyesinde benzer empedans sapmaları göstermiştir. Hücre tipleri birbirleriyle karşılaştırıldığında HCT116 ve HEK293 hücre hatları, 1XPBS solüsyonunda benzer empedans sapmaları üretirken, 0.1XPBS konsantrasyona sahip solüsyonlarda aralarındaki empedans sapmalarında belirgin bir fark meydana gelmiştir.

Ortam iletkenliği hücre iletiminden daha düşük olduğunda, hücreden daha fazla akım geçer ve empedans kayması negatiftir. Böylelikle hücre tipi hakkında daha fazla bilgi toplanır ve tanısal duyarlılık artar. 200 mM sükroz çözeltisinde kanserli lenfosit hücreleri ile sağlıklı kan hücreleri arasında belirgin bir empedans sapması farkı vardır. Üretilen sistemin sağlıklı kan hücrelerini ayırt etmede en yüksek hassasiyete sahip olduğu aralık 200mM sükroz çözeltisi için 0.1kHz ve 10kHz frekans aralığıdır.

Belirli bir frekansta kaydedilen empedans kayması hedef hücre tipi ve evresine yönelik tanılama olanağı sunmaktadır. Kanser hücrelerinin tanılanması ilaç testlerinde, ilacın çalışma mekanizması ve hücre biyolojinin anlaşılmasında oldukça kritiktir. Farklı kimyasal ve ilaç konsantrasyonlarının hücre üzerindeki etkisinin bu proje ile geliştirilen sistem ile takip edilmesi, tanılanması ve iyileştirilmesi mümkün kılınmaktadır.

Dielektrofrez ile ayrıştırma bölgesi için numerik analizler ile ayrıştırma parametreleri araştırılmıştır. Üretilecek mikrokanal ve mikroelektrot geometrileri bu analizler sonucunda belirlenmiştir. Deneysel çalışmalar farklı çaptaki polistren parçacıklar ile başlayıp, çeşitli biyolojik hücreler için de ayrıştırma koşulları belirlenmiş ve bu koşullar göz önünde tutularak sürekli akışın olduğu sistemlerde ayrıştırma gerçekleştirilmiştir. Polistren parçacıklar için %100 verimle ayrıştırma gerçekleştirilirken Jurkat, Daudi, HL-60 ve THP-1 hücreleri ile yapılan çalışmalarda da frekansa bağlı ayrıştırma bölgeleri incelenmiş, Jurkat ve Daudi ile yapılan deneylerde ayrıştırma sağlanmış ve Daudi hücresinde 23 kat zenginleştirme gerçekleştirilmiştir.

Dielektroforez ile ayırma ve empedans analizli sistemler de üretilmiş olup, K562 hücrelerinin bu sistemle yönlendirildiği ve istasyonlarda toplandığı deneysel çalışmalarda kayıt altına alınmıştır. Nihai sistemin ayrıştırma verimliliğini ölçmek için, sisteme entegre edilen her hücre tipi farklı bir renkli floresan boya ile etiketlenmeli ve floresan mikroskop altında izlenmelidir. Ayrıca dielektroforez ile ayırma sonrası çıkışlardan toplanan hücreler akış sitometrisi ile sayılmalı ve ayırma etkinliği gösterilmelidir.

Bu tezde mikro üretim teknolojileri kullanılarak çip-üstü organ sistemleri geliştirilmesi hedeflenerek sürekli akış içeren dinamik koşullar ve akış olmayan statik koşullar altında hücre farklılaşmasına yönelik sonuçlar da toplanmıştır. Böbrek proksimal tübül hücreleri kullanılarak çip-üstü böbrek sistemleri üretilmiş, mikroakışkan sistem içinde ve akış altında kültüre edilmiş, canlılıkları ve hücre dokusunun bariyer özelliği elektriksel direnç değerleri ile takip edilmiştir. Çip-üstü akciğer sistemlerinde insan alveol hücreleri kullanılarak statik koşullar altında iki farklı tipte hücre aynı mikroakışkan sistemde kültüre alınmış ve canlılıkları, hücre dokusuna ait bariyer özelliği aynı yöntemler ile takip edilmiştir.

Literatürde çip üstü organ (organ-on-a-chip) olarak adlandıran, doku ve organ seviyesi fizyolojisini simüle etmek için düzenlenmiş, farklı hücrelerin canlılığını koruduğu, hücrelerin tek katmanlı olarak yüzeyinde barındığı sürekli ve boşluklu yapıya sahip membran içeren, mikrokanallarda ortam için gerekli sıvı akışının ve mekanik etkilerin oluşturulduğu bir mikroakışkan hücre kültürü platformu geliştirilmesi son birkaç yıldır araştırmaların giderek arttığı güncel bir konu haline gelmiştir. Çok hücreli mimarileriyle doku-doku arayüzlerini, fizyokimyasal mikro ortamları ve doku hücreleriyle temas eden kılcal damar geçirgenliğini simüle eden bu platformlar, geleneksel 2D veya 3D kültür sistemleri ile mümkün olmayan doku ve organ ortamı oluşturarak, canlı hücrelerin biyokimyasal, genetik ve metabolik aktivitelerinin, fonksiyonel doku ve organ bağlamında gerçek zamanlı görüntülemesine ve analizine olanak sağlarlar.

Bu çalışmada, mikroakışkan sistemleri üretiminde yaygın olarak kullanılan mikro üretim aşamaları kullanılmıştır. Geliştirilecek çip üstü organ platformunda, böbrek tübülleri ve akciğer alveolleri yapılarında membranın alt ve üst tarafında tek katmanlı hücre kaplanmasıyla doku yapısı taklit edilmiştir. Alt ve üst kanal içerisine sağlanan besiyer akışı ile inkübasyon koşullarında oksijen, karbondioksit ve besin alışverişi sağlanarak hücresel canlılığının korunup korunmadığı MTT testi ile ve hücre dokusunun bariyer özelliği elektriksel direnç (TEER) ölçümleriyle karakterize edilmiştir.

Mikrokanalın alt ve üst yüzeylerinde metal elektrotlar bulunan ve ortasında membran bulunan mikroakışkan sistemler, çip üstü organ platformları için başarıyla üretilmiştir. Özellikle çip üzerinde böbrek uygulamasında tatmin edici sonuçlar kaydedilmiş ve dinamik koşullarda mikroakışkan sistemdeki hücre kültürlerinin sıkı bağ dokularındaki artış elektriksel ölçümlerle kaydedilmiştir. Çip üstü böbrekte dinamik koşullarda başlangıçta bir miktar hücre canlılığı kaybı olmasına rağmen, hücre canlılığının hızla düzeldiği ve arttığı görülmektedir. Hücre konsantrasyonları aynı olmasına rağmen dinamik koşullarda hücrelerden elde edilen direnç değerleri statik koşullara göre 7 kat daha yüksektir. Bu durum, hücre farklılaşmasının gerçekleştiğini ve sıkı bağ dokularının oluştuğunu göstermektedir.

0-48 saat aralığında çip-üstü böbrek sistemlerinde statik ve dinamik koşullar altında kültüre edilen böbrek tübüllerinin canlılıkları MTT testi ile kaydedilmiş, sıkı bağ oluşturma oranlarının farklı olduğu TEER sonuçları ile kaydedilmiştir. Hücre canlılıkları ölçemeye yönelik MTT testi ile elde edilen sonuçlar TEER ile uyum içinde olup, dinamik koşullar altında 48 saat içerisinde böbrek hücrelerinin canlılıklarının statik koşullara kıyasla daha yüksek olduğu görülmüştür.

Çip-üstü akciğer sistemlerinde, iki farklı hücre tipi birlikte başarılı bir şekilde kültürlenmiştir. Canlılık ve hücre bariyer direnci değerleri statik ve dinamik koşullar altında kaydedilmiştir. MTT testi sonuçları incelendiğinde, statik koşullarda hücre canlılığı dinamik koşullara göre ilk 24 saat daha düşük kalmış ancak hücre canlılığı, böbrek uygulamasında görüldüğü gibi 48 saat sonunda statik ve dinamik koşullar için yakın değerler göstermiştir. Çip-üstü akciğer sistemi üzerinde, statik ve dinamik koşullar için alınan TEER değerleri, hücre bariyerinden okunan direnç değerinin dinamik koşullardan daha yüksek olduğunu ve hücre aralarında sıkı bağ dokuların oluştuğunu göstermektedir ve hücre farklılaşmasının gerçekleştiğini göstermektedir.

Üretilen çip-üstü akciğer sistemlerinde statik koşullar altında iki farklı hücre tipinin bir arada başarı ile kültüre edilmesi ile 0-48 saat aralığında canlılıkları ve hücre bariyeri direnç değerleri TEER ölçümü ile kaydedilmiştir. MTT testi ve TEER ölçümleri ile alınan sonuçlarda kayma gerilmesi ve mekanik gerilme altındaki akciğer hücrelerinin, statik koşullardaki hücrelere göre daha yüksek canlılığa sahip olduğu görülmüştür.

Proje çıktısı olarak ürettiğimiz üç boyutlu mikroakışkan doku/organ çip üstü kültür sistemi prototip ürün olarak geliştirilmiş olup doku geliştirme, organ fizyolojisi, ilaç tarama ve geliştirme araştırması, moleküler taşıma mekanizmaları, toksisite testi ve biyobelirteç tanımlama gibi farklı alanlarda kullanılabilecek bir teknoloji platformudur. Özellikle ilaç geliştirme, nihai ilacın pazara sunulma sürecini kısaltarak ve kişiye özel ilaç geliştirme alanında araştırmacıların ve bilgi birikiminin gelişmesine önemli katkı sağlayacak ürünler için yeni projeler ve iş birlikleri yaratacaktır.

1. INTRODUCTION

Significant advances in understanding of cancer diseases at molecular level have led to the development of effective new therapies based on tumor cell specific changes. However, there may also be cases in which cancer cells are resistant to treatment. The formation of resistant subclones within heterogeneous tumors poses a significant barrier to the effective treatment of cancer (Haber et al. 2011; Hyman et al. 2017).

Sampling of circulating tumor cells (CTCs) provides a suitable solution for studying tumor heterogeneity. Circulating tumor cells can be an example that represent tumor cells spread to different tissues of a single patient. In addition, it is possible to examine the tumor metamorphosis over time with samples taken from the patient's blood at regular intervals.

The measurement method applied in a cell population may be designed to cover all cells and give a single average value for the population. However, such measurements do not record changes from cell to cell within the same population. Cell variations can be recorded statistically in cell populations where cells are measured individually. Since direct measurements are taken from each of the cells in the population, the noise from the environment and the error that may occur in the measurement are minimized. The response of each cell in the population which is sensitive to external stimuli or changing ambient conditions can be accurately measured.

Recent advances in microfluidic-based systems have enabled the development of highly efficient platforms capable of capturing and isolating circulating tumor cells, which are very rare in blood. Thus, the study of CTCs as a single cell has led to an idea of tumor heterogeneity and treatment resistance in various cancers.

If it is desired to obtain individual information from the cells in the population, the cells must be separated individually and captured in the measurement areas or passed through the measurement area in sequence. Ideally, the proposed method should keep the need for skilled people and equipment to a minimum, and the results should be more efficient than conventional methods. Microfluidic-based systems can be designed to suit a single cell size, cells can be captured individually at stations or passed through the individual measuring area in a sequence. It produces fast and

reliable results with systems that are produced in much smaller volumes than conventional laboratory equipment and with a low sample volume in microliters.

Lab-on-a-chip (LOC) can meet the need for high-efficiency, low-production, portable systems for point of care applications and rare cell detection. It is possible to produce these systems in a few centimeters as an integrated system that can meet several different laboratory conditions together (Neužil et al., 2012; Rios et al., 2012; Trietsch et al., 2011). LOCs are able to offer faster and cheaper solutions as they achieve results with low volume samples. LOCs are effectively used in biomedical and environmental applications such as fluid transport, drug transport, virus and bacteria identification and cell / particle orientation, focusing and separation.

The main objective of this study was to separate the cell type of interest from a population containing various types of cells by dielectrophoresis (DEP) based methods followed by individual capture of this cell type and performing a secondary physical / chemical analysis on it. Although the prototypes for this purpose are examined separately as separation region (1st region) and analysis region (2nd region) for ease of research, the final product is integrated on a single chip.

The Clausius-Mossotti (CM) factor, which determines the DEP behavior (positive or negative) of different cells for the separation zone was investigated. Depending on the numerical results obtained for the systems with continuous flow, the conditions enabling particle and cell separation in the selected design were investigated. In the analysis region, impedance spectrometers of different types of cell groups in media with different conductivities were recorded on the cells captured individually.

The cells are not found in the body in a stationary environment. Therefore, experimental studies conducted in stationary cell culture environments cannot go beyond providing a preliminary idea about the possible drug effect. In addition to stationary two-dimensional cell cultures, systems have been developed that include fluid flow in order to make the living environment more accurate. Microfabrication methods can be used to develop systems that are compatible with biological systems, with proper shear stresses, cell-liquid ratios, and the time of physiological fluid in tissue reservoirs. It has been seen that cellular functions and gene expressions differ even with the shear stress effect of the medium passing over the cells alone (Zhang et al., 2009; Galbraith et al., 1998; Fernandez et al., 2007).

In addition to the DEP + EIS based microfluidic system, experimental studies have been carried out on the development of potential organ-on-a-chip systems to increase the accuracy of drug screening tests.

2. LITERATURE REVIEW

In drug and biotechnology applications, the interest in cell behavior and biochemical analysis of the cell is increasing day by day (Mateo et al., 2014; Karabacak et al., 2014; Alix-Panabiëres et al., 2014). Different types of cells have different characteristics and depending on these unique features, cell enrichment, orientation or separation is possible in microfluidic based systems. (Jin et al., 2014; Hajba et al., 2014; Cemazar et al., 2013; Chen et al., 2012). The ability to individually isolate / capture cells of a particular cell type from a complex cell population is critical for the diagnostic analysis of target cells. The ability to individually isolate / capture cells of a particular cell type from a complex cell population is critical for the diagnostic analysis of target cells.

Microfluidic based cell separation methods can be examined roughly in two main categories as labeled and label-free methods (Shields et al., 2015). Systems without any labeling do not cause a change in properties such as cell viability, size, shape, density, elasticity, and polarity. This means that the cell is only separated based on its specific physical / chemical properties. Therefore, these methods gain importance and attract attention. In microfluidic-based systems, cells can be separated by hydrodynamic forces, without labeling and applying any external force. Depending on the method to be preferred, high flow rates up to 2000 µl/min are applied and the flow rate can cause physical damage to the cell and reduce cell viability. Active systems with external force applied to the microfluidic system are the solutions that can be applied at low flow rates where cell viability is not affected. These systems can be listed as acoustophoresis, magnetophoresis, dielectrophoresis and optophoresis based systems. While acoustophoresis can be applied to separate cells of different sizes, magnetophoresis is a method that requires labeling of cells with magnetic beads. As an example of electrokinetic-based systems in said methods, cell separation by dielectrophoresis enables efficient cell separation in a much wider range of cell types.

The dielectrophoresis is a force acting on a particle/cell under an inhomogeneous electric field (alternating current or direct current). When a particle/cell is polarized under an inhomogeneous electric field, a net polar moment (dipole moment) act on it.

Each cell type has a unique polarity, which makes it possible to efficiently target the selected cell type (Gascoyne and Shim, 2014).

If the applied electric field is provided with alternating current, DEP behavior varies positively or negatively depending on the electrical properties of the particles and the surrounding medium as well as the frequency applied. The dielectrophoretic force (2.1) is given as follows (Yun et al., 2013):

$$F_{DEP} = 2\pi\, \varepsilon_0\, \varepsilon_m\, a^3\, Re(f_{CM})\, \nabla E^2 \qquad (2.1)$$

∇E^2 is the gradient of the square of the electric field applied, a is the diameter of a particle, ε_0, the electrical permeability (permittivity) of the vacuum, ε_m, the permeability of the liquid medium in which the particle is, $Re(f_{CM})$ refers to the real part of the Clausius-Mossotti (2.2) factor and is defined as follows:

$$Re(f_{CM}) = (\varepsilon_p^* - \varepsilon_m^*)/ (\varepsilon_p^* + 2\varepsilon_m^*) \qquad (2.2)$$

Here ε_p^* and ε_m^* are the complex electrical permeability of the particle and its environment (2.3), respectively, and is defined as follows:

$$\varepsilon^* = \varepsilon - j\frac{\sigma}{w} \qquad (2.3)$$

The complex electrical permeability depends on the frequency (w) of the alternative electric field applied and the conductivity of the medium (σ). This affects the polarity depending on the conductivity of the environment in which the cell or particle is located and the frequency of the applied electrical field which determines whether the DEP force acting on the cell will act positively or negatively depending on whether the CM factor is positive or negative, and thus the direction of the force. If the particle's polarization is larger ($f_{CM} > 1$) than the polarity of the medium, positive DEP (pDEP) occurs and the particle moves into areas where the electric field is dense. In cases where the polarization of the particle is less than the polarization of the medium ($f_{CM} < 1$), negative DEP (nDEP) occurs and the particle is pushed from the areas where the electric field is dense.

One of the reasons why cancer recurrence and cancer treatment is not successful is the formation of metastases and the resistance of cancer cells to the drugs administered. Metastasis is the spread of the cancer cell from the organ in which it first formed to another organ. Drug-resistant cancer cells cannot be completely treated (Zhou, 2010) and the detection of very few remaining cancer cells is quite difficult by conventional methods. DEP based microfluidic systems offer a possible

solution since it is effective in detecting and separating rare cells (Gascoyne and Shim, 2014).

Although K562 and K562AR cells are both the same type of leukemia cells, they differ in their dimensional and internal structural features. K562 cell is sensitive to drugs while K562AR cell is resistant to drugs during cancer treatment. Identification of K562AR leukemia cells is important for successful cancer treatment. The properties of K562 and K562AR cells are given in Table 1.

Table 2.1 : Electrical properties of K562 and K562AR leukemia cells (Demircan et al., 2015).

Cell Type	$\sigma_{cytoplasm}$	$\varepsilon_{cytoplasm}$	$\sigma_{membrane}$	$\varepsilon_{membrane}$	r_{cell}
K562	0.23	40	$1.8x10^{-5}$	8	8.35μm
K562AR	0.5	40	$2x10^{-5}$	9	8.35μm

In line with studies with K562 and K562AR cells, the dielectrophoretic behavior of K562 and K562AR leukemia cells at different frequencies has been presented (Demircan vd., 2015). At the frequency value of 48.64MHz, K562 cell was recorded at threshold frequency value (f_{CM} = 0, F_{DEP} = 0), and K562AR cell was affected by pDEP and it has been shown that these two cell types can be separated by DEP.

Fang Yang et al. (Yang et al., 2013) aimed to separate two similar cancer cells from each other. One of these cancer cells is LNCap, the prostate cancer cell, and the other is the large intestine cancer cell HCT116. Since the DEP force depends on the diameter of the cells and the dielectric properties of the cells, they continued their work by predicting that two cancer cells will separate with the frequency applied. They presented a persuasive study that if two cancer cells with a size of approximately 20μm can be separated, other cancer cells can also be separated. First, they observed how both cancer cells behave at which frequencies. The cells affected by different DEP strengths in three solutions prepared with different conductivities (0.025X PBS-Phosphate buffered saline solution 600μs / cm conductivity, 0.05X PBS solution 900μs / cm conductivity and 0.1X PBS solution 3000μs / cm conductivity). In 0.1X PBS solution, it was observed that the difference between the DEP forces acting on HCT116 and LNCap cells was highest. While the DEP power of HCT116 cells at 2.5MHz frequency is zero, n-DEP was effective on LNCap cells. While LNCap cells are directed at a frequency of 2.5MHz, it is predicted that HCT116 cells will be dragged along with the flow without being affected.

Another research group, Mohammed A. and his team (Alshareef et al., 2013), aimed at separating and identifying MCF7 breast cancer cell and HCT116 large intestine cancer cells using DEP force. The margin of error in defining metastasis by traditional methods is high. With the determination of the characteristics of cancer cells, they considered two different cancer cells with the idea of making a more accurate diagnosis. Firstly, studies were carried out for each cell to understand the frequency - DEP force relationship in different PBS solutions (0.025X PBS solution, 0.05X PBS solution, 0.1X PBS solution). In this study, it is seen that the difference between DEP forces is higher in low frequency ranges (<5MHz). In 0.1X PBS solution, it was preferred in experiments because there is more difference between the threshold frequencies of the cells. As a result of the studies carried out in the range of 1-5MHZ, it was found that the separation in the frequency value of 3.2MHZ is the most effective. It is shown that MCF7 cells are directed in the microchannel under the influence of nDEP, since HCT116 cells are not affected by DEP at the selected frequency value.

Electrochemical impedance spectroscopy (EIS) is an important measurement system in cell biology in the analysis of cellular structure, cell physiology and cell-disease interaction studies. When recording impedance values, they are plotted as time-dependent or frequency-dependent values. These data from the expanded parameters give information about the capacity and resistance of the cell. In these simple equivalent circuit models (Randles circuit model), the dielectric and electrical properties of the cells are determined by using these values (Park et al., 2010).

Measuring cellular resistance without the need for any molecular labeling can provide important information for researchers, especially about the mechanisms of cell functioning in the occurrence and progression of a disease. For example, the membrane specific capacity of cancerous tissue cells differs from normal cell membranes. White blood cells are known to have different capacitance values among themselves depending on the surface geometry of the cell membrane, and cell membranes with specific apoptosis or necrosis conditions have different capacitance and conductivity values compared to those in normal mode. In a study (Anh-Nguyen, 2016), MCF-7 breast cancer cell attachment, adhesion, spreading and long-term monitoring of the response of these cells to anticancer drug Cisplatin are presented on the same platform. These cellular activities and responses of cancer cells to drug therapy are demonstrated by the impedance spectrum of the target cells. In another study (Dastider, 2016), a microfluidic platform consisting of two consecutive dielectrophoresis and impedance measurements for the detection of E.coli, a low concentration (39 CFU / mL - CFU: colony forming unit, number of live cells)

foodborne pathogen, was presented. While the positive dielectrophoresis pulls the bacteria towards the center of the microchannel, anti-E.coli coated finger electrodes in the consecutive region detect the bacteria flowing along the microchannel.

There are also notable examples of microfluidic systems in combination with DEP + EIS. In a study with a simple design (Hamada, et al. 2013), Escherichia coli (E.coli) bacteria were directed in the microchannels by negative DEP, and impedance measurement was performed by capturing the bacteria under positive DEP on secondary electrode region. Under the effect of nDEP in the first part, bacteria are pushed towards the lower part of the microchannels away from the electrodes, where its concentration is increased and it is made easier to trap with pDEP. It was stated that by adding the nDEP region to the system, the capture efficiency in the pDEP region is doubled. The signal collected in the pDEP region was monitored on the computer and the impedance shift that occurred when the bacteria was captured was examined. It was emphasized that the number of captured E. coli bacteria should be above a certain threshold concentration value in order to be measurable. This study proposed a solution with a DEP + EIS integrated system to a priority issue such as the detection of E.coli bacteria in drinking water, but as stated, the measurement accuracy should be increased. In another design (Kim, et al. 2015) aimed at determining the concentration of E.coli bacteria in drinking water, it operates in two stages and under the influence of pDEP as a pre-concentration and capture region. In this study, it was emphasized that E.coli bacteria were detected with a sensitivity of 300 CFU / mL.

In many biological studies, cell lysis method is used to extract cell proteins or DNA. In an exemplary study (Ameri, et al. 2014), red blood cells were directed to the microwells by alternating current (AC) DEP and cell lysis was achieved by applying direct current (DC) through the same electrodes in these wells. In that study, impedance measurements were made before and after the signal was applied and it was recorded that the impedance value decreases as the cells fill the microwells, and reaches to minimun when the cell lysis was achieved. It is also emphasized that the system can meet all power needs with a single AA battery. The study suggests a solution as a portable system for researches where the target cell capture and cell lysis is critical.

In another study based on DEP + EIS (Wagenaar, et al. 2016), it was aimed to separate the sperms with morphological disorders from healthy sperms. This system, which operates fully automatically, healthy sperm cells was separated from 3μm polystyrene particles for proof of concept. In this method, there are three active

regions in order as focusing by nDEP, classification by EIS and spearation by nDEP. In the first region, all particles and sperm are focused in the microchannel center to pass through the measurement electrodes in the second region in a concentrated single row. The measurement electrodes identify these structures due to the impedance shift that occurs when the cell / particle passes and determine which of the two separate electrode pairs that will be activated and lead to two different collection outputs. The entire system is controlled by an algorithm written on LabView and offers a high potential for similar work.

The effects of the drugs used in the treatment of diseases on the real patient should be predicted in the most accurate way in preclinical studies. With the methods used in the studies conducted for this purpose, the drug trials foreseen reach high costs. Moreover, experimental methods on animals to verify drug effect are often very long, expensive and ethically controversial, and do not always reflect human physiology. Since the methods applied in the pharmaceutical industry, as well as the chemical and cosmetic industries, cause similar problems, alternative methods with higher clinical accuracy are sought. As a method that can put aside all these high costs, long trial-verification times and unethical decisions, it is possible to carry out low-cost, faster and more accurate drug development research with an optimum platform. These platforms are called in literature as “organ-on-a-chip”, “body-on-a-chip” or “human-on-a-chip”. These unique platforms are the systems that model the most realistic, physiologically correct, functional, single or multiple tissues, organs or diseases (Swinney and Anthony 2011; Wu et al., 2010). These platforms provide faster results in the screening of possible drug combinations and provide a solution for the development of individual drug by creating tissue / organ sample of the real patient (Esch et al, 2011).

Today, drug development studies consist of various stages such as preclinical, clinical and marketing as shown in Figure 2.1 (Dietzel, 2016). The first step in drug development is to identify the most suitable compounds by verifying the large number of compounds envisaged by in vitro experiments. With animal trials to observe the in vivo drug effect of these compounds, the number of suitable drug compositions is further reduced and the next step is to proceed to the clinical stages. In clinical stages, suitable drug composition is sought after testing on human subjects. Preclinical stages require much higher cost and time than clinical stages. Inaccurate selection of the methods to be applied in the preclinical stage and failure of the medication prescribed at other stages increases the costs and may cause significant damages on the patients, and may even lead to the results that require the withdrawal of the

drug from the shelves after it is placed on the market. Therefore, from simple two-dimensional cell cultures to on-chip organ systems, existing methods for optimal representation in-vitro and in-vivo pre-clinical studies are the most important steps in the discovery of potential drugs.

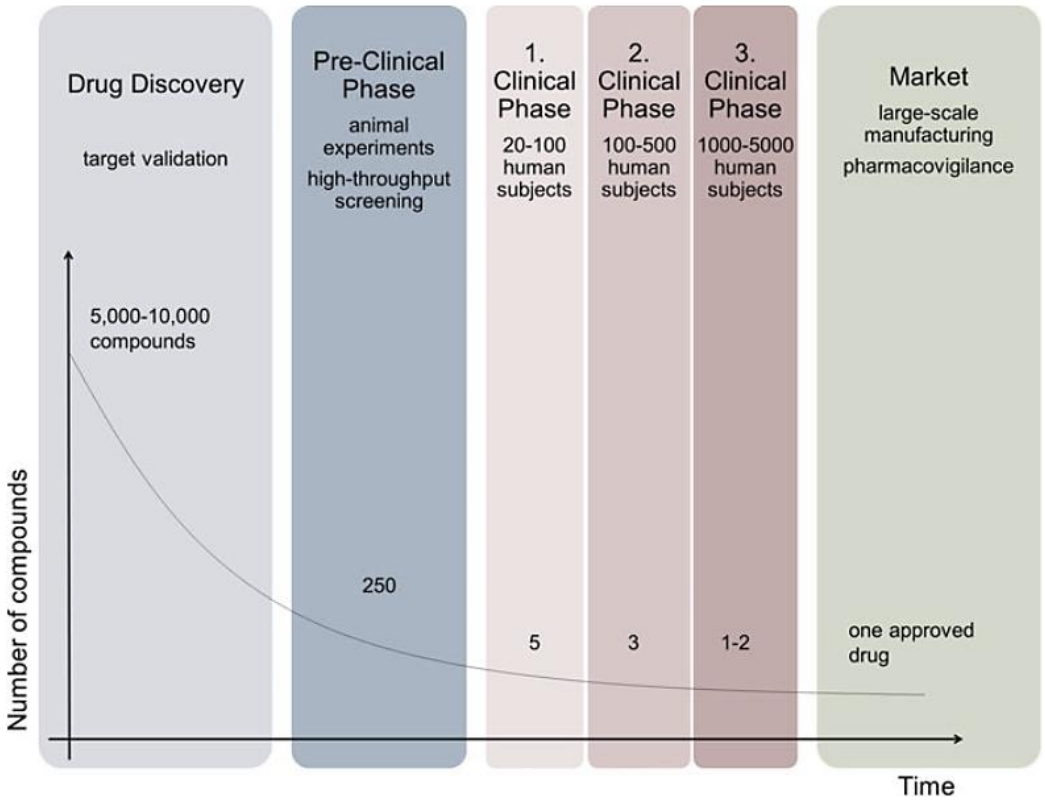

Figure 2.1 : Phases of drug development (Dietzel, 2016).

Experiments on two-dimensional static cell cultures provide an impression of the therapeutic effect of potential compounds on the targeted tissue. However, it is not predictable how the whole body will be affected by these compounds (Esch et al., 2011). The clinical benefit or toxicity of a drug cannot be guaranteed by numerous non-clinical experiments and animal tests. Since animal tissues differ physiologically and do not match the complexity of human tissue, they cannot be an alternative (Meer and Berg, 2012; Boughton et al., 2011). Especially in advanced drug trials, the results show that the study of human diseases on animal tissues is not sufficient. (Huh et al., 2011). Oncology drugs have a 5% success rate. Only this rate shows that the success of such a preliminary study is very low (Esch et al., 2011).

One way to improve the drug-screening method is to work with three-dimensional cell cultures that better reflect in-vivo conditions rather than working with two-dimensional cell cultures in uniform and monolayer form. Multicellular spheroids (spherical structures), hydrogels, natural (usually animal) intercellular matter (connective tissue)

and polymer or animal porous scaffolds are widely used in studies with three-dimensional cell cultures (Gurski et al., 2009; Kievit et al., 2010; Hutmacher, 2010). Three-dimensional cell cultures have many advantages over two-dimensional cell cultures. For example, the mechanical properties of hydrogels can be precisely controlled, and phenotypic behavior of the cells can be defined (Engler et al., 2006; Discher et al., 2005; Huebsch et al., 2010). Various hierarchical structures and geometric shapes can be created to form a targeted tissue type. Figure 2.2 shows a schematic representation of two-dimensional and three-dimensional cell cultures. Like two-dimensional cell cultures, three-dimensional cell cultures are far from representing a realistic structure when they are considered only in static conditions and the mechanical and dynamic flow conditions to which the cells are exposed are ignored.

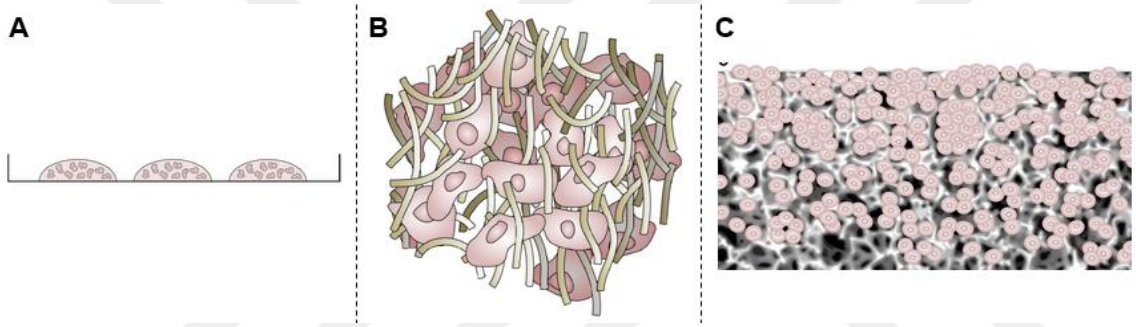

Figure 2.2 : Schematic representation of two-dimensional and three-dimensional cell cultures (A) Two-dimensional uniform cell culture sample in a Petri dish (B) Three-dimensional cell culture sample formed with hydrogel. (C) Three-dimensional cell culture sample formed in a porous scaffold. Cells retain their three-dimensional structure without flattening in the porous scaffold and mimic the three-dimensional tissue structure by establishing inter-pore bonding (Knight and Przyborski, 2015).

Liver poisoning is one of the primary parameters examined in the emergence of new drugs. For this reason, intensive research has been carried out in the development of three-dimensional hepatic spheroids (liver spherical tissue) in drug development studies (Leite et al., 2012; Yip and Cho, 2013; Tostoes et al., 2012) and high yield commercial products. In literature, there are studies that draw attention to the differences between two-dimensional and three-dimensional cell cultures (Lee et al., 2009). The toxic effects of gold and CdTe (cadmium telluride) nanoparticles on two-dimensional cell cultures and three-dimensional spheroids were investigated. The results showed that the toxicity in spheroids decreased significantly compared to two-dimensional cell cultures. The toxic effect of the three-dimensional structures caused the phenotype to change and the transport of nanoparticles within the tissue was prevented due to complex cell relationships.

In addition to two-dimensional and three-dimensional cell cultures, it is also possible to examine living tissues taken in biopsy or cross-section of a tissue in an in vitro experiment. However, since these tissues lose their vitality within a few days, it is not possible to make a long-term and high-yield study (Midwoud et al., 2010).

It is not possible to mimic a living organ even if some elements of tissue-specific microenvironment can be provided in studies with a uniform cell culture. Studies with cell cultures lack tissue-tissue interactions within a multi-scale architectural structure. An example of the interaction between parenchymal cells and connective tissue providing the vascular endothelium (vascular endothelial cells) and its surroundings can be shown. Such interaction is highly critical for the functioning of almost all organs. Generally, cell cultures are not exposed to mechanical effects, liquid shear stress, stress and compression that must be exposed in vivo (Mammoto et al., 2013; Ingber, 2003). In the absence of fluid flow, it is not possible to investigate the interaction of culture cells with blood circulation and cells in the immune system (Bhatia and Ingber, 2014).

The organ is composed of two or more tissues that come together in a hierarchical structure and the tissues are composed of different types of cell groups. The basic way to mimic organ functions is to combine two or more tissues. In recent years, great steps have been taken in this field.

Organ-on-a-chip (or on-chip organ) systems combine the key elements of a particular human tissue or organ and the interaction between them in physiological detail. Figure 2.3 shows a schematic description of the on-chip organs from two- and three-dimensional cell cultures and their functions studied in the literature (Meer and Berg, 2012). These systems are much more accurate models mechanically and physiologically that perform tissue-organ activities compared to three-dimensional or two-dimensional cell culture models (Huh et al., 2011). When we look at the latest studies in this field, it is not correct to evaluate the structures produced as a complete organ. However, it is seen that the microarchitecture of the functional unit of a particular organ or tissue-tissue interface is likened, and the structures of the organ that are artificially designed with dynamic mechanical and biochemical stimuli are produced on this architectural structure. Generally, on-chip organ systems are formed by utilizing biological microelectromechanical systems (Bashir, 2004), microfluidics (Whitesides, 2006) and biomimicking (Bhushan, 2009).

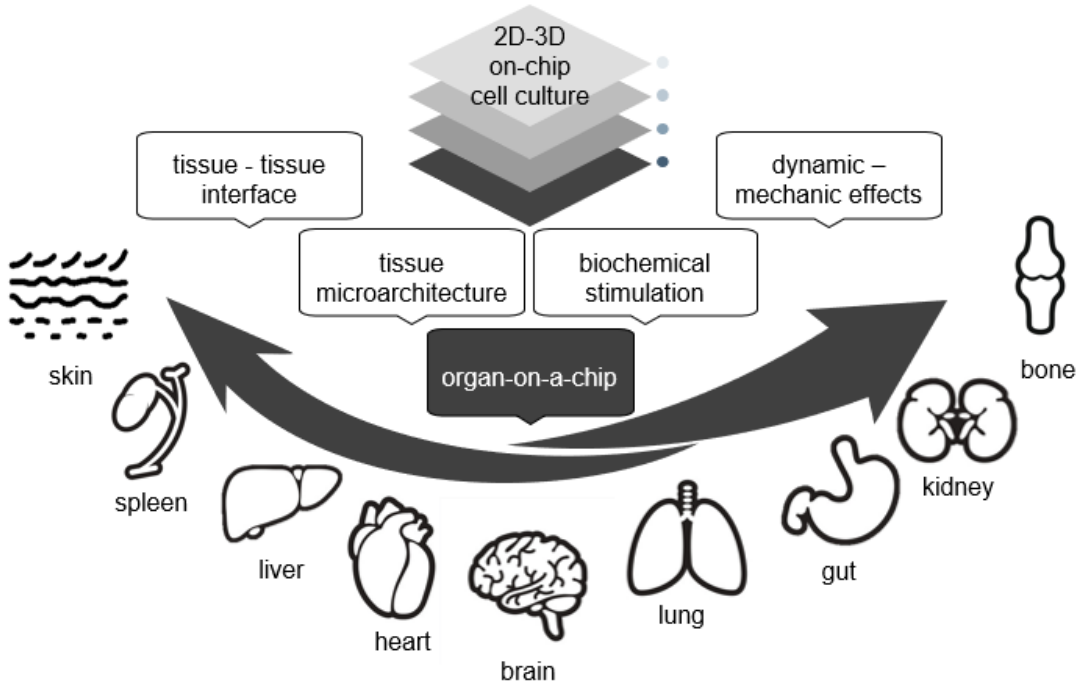

Figure 2.3 : Organ-on-a-chip concept and schematic representation of the studied organs (Meer and Berg, 2012).

The simplest system that can be considered as an on-chip organ is a system in which uniform culture cells are found in a single microfluidic reservoir and perform tissue-specific functions. Examples of cells herein are hepatocyte or tubular epithelial cells. A typical approach to forming an endothelial barrier is the creation of an air-liquid interface with a porous membrane layer between two microchannels (Jang et al., 2013; Huh et al., 2012; Huh et al., 2007). In more complex designs, there are systems in which two or more microchannels are connected to porous membranes and different types of cells are lined up on both sides of the membrane for inter-tissue interaction (Huh et al., 2012; Huh et al., 2010; Kim et al., 2012). The capillary interface with the alveoli of the lung or the blood-brain barrier can be examined on these systems. These systems can be constructed to include physical forces such as physiologically relevant fluid shear stress, repeated stress and mechanical stress.

There are many on-chip organ systems in the literature, but the first lung-on-a-chip study (Huh et al., 2010), published by Science magazine as the first organ-on-a-chip, stands out. Since this study, published in 2010, many organ types have been developed on microfluidic-based chips.

The general approach in on-chip kidney applications is to produce a homogeneous tissue layer on the upper surface of the membrane. When the structure of the kidney is examined, the nephron is seen as the functional building block. It provides blood filtration by considering the balancing of water and soluble substances in the blood. It

ensures the reabsorption of useful substances into the blood, while removing other wastes as urine. The nephron can be examined as three main structures. The first section provides passive mechanical filtration of the glomeruli, blood, and retention of cells and large proteins. In the second section, the blood and filtered fluid reach the proximal tubule, where reabsorption occurs. Finally, all filtration is complemented by osmosis, diffusion and reabsorption in the Henle loop. Figure 2.4 shows the schematic representation of the nephron forming parts in in vivo and how it is modeled in vitro.

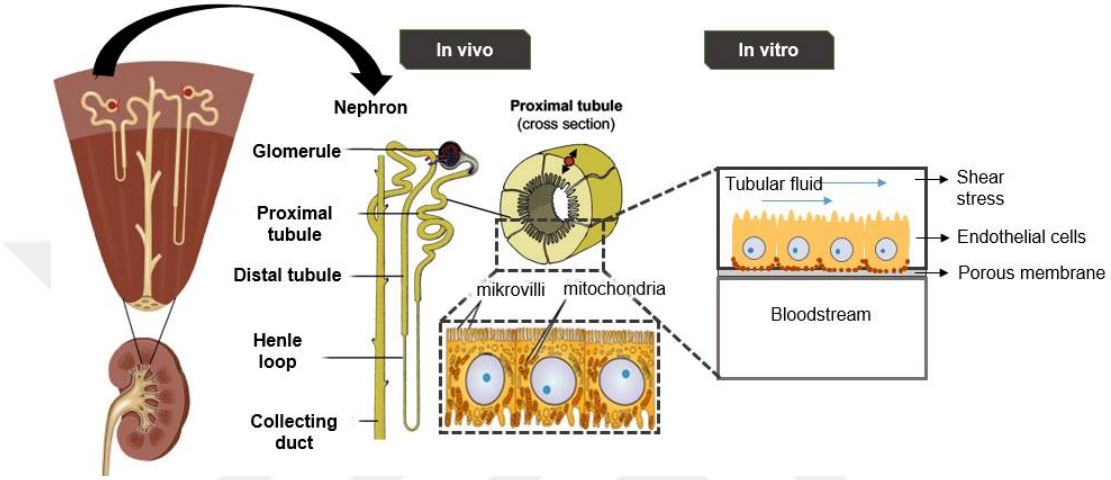

Figure 2.4 : Schematic representation of nephron structures in vivo and in vitro.

Although a system in which various structures forming the nephron are connected in series and studied numerically (Weinberg et al. 2008), no experimental study has been produced in the literature on a whole nephron structure. Generally, it was observed that proximal tubule cells were cultured on one surface of the membrane and over-chip organ systems were studied. The important elements that make up the nephron are summarized in Figure 2.5. In Weinberg's study (Weiberg et ali 2008), an integrated nephron structure was examined numerically and the dimensions and filtration parameters of the substances in the blood that could be applied on an on-chip organ platform were determined.

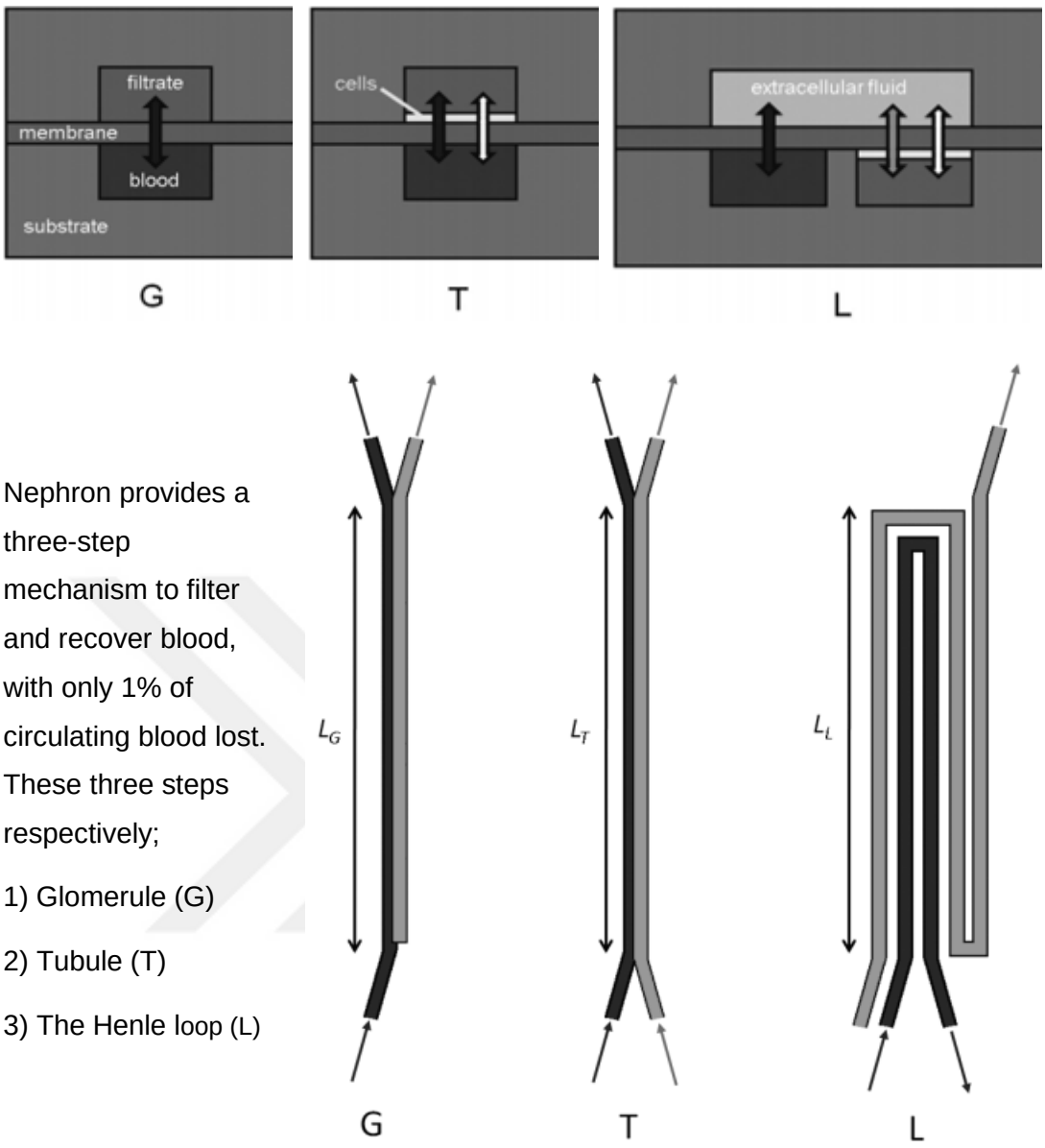

Figure 2.5 : Schematic drawing explaining the nephron structure in the kidney functionally (Weinberg et al, 2008).

The simplest approach of the kidney-on-chip platforms which is separated by membrane for the first time in the literature appears to be a microfluidic system with mouse cells, where dynamic conditions in the upper part and static conditions in the lower part takes place (Jang and Suh, 2010). Figure 2.6 shows this system in detail.

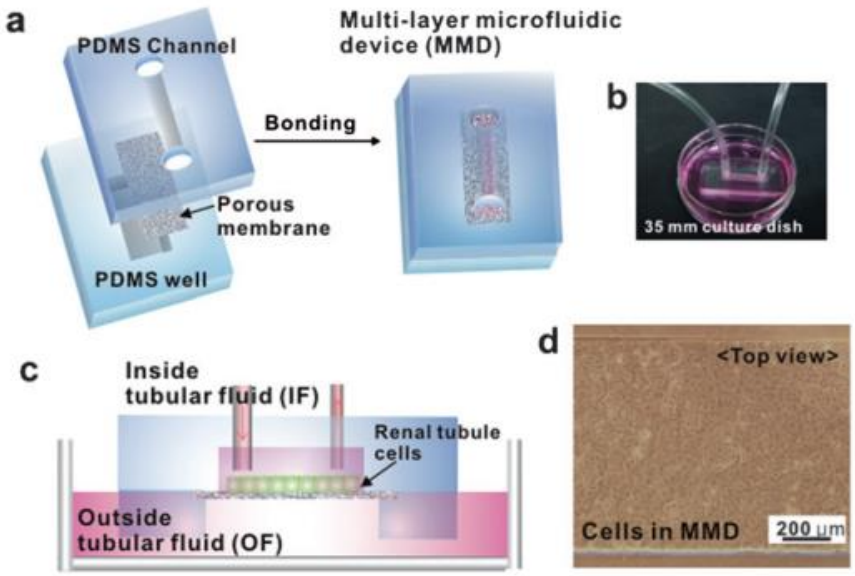

Figure 2.6 : Microfluidic based kidney-on-a-chip system created by using a porous membrane for the first time in literature (Jang and Suh, 2010).

Under the effect of shear stress, it was investigated whether the mouse cells fulfilled renal cell function. The top microchannel width is 1mm, length is 1cm and depth is 100μm. The lower chamber was cut into a coarser structure (2mm width, 0.6cm length, 1-2mm depth) and a 10μm thick Transwell polyester membrane with 0.4μm diameter pores was used. Tissue was cultured from mouse kidneys to cultivate inner medullary collecting duct (IMCD) cell culture. IMCD cells were incubated in hypertonic cell culture for 3 days at 37°C and 5% CO_2. After 3 days, a conformal cell layer was obtained on the membrane. The cells were then subjected to shear stress of 1 dyne/cm^2 with a syringe pump and hypertonic medium (Dulbecco's Modified Eagle Medium (DMEM) / F12 with 1% fetal bovine serum (FBS), 640 mOsm / kgH2O) at 37°C for 5 hours. Cells exposed to the flow for 5 hours show a very clear apical and basal cell polarization as shown in Figure 2.7 and vertical elongation.

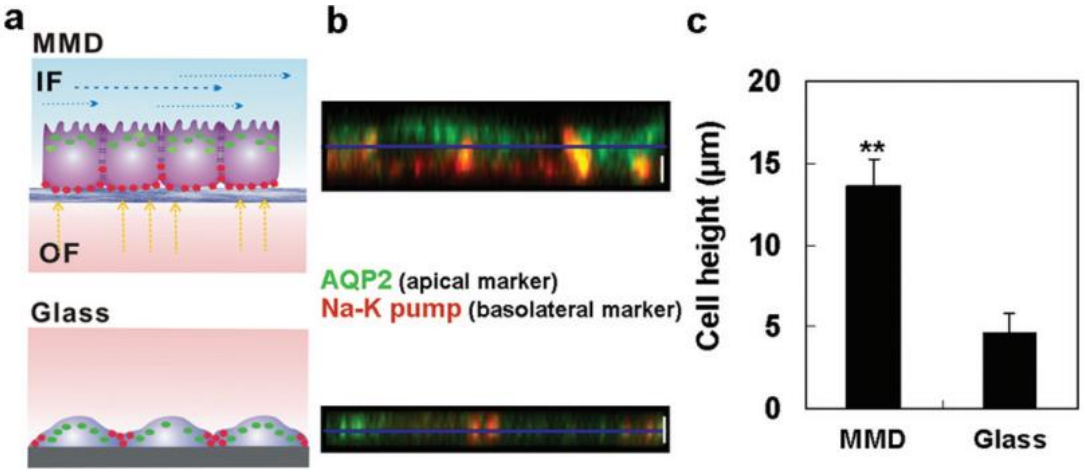

Figure 2.7 : IMCD cells were formed a) on a membrane and a glass surface. b) AQP2 (apical marker) and Na-K-pump (basolateral marker) show the structure change of cells after 5 hours of flow. c) Quantitative analysis of cell lengths in both environments (Jang and Suh, 2010).

In literature, the first study with human cells emerges as the study of the same group (Jang et al., 2013). Primary human proximal tubule epithelial cells were used in this study (Figure 2.8). Cells cultured in renal epithelial growth medium (REGM; Lonza) with FBS (0.5%), human transferrin (10 mg mL^{-1}), hydrocortisone (0.5 mg mL^{-1}), insulin (5 mg mL^{-1}), triiodothyronine ($5x10^{-12}$ M), epinephrine (0.5 mg mL^{-1}), epidermal growth factor (EGF) (10 mg mL^{-1}), and antibiotics (100 U mL^{-1} penicillin and 100 mg mL^{-1} streptomycin). Cells (2x10 5 cells / cm-2) were incubated at 37°C and 5% CO_2 in REGM for 3 days. At the end of day 3, following the forming a conformal cell layer, the cells were exposed to a shear stress of 0.2dyne/cm^2 by syringe pump at 37°C.

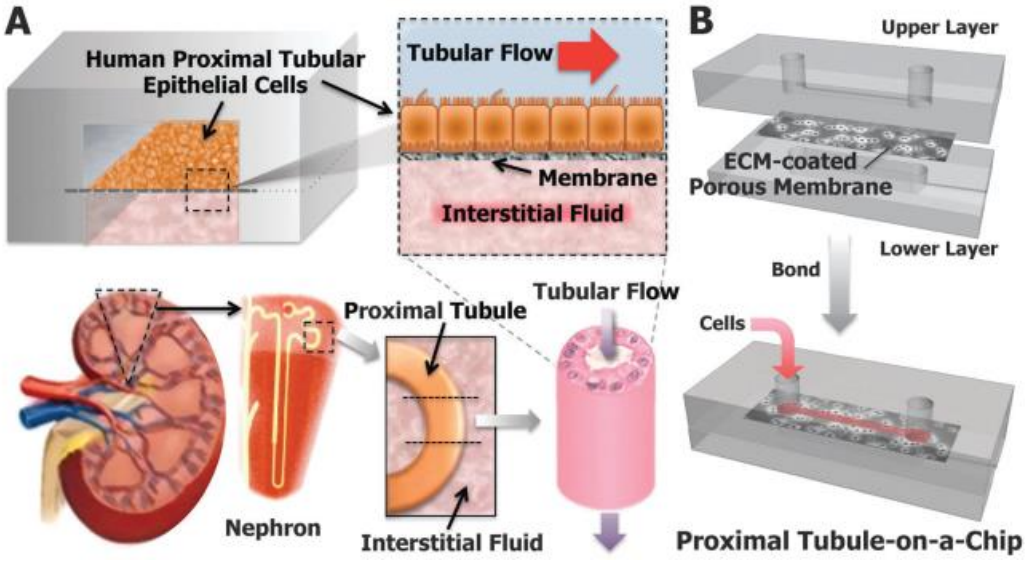

Figure 2.8 : Microfluidic-based kidney-on-a-chip system with a porous membrane generated by human epithelial proximal tubule cells (Jang et al., 2013).

Some researchers have attempted to model renal pathological diseases such as renal fibrosis (Moll et al. 2013) and kidney stone formation (Wei et al. 2012). These studies aim to reproduce a specific disease state. Particularly in the study of Wei et al., A design very close to that presented above. It can be seen that the above-chip kidney systems can provide answers for monitoring the effects of physiological conditions on the tissue/organ as well as being a platform for studying various diseases.

3. DIELECTROPHORESIS

The main purpose of this study is to capture the cell type of interest from a population containing various types of cells by dielectrophoresis (DEP) based methods and to perform a secondary physical / chemical analysis on this cell type. Although the designs produced for this purpose are examined separately as separation region (region 1) and analysis region (region 2) for the convenience of the research, they are integrated together on a single chip in the final product.

3.1 Design and Simulations

The design to be used for DEP-based cell separation is provided in the Figure 3.1. While a planar microelectrode array placed on the microchannel bottom surface is enough to generate an effective DEP force, it does not involve complex fabrication steps and is cost-effective considering single-use chips. In the system to be produced, there are interdigitated titanium electrodes and PDMS (polydimethylsiloxane) microchannels on the glass base.

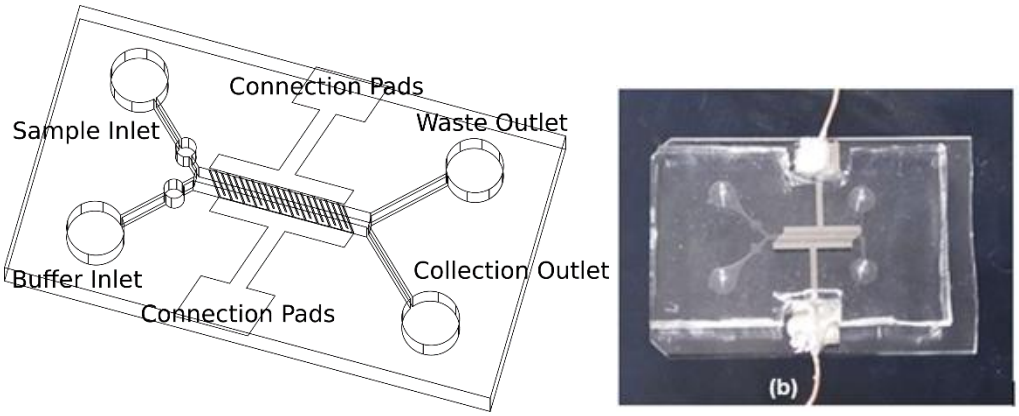

Figure 3.1 : Preferred DEP-based separation design under continuous flow a) Schematic view is shown in different colors to indicate that the electrode pair has opposite polarity applied. In the detail in the figure, it is shown that the width of the electrode fingers and the gap between them is 50μm. b) System for DEP-based separation.

Figure 3.2 shows the orientation under the force pDEP and nDEP when the fluid velocity is zero. Also shown are the boundary conditions for two-dimensional electrostatic simulations. The initial conditions are zero ($\phi = 0$) for all surfaces except

electrodes. The electrode pair is of equal size but opposite polarity. Since the microchannel bottom surface was covered with electrodes, periodic boundary conditions (PBC) were also applied, assuming that a single pair of electrodes was repeated infinitely. The electrode width (w) and the gap between the electrodes (g) are equal and 50 µm.

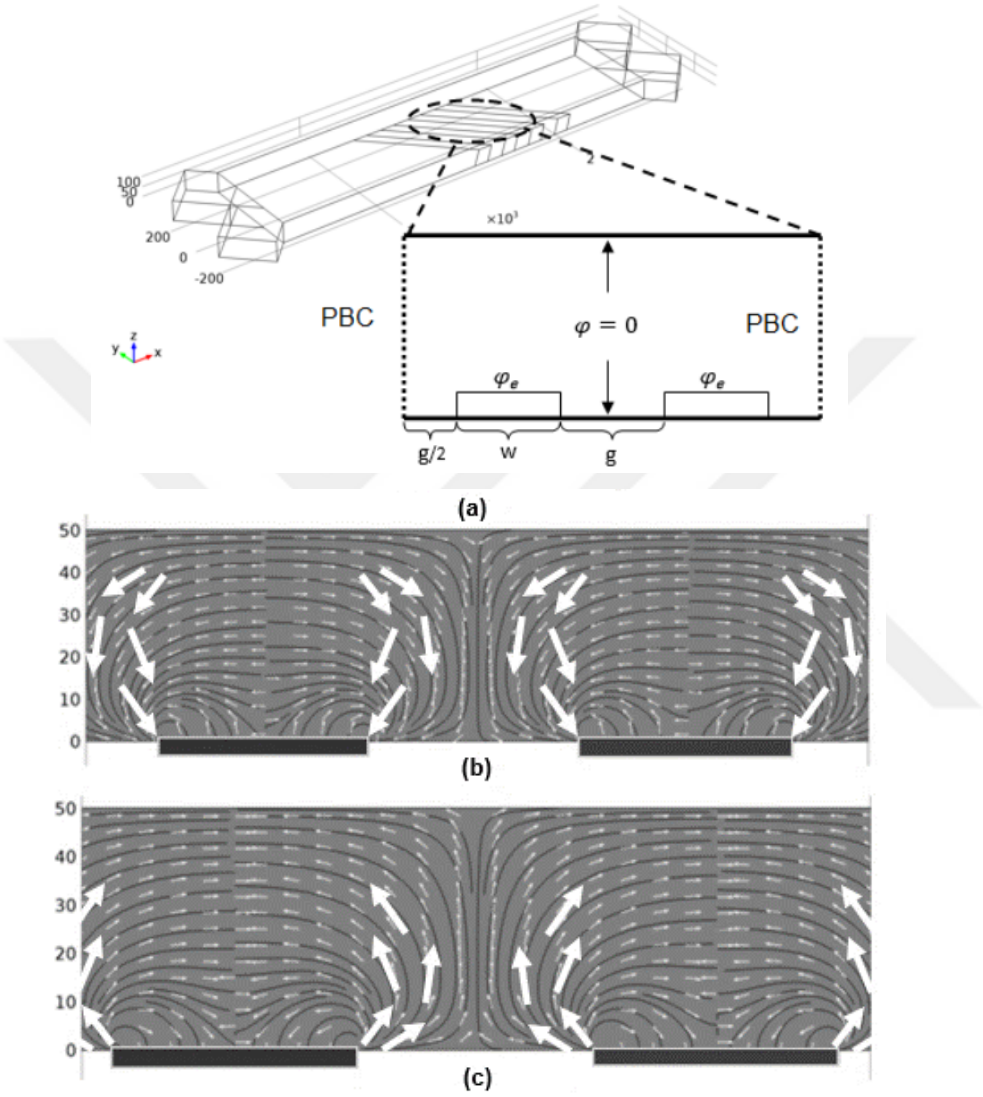

Figure 3.2 : In the case where the fluid velocity is zero, a) boundary conditions for electrostatic simulations. b) The particles are attracted towards the electrode edges under the pDEP conditions. c) A pushing force is generated outward from the electrode edges under the nDEP conditions.

The microchannel is 500 µm wide and 1 mm long. Since the electrodes are placed on the lower surface of the microchannel, the electric field strength reaches the highest value on the lower surface and there is a significant loss in the electric field strength towards the upper surface as seen in Figure 3.3. An effective electric field strength that can provide cell / particle orientation must be maintained throughout the channel

height. Therefore, the microchannel height is limited to 20 μm in the system to be produced. If the microchannel height is 50 μm or 100 μm, the cells / particles pushed to the surface under the effect of nDEP are moved away from the lane where DEP force is effective and drift through the microchannel.

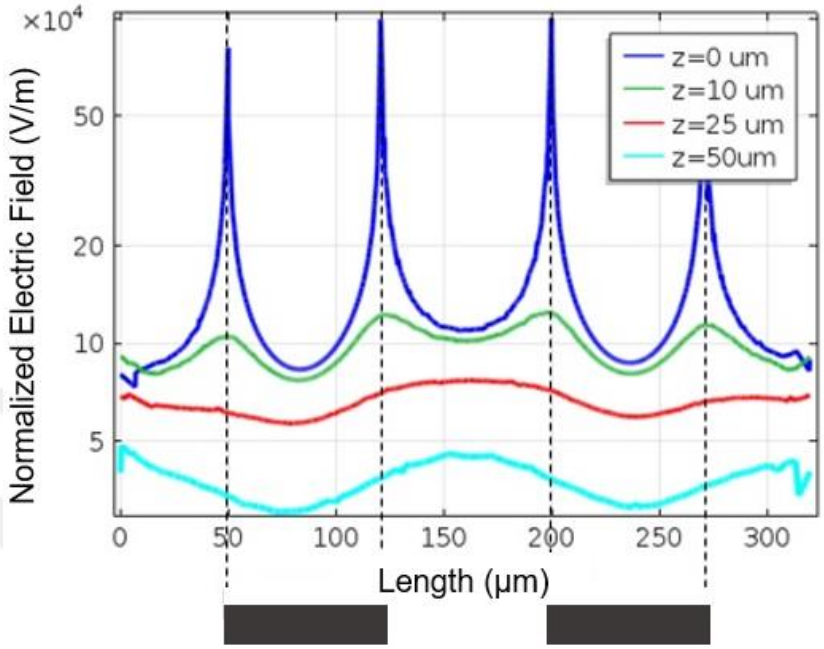

Figure 3.3 : Variation of electric field strength due to microchannel height. (y-axis logarithmic).

The total force acting on the cell / particle is also a combination of the hydrodynamic drag force and the DEP force with the fluid velocity being different from zero. Interdigitated electrodes were placed on the microchannel bottom surface at a 45° angle to the flow direction to provide DEP force. The particles in the microchannel are under the influence of dielectrophoresis and hydrodynamic forces. In situations where the particle is less polarizable than the liquid medium, the dielectrophoretic force will exert a pushing force out of the microelectrodes as the negative dielectrophoresis will be effective on the particle. Since the hydrodynamic force simultaneously push the particles along the flow, these two main forces acting on the particle conflict with each other. The ability to direct the particle with the net force acting on it varies depending on which of these two forces is dominant. In the case where the hydrodynamic force is bigger, $F_{HD} \geq F_{DEP}$ follows the particle flow path since the dielectrophoretic force barrier will be overcome, and in the case where the hydrodynamic force is low, it is possible to direct the particle with the dielectrophoresis. As shown in Figure 3.4, under these conditions the net force acts along the angle of the electrode and enables cell / particle orientation under nDEP conditions. The flow velocity exceeding the

dielectrophoretic force barrier is called the threshold velocity (3.1) and is expressed as follows:

$$V_{th} = \frac{F_{DEP}}{6\pi\eta\alpha sin\theta} \tag{3.1}$$

where η is the viscosity of the liquid and α is the particle radius. The threshold velocity depends on the dielectrophoretic force, viscosity of the liquid, the particle radius and the angle of arrangement of the electrodes. At flows faster than the threshold velocity, since the dielectrophoretic force barrier will be overcome, the particles will be entrained along the flow and will not be directed as desired by the dielectrophoresis. Since different particles have different threshold velocities, it is possible to separate the particles by regulating the fluid flow even if they are subjected to dielectrophoresis force of the same type (positive or negative) (Oh et al., 2009; Wu, 2008; Meinhart et al., 2003; Castellanos et al., 2003).

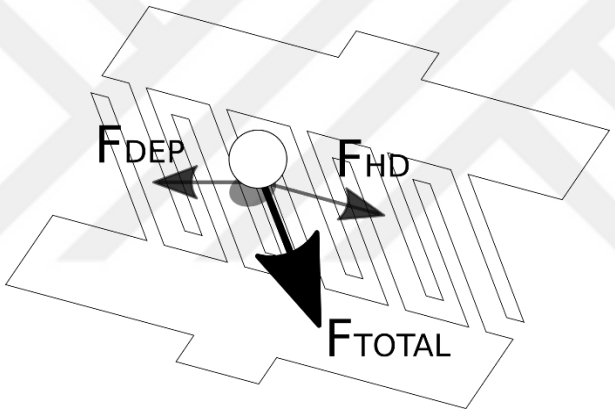

Figure 3.4 : When the fluid velocity is different from zero, the direction of the resultant force Ft formed by the hydrodynamic force (F_{HD}) and DEP force (F_{DEP}) is in the direction of the electrode angle.

In order to investigate the forces that occur on particles of different sizes, where the fluid velocity is different from zero, using finite element methods including multiple physics and simulations are made to contribute to the development of experimental studies. The electrostatic boundary conditions applied in these simulations are given in Figure 2 before. Simulations are designed to compute the electrostatic and laminar flow together and examine the movement of particles in an environment of such properties. The electric field is formed using the alternating current voltage applied to the electrodes and is not affected by the flow and computed with static solver. Likewise, a static solver is used for the flow profile regime. The motions of the particles were solved as time-dependent by adding electrical field and flow profile equations,

adding the properties of the particle, dielectrophoresis force, flow dependent drag force to the model.

The operation steps are listed below.

For the computation of electric field and fluid flow;

- Selection of effective physics and solvers in the system
- Creation of geometry
- Definition of material properties and materials
- Boundary conditions of the electric field and flow on the geometry, determination of inputs and outputs
- Establishment of mesh
- Determination of the solution method (static or time dependent) and solving the problem

To monitor particle movements in the next step;

- Solving time-dependent particle positions
- Graphical acquisition and interpretation of results

The material information used in the simulations is given in Table 3.1, with a few of the known biological cell parameters and Table 3.2 shows the solved equations. The CM factor of the polystyrene particle in DI-water was calculated numerically and is shown in Figure 3.5. Considering this graph, it is possible to direct the polystyrene particles under the influence of nDEP by applying the electric field at the frequency of 2 MHz.

Table 3.1 : Material properties.

Material	Property	Value	Unit
DI-water	Density	1000	kg/m^3
	Dynamic viscosity	0.001	Pa*s
	Permittivity	120	1
Polystyrene particles	Density	1050	kg/m^3
	Diameter	9.8, 3.2	µm
	Permittivity	2.55	1
Red blood cells	Membrane conductivity	$1x10^{-6}$	S/m
	Membrane permittivity	4.44	
	Diameter	5	µm
Thrombocyte	Membrane conductivity	$1x10^{-6}$	S/m
	Membrane permittivity	5	1
	Diameter	1.8	µm
K562 leukemia cells	Membrane conductivity	$7x10^{-4}$	S/m
	Membrane permittivity	10-15	1
	Diameter	17-22	µm

Table 3.2: Equations solved in models

Definition	Equation
Dielectrophoresis	$F_{DEP} = 2\pi r^3 \varepsilon_0 \varepsilon_m K \nabla \lvert \nabla V \rvert^2,\ E = -\nabla V$
Classius-Mossotti factor	$Re(f_{CM}) = Re\left[\left(\varepsilon_p{}^* - \varepsilon_m{}^*\right)/\left(\varepsilon_p{}^* + 2\varepsilon_m{}^*\right)\right]$
Hydrodynamic drag force	$F_{drag} = \frac{1}{\tau_p} m_p (u - v),$ $\tau_p = \frac{\rho_p {d_p}^2}{18_\mu}$

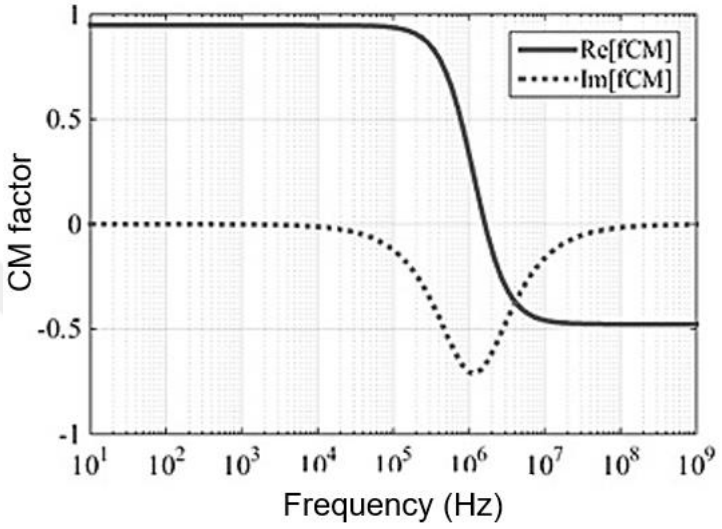

Figure 3.5 : Numerically calculated CM factor for polystyrene particle in DI-water.

Instead of using the actual geometry, which is intended to be fabricated for experimental studies, a characteristic element is selected and studied on it. In the formed geometry, two interdigitated electrodes were placed on the microchannel bottom surface and the total amount of orientation in the unit path was examined. As the number of electrodes increases, the total amount of orientation will increase. Since the electrode heights are quite small compared to the channel height, they are neglected in the simulations. In the analysis, a fine meshed triangle element network was used. The largest element size was 11.1 μm, the smallest element size was 1.2 μm and the largest element growth rate was 1.1 μm. As can be seen in Figure 3.6, there is a DEP force acting on the 9.8 μm particles but not enough DEP force is generated for the 3.2 μm particles. It is seen that a size-based separation is possible. In addition to the electrostatic conditions, the velocity of the fluid is given as flow rate and is 5 μl/min and the voltage applied to the electrodes is 10 V_{pp} at 2 MHz.

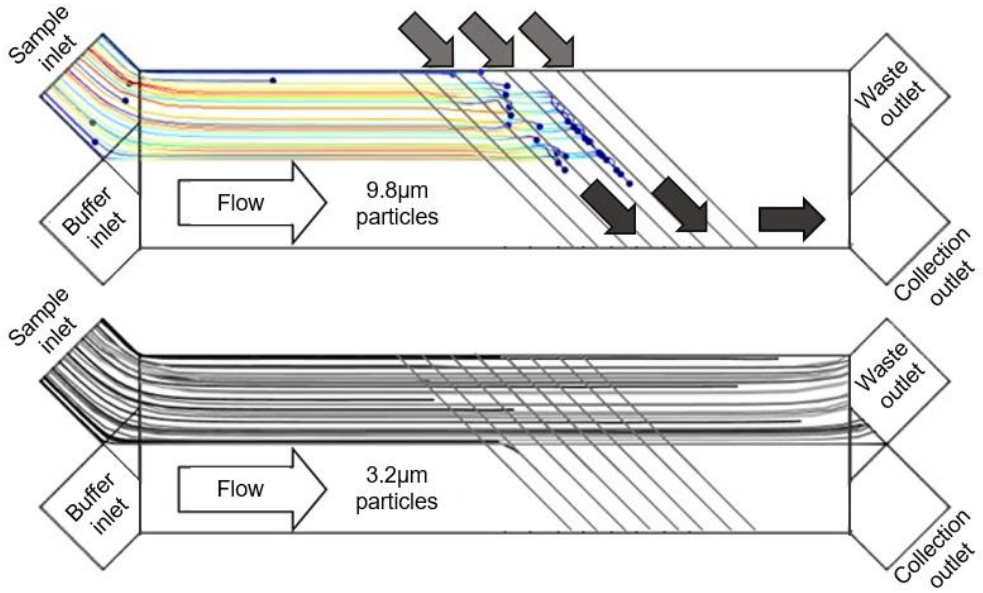

Figure 3.6 : The result from which the orientation of polystyrene particles of 3.2 μm and 9.8 μm in DI-water is obtained. The paths of the particles along the microchannel are plotted.

Figure 3.7 shows the time-dependent position change due to the DEP force acting on the particles of different sizes. Based on these results, it has been shown that polystyrene particles of different sizes can be oriented with the determined design and the fabrication of the selected design is made and the experimental outputs are compared with the simulations.

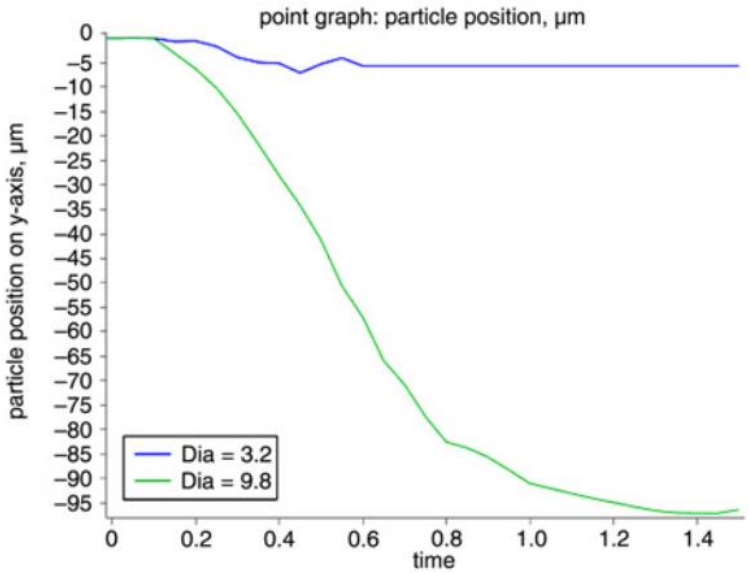

Figure 3.7 : Time-dependent positions of particles on y-axis.

3.2 Fabrication

The fabrication of the designed systems begins with the fabrication of chrome masks containing electrode and microchannel designs. Heidelberg “DWL 66FS - Heidelberg Instruments” is used to transfer the pattern on to the AZ1500 series photoresist coated mask.surface. AZ351B developer was applied, and the areas exposed to UV light were removed from the surface by wet etching and exposing Cr surface. The fabrication of the glass mask was completed by removing Cr under the patterned photoresist layer by Etch 18. As a final product, the patterns transferred to the mask were transparent.

For the production of microelectrodes, glass slides are coated with photoresist, patterned and metal coating was made. Cleaning the glass slides is very important in order to obtain a homogeneous photoresist thickness. The glass slides were placed in 1 molar KOH (potassium hydroxide) solution for 10 minutes in an ultrasonic mixer and rinsed with DI-water. After that, glass slides were placed in acetone for 10 minutes in an ultrasonic mixer and rinsed with isopropyl alcohol and DI-water, respectively. Here, KOH has been used to remove organic dirt from the surface, and acetone to remove inorganic dirt. 400nm thick AZ 1505 positive photoresist (AZ Electronic Materials) was coated on the glass substrate with a "Laurell WS-400E" spin coating device. “SÜSS MA6 Mask Aligner” was used for photolithography. Mid UV (260nm-325nm) wavelength light source, which can provide 24mJ / cm energy per second, was used. After UV expose, microelectrode patterns were made by AZ351B developer applied to glass slides.

Ti coating was made on photoresist-coated glass slides with physical vapor deposition. Ti target materials were evaporated by direct current (DC) magnetron sputtering. After 200 nm Ti was coated on photoresist coated glass slides, the photoresist was removed from the surface with acetone and electrodes were obtained on the glass surface in desired designs.

PDMS, is a commercially available silicon-based polymer with its curing-agent. PDMS is mixed by adding a curing-agent in the ratio of 1:10 (w/w). In order to remove air bubbles formed during mixing, degassing process is applied in vacuum environment. Then the mixture is poured to a SU-8 mold and left in an oven at 65°C for 4 hours to solidify. SU-8 is a widely used negative photoresist as a mold material in the fabrication of microfluidic-based systems. PDMS microchannels peeled from the SU-8 mold and are adhered to the microelectrode coated glass surface with oxygen plasma. A few drops of methanol are poured onto the glass surface prior to bonding

to obtain a lubricating interface. Microchannel and microelectrodes are aligned under optical microscope. Subsequently, methanol was removed from the interface by placing the microfluidic chips in a vacuum oven at 50°C for 15 minutes. Copper wires are fixed with silver-epoxy mixture on the connection pads on the chip so that the electrodes can be signaled over copper wires. Schematic view of fabrication steps of PDMS microchannels and microchannels with metal electrodes placed on bottom side are shown in Figure 3.8 and Figure 3.9 respectively.

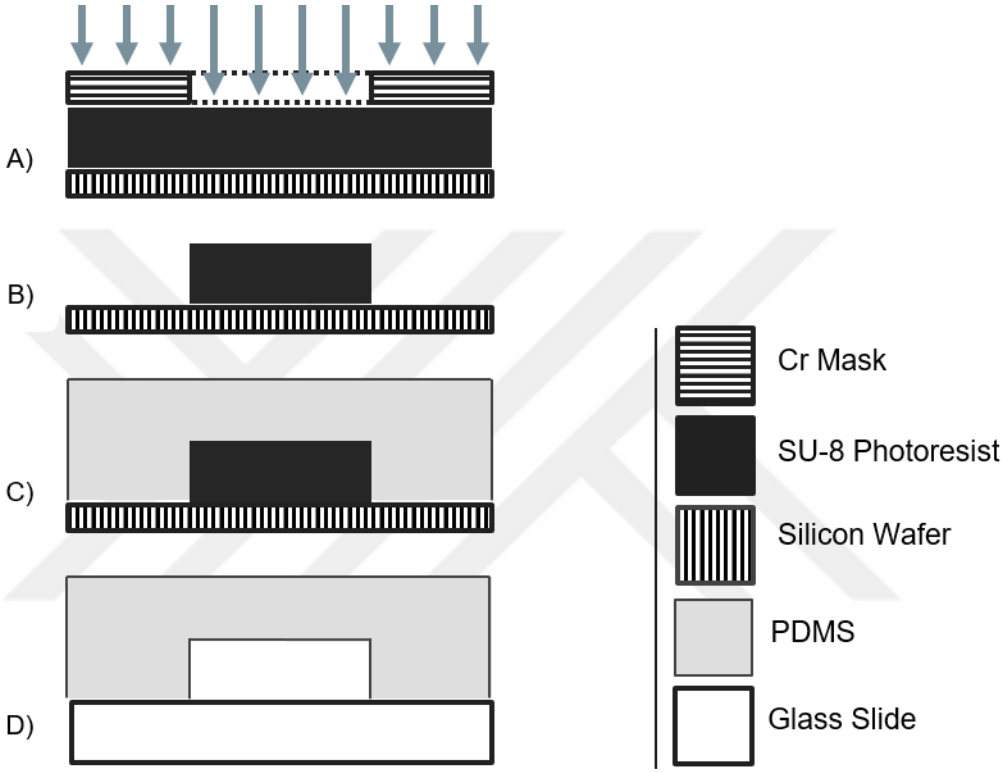

Figure 3.8 : Fabrication steps of PDMS microchannels. A) Desired pattern is transferred onto the photoresist by UV optical lithography. B) Patterned photoresist is solidified on the hot plate to be used as a mold. C) PDMS is poured onto the mold and solidified on the hot plate. D) PDMS is peeled from the mold and adhered to a glass slide if there is no metal electrodes needed in the design.

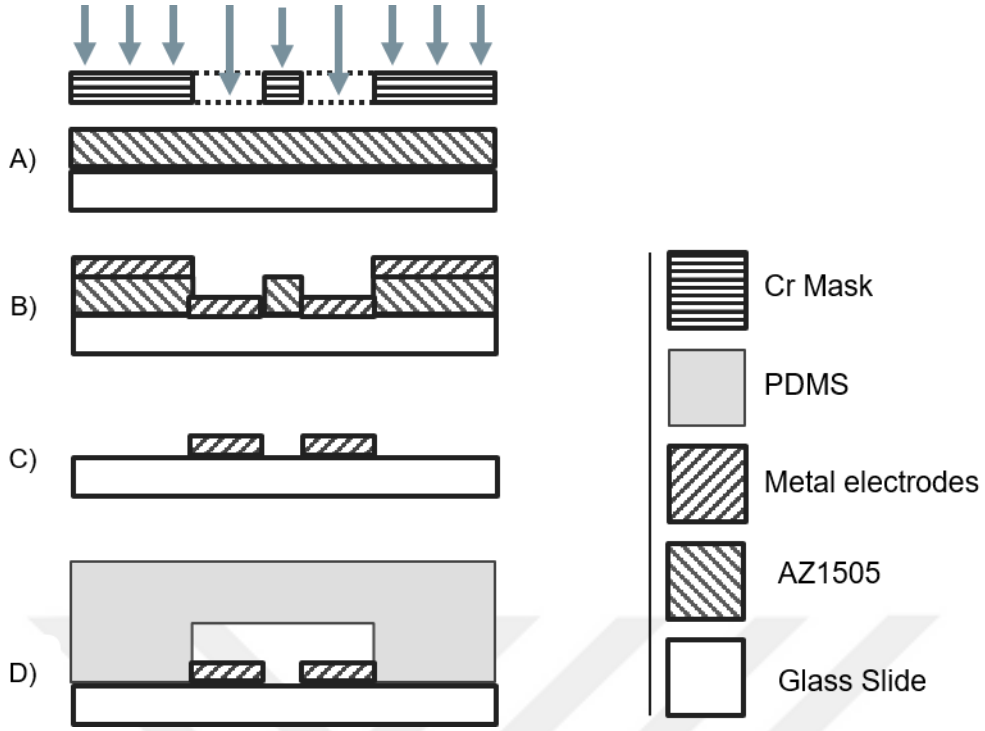

Figure 3.9 : Fabrication steps of microchannels with metal electrodes placed on bottom side. A) Desired electrode pattern is transferred onto the photoresist by UV optical lithography. B) Preferred metal (Ti or Cr / Au) is coated on the photoresist coated sample by physical vapor deposition method. C) The electrodes of the desired pattern are provided on the glass slide with the removal of photoresist. D) Alignment and assembly of the prepared PDMS microchannels and metal electrodes.

3.3 Experimental

The behavior in DI-water was examined in the experiments carried out with polystyrene particles, and in the next steps the effect of the particles on the electrokinetic transport was investigated by changing the conductivity of the medium. DI-water conductivity was measured as 2.5x10-4 S / m with “HC 3010 conductivity meter, Trans Instruments (Singapore)”. The CM factor of the polystyrene particles in DI-water was calculated numerically by the software MathWorks Matlab R2013a (USA) and as shown in Figure 3.10, pDEP is active at low frequencies and nDEP is active at high frequencies. In the experimental studies, the opposite phase signal at the 5 V_{pp} sine wavelength was applied to the electrode pair at different frequency ranges.

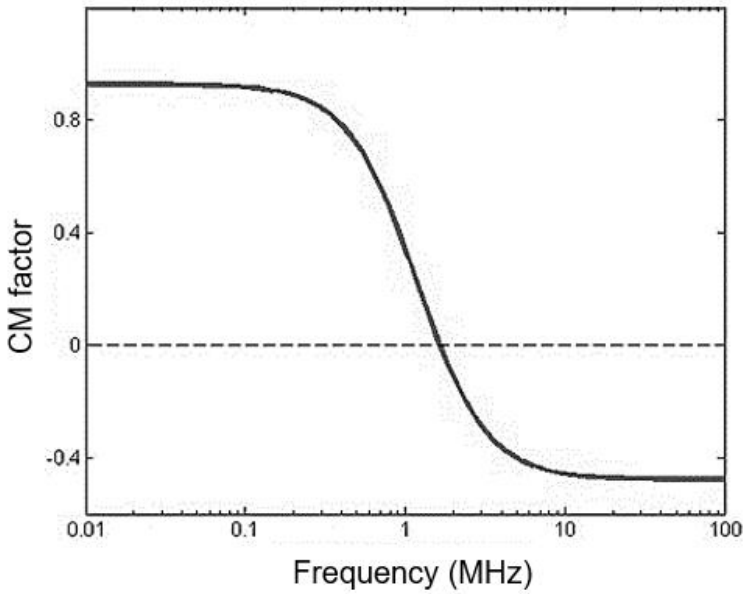

Figure 3.10 : Variation of the CM factor depending on the electric field frequency for particles in DI- water ($2.50x10^{-4}$ S / m). pDEP is effective if CM> 0 and nDEP is effective if CM <0.

The LOC presented in Figure 3.1 is placed under a fluorescent microscope and copper wires (50μm in diameter) are fixed to the titanium electrode connection pads with silver epoxy. 81150A Pulse Function Arbitrary Noise Generator, Agilent Technologies (USA) signal generator and crocodile-end jumper cables were connected to the electrode pair and an alternating current at $10V_{pp}$ is applied. The test apparatus is shown in Figure 3.11.

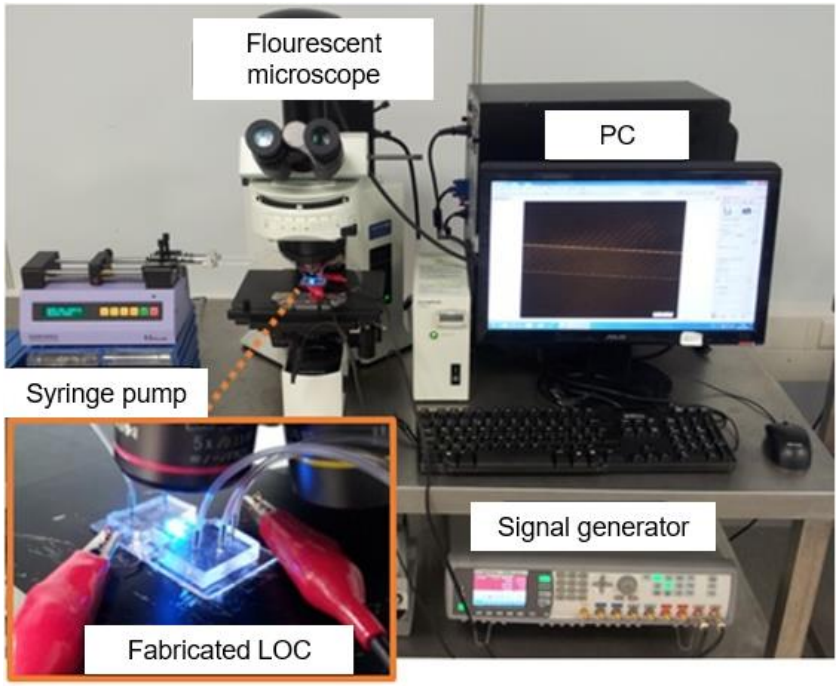

Figure 3.11 : Experimental setup for systems with continuous flow.

In the preliminary studies, the frequency ranges where polystyrene particles were affected under pDEP and nDEP were determined and it was observed that nDEP was effective over 700 kHz in DI-water. The frequency of 2MHz, where nDEP is most effective, has been kept constant in experimental studies. Fluid velocity is provided by a “Harvard Pump 11 Plus Dual Syringe” syringe pump and Hamilton 100 µl syringes connected to both ports of the microchannel. In the experimental results presented in Figure 3.12, it was observed that the separation between 1-10 µl / min was realized at high efficiency and the separation decreases at higher flow rates.

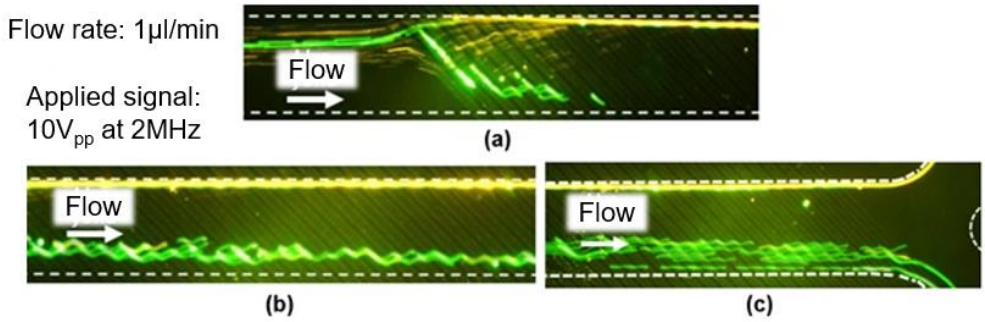

Figure 3.12 : Once polystyrene particles meet the electrodes, they are oriented depending on their size. a) the region where the particles meet the electrodes in the microchannel, b) the center of the microchannel, c) waste and collection outlets at the end of the microchannel.

In order to be able to direct live cells under continuous flow, the separation parameters must be determined. Among these parameters, the characteristic CM frequency (frequency value where CM = 0) of each cell which has an important place in the orientation with DEP should be determined. For this purpose, the medium and the electric field frequency that cells can be directed by DEP were investigated. The medium in which the living cells will be placed during the experiment must be isotonic so that the cells do not undergo physical change and should be at a conductivity level where they can be directed under an effective DEP force, as we examine with polystyrene particles. The media prepared for the cells we studied in the literature are quite similar (Yasukawa et al., 2013; Shafiee et al., 2010; Sano et al., 2011; Yasukawa et al., 2012). Basically, while preparing the isotonic solution with sucrose, glucose or dextrose, it is seen that a certain ratio of PBS (phosphate buffered saline) or RPMI medium is added to keep the medium at the desired conductivity. For live cell studies, 2.5% by volume and 10% by volume of PBS were added to 200 mM sucrose solution, and values close to the conductivity values in the literature were obtained. These values were 0.4 mS / cm and 1.604 mS / cm, respectively. Thus, it is aimed to investigate the direction of effective DEP force in different conductivity media. According to the experiments, the results in Table 3.3 were collected.

Table 3.3 : DEP force directions on biological cells depending on frequency in different conductivity media.

Medium Conductivity	**0.4 mS/cm**					**1.604 mS/cm**				
Frequency / Cell Type	50 kHz	500 kHz	750 kHz	1 MHz	5 MHz	50 kHz	500 kHz	750 kHz	1 MHz	5 MHz
HL-60	**--**	**-**	**++**	**++**	**++**	**--**	**--**	**--**	**+**	**++**
Jurkat	**--**	**--**	**--** *600 kHz	**++**	**++**	**++**	**--**	**--**	**--**	**++**
Daudi	**--**	**--**	**--** *600 kHz	**++** *700 kHz	**++**	**++**	**--**	**--**	**--**	**++**
THP-1	**--**	**--**	**--** *700 kHz	**++**	**++**	**++**	**--**	**--**	**-**	**++**

++ = *pDEP,* **+** = *weak pDEP,* **--** = *nDEP,* **-** = *weak nDEP*

As can be seen here, nDEP is active on biological cells at low frequencies and pDEP is active at high frequencies. As the conductivity of the medium increases, the characteristic CM factor shifts towards high frequencies. The main conclusion to be drawn from Table 3.3 is that the cells in the respective medium can be separated from each other at the frequency value in the regions highlighted in green. It is envisaged that THP-1 and Daudi cells can be separated at 700 kHz in medium with a conductivity of 0.4 mS / cm and HL-60 cell type at 1 MHz frequency can be separated from Jurkat and Daudi in medium with conductivity of 1.604 mS / cm. In addition, in the regions highlighted with blue, it is envisaged that the relevant cells will be separated, although the force direction acting on the cells at the current frequency values are the same, magnitudes of DEP force is at different intensities. Accordingly, in the medium with a conductivity of 0.4 mS / cm, the HL-60 cell type can be separated from the other three types at 500 kHz frequency. In the medium with a conductivity of 1,604 mS / cm, the THP-1 cell type can be distinguished from the other three types in the 750 kHz frequency range. It is envisaged that THP-1 cells can be separated from Jurkat and Daudi in the frequency range of 1 MHz.

Experimental studies were carried out to differentiate Jurkat and Daudi cells with the experimental setup used in the experiments with continuous flow with polystyrene particles. The behavior of Jurkat and Daudi cells depending on the electric field frequency is quite similar. Table 3.4 shows that these two cell types have only 1 micrometer size difference in size distribution measurements with the EVE Automatic Cell Counter. When all similarities are considered, it is difficult to differentiate these two cell types and they are not included in the literature.

Table 3.4 : Concentration distributions of Jurkat and Daudi cells.

Jurkat		**Daudi**
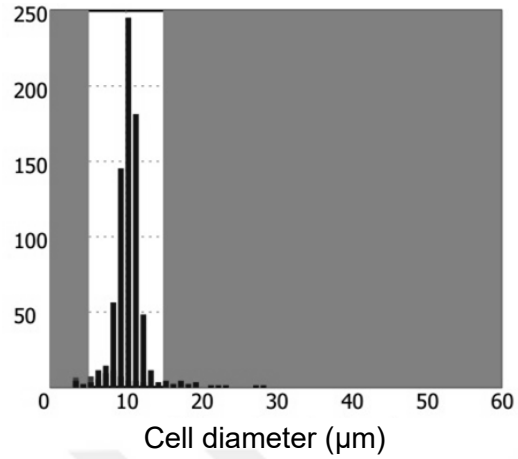		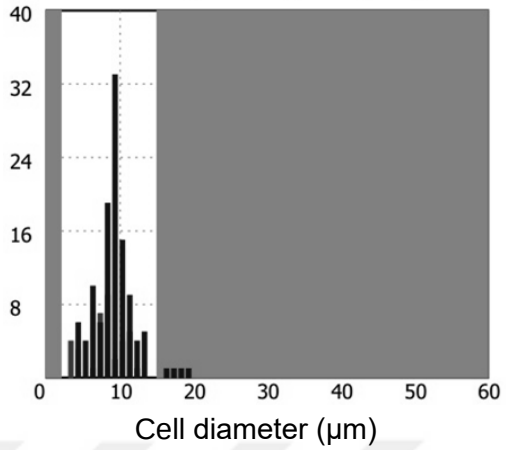
Total cell concentration	$3.9x10^6$ cell/mL	$7.4x10^5$ cell/mL
Viable cell concentration	$3.6x10^6$ cell/mL	$5.6x10^5$ cell/mL
Dead cell concentration	$2.5x10^5$ cell/mL	$1.8x10^5$ cell/mL
Viability	93%	76%
Average viable cell diameter	10.1µm	9.0µm
Average dead cell diameter	8.1µm	7.6µm

Cells were labeled with fluorescent dye (Jurkat cells; CFSE and Daudi cells; Far-red) for better observation under fluorescence optical microscope. Prior to the experiments, the cells were centrifuged for 5 minutes at 1000 rpm (round per minute) separated from the supernatant and pelleted. 0.8 µl of CFSE and 0.8 µl of Far-red were applied to concentration of $10x10^6$ Jurkat and Daudi cells respectively and the cells were dissolved in diluted CFSE. After 5 minutes of incubation, the cells were washed 2 times with FBS + PBS solution and mixed in medium with a conductivity of 0.4 mS / cm. Jurkat and Daudi cells were mixed to be equal in number in the medium, prepared at a 1: 1 concentration.

When 3 µl / min flow rate and $10V_{pp}$ 700kHz signal were applied, all cells were found to be under the effect of pDEP and trapped on electrode surface as in seen in Figure 3.13(a). During the experiments, the frequency was reduced in a controlled manner

to 620 kHz, where Jurkat cells were observed to be directed under nDEP as in Figure 3.13 (b).

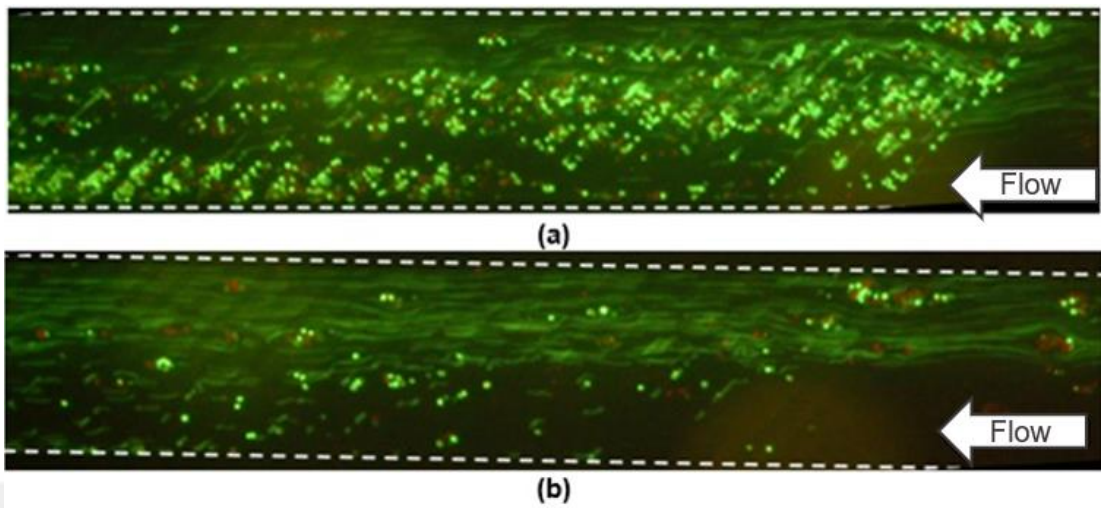

Figure 3.13 : 3µl / min flow rate and 10V_{pp} a) At 700kHz; Jurkat and Daudi cells were observed to be collected on the electrode surface under the influence of pDEP b) When the applied frequency was reduced to 620 kHz; Jurkat cells were observed to be directed under nDEP where Daudi cells were not affected by this change.

At the end of the microchannel, it was observed that Jurkat cells were mostly collected from outlet 1, as shown in Figure 3.14, whereas the majority of Daudi cells with similar characteristics were collected from outlets 2 and 3.

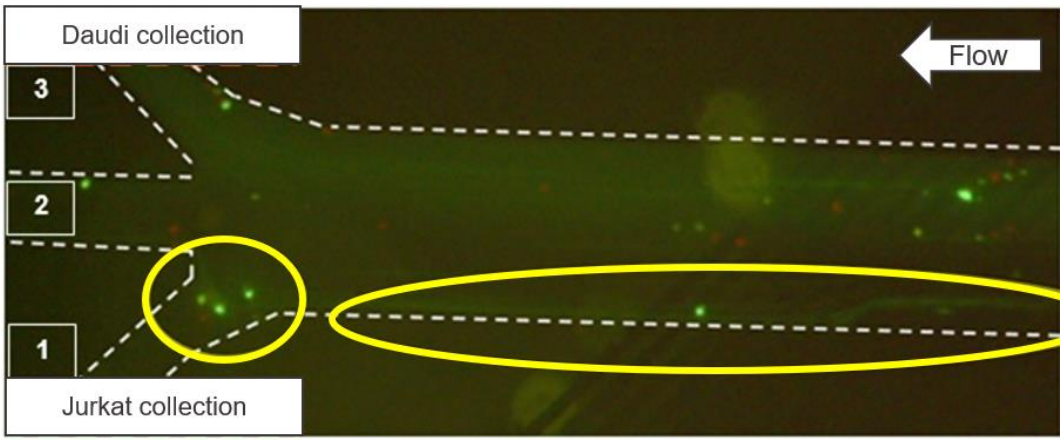

Figure 3.14 : There are three outlets of equal width at the end of the microchannel. Outlet 1 is intended to collect Jurkat cells while outlets 2 and 3 are Daudi cells collection outlet.

As a result of the experiment carried out with live cells in the continuous flow system, cells collected from outlet 1 and cells collected from outlets 2 and 3 were counted to determine cell type by a flow cytometer. Figure 3.15 shows the counting of cells collected from outlet 1. Since the Jurkat cells were expected to be larger in number than other outlets, the amount of CFSE irradiation (CFSE (+)) cells was determined

and it was recorded as 11.6%. The amount of non-CFSE radiation (CFSE (-)) was found to be 88.4% and 59.4% of these cells did Far-Red radiation (Far Red (+)). In total, a non-irradiating cell was found in a percentage slice of 36.7% (88.4% x 40.8%). It is predicted that non-luminescent cells may be dead or the effect of fluorescent dye loses over time.

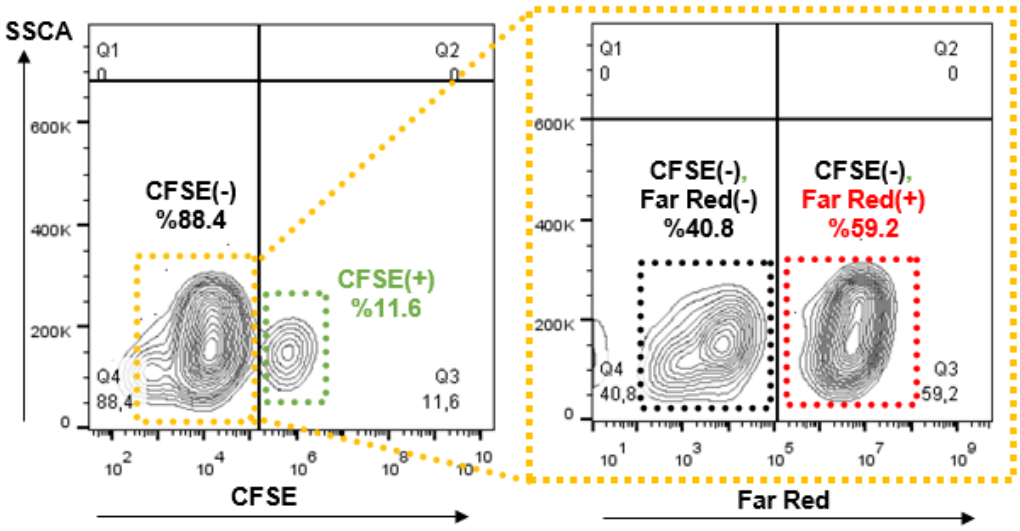

Figure 3.15 : Flow cytometer count results of cells collected from outlet 1. While 11.6% of the collected cells were Jurkat cells, 59.2% of CFSE non-irradiating cells were Daudi cells.

The cells collected from outlets 2 and 3 were counted together and the counting result obtained in Figure 3.16 was obtained. 44.7% of the cells collected here showed Far Red radiation (Far Red (+)), while only 3.41% of the amount that did not show Far Red radiation showed CFSE radiation. This shows that a very small amount of Jurkat cells are collected from these outlets. 53.42% of the cells collected from outlets 2 and 3 do not emit any color.

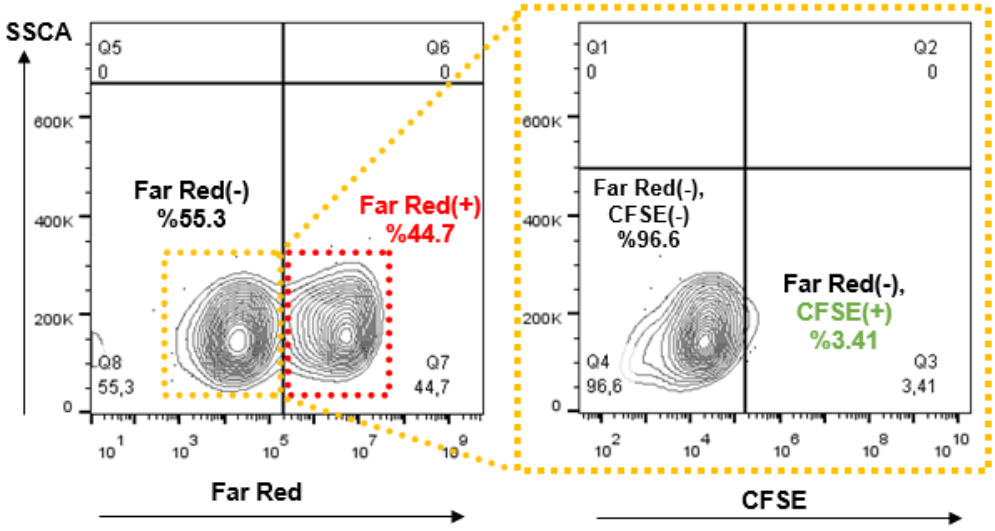

Figure 3.16 : Flow cytometer count results of cells collected from outlet 2 and 3. While 44.7% of the collected cells are Daudi cells, 3.41% of the cells that do not make Far Red radiation are Jurkat cells.

Table 3.5 summarizes the results of our study to separate Jurkat and Daudi cells. As a result of our efforts to separate Jurkat and Daudi cells in a 1:1 concentration ratio in a LOC system, it is seen that Daudi cells are collected from the outlets 2 and 3 and enriched almost 24 times more than the outlet 1.

Table 3.5 : Enrichment ratios of Daudi cells from each outlet

Outlet #	% CFSE	% Far Red	% Non-irradiating CFSE(-), Far Red(-)	Enrichment Rate
1	11.6	52.33	36.07	4.51 times more Daudi
2 and 3	1.89	44.7	53.42	23.65 times more Daudi

A single inlet microchannel design was also used to study of Jurkat enrichment. The cells are labelled with a fluorescent marker (CFSE) for easier observation of the cell movement under a fluorescent optical microscope. Before the test, cells are pelletised by centrifugation at 1000 rpm for 5 min and supernatant is discarded. About 0.8 µl CFSE is applied for 10 × 106 cells and cell pellet is dissolved in diluted CFSE. Dissolved cells are incubated at room temperature for 5 min. After washing the cells two times with 5 ml 5% FBS+PBS solution as blocking dye, cell pellet is dissolved in PBS.

The experimental results for Jurkat cells are given in Fig 3.17. nDEP is effective in PBS medium under applied signal which is 10 V_{pp} at 550 kHz. The deflection on the y-axis becomes clear below the flow rates of 3 µl/min. As in the case of polystyrene particles, Jurkat cells with larger diameters are deflected on the y-axis along the

microelectrode geometry and given in Figs 3.17(a-b). It is experimentally observed that near the end of microchannel, cells with larger diameters are completely focused on one side of the microchannel as in Fig. 3.17(c). The cells with smaller diameters are not affected by a dominant dielectrophoretic force and leave the channel without any deflection. Distribution of small cells are expressed with blue circles for each individual cell in 3.17(d-e). The enrichment of Jurkat cells based on their diameter is achieved with the current design.

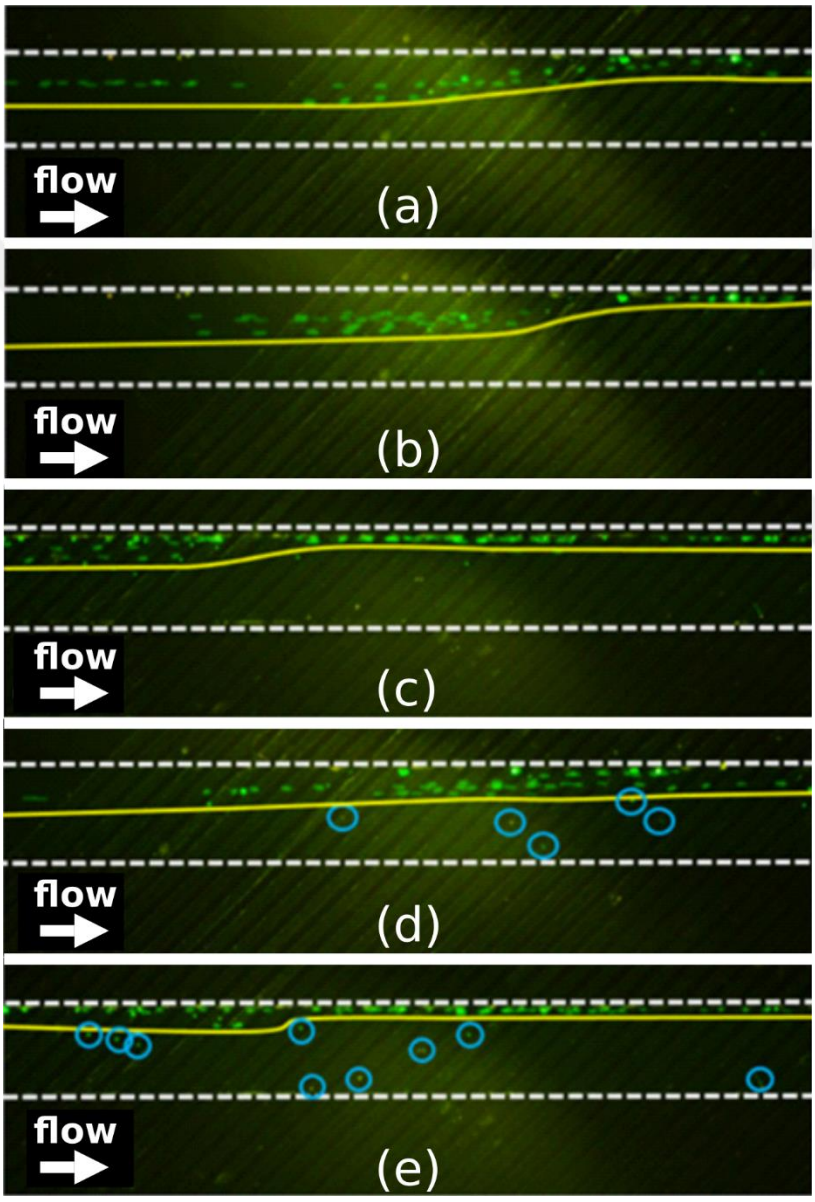

Figure 3.17 : Experimental results for Jurkat cells. The enrichment of cells is expressed with yellow line and the microchannel sidewalls are expressed with white dash a–c Cells with larger diameters are focused on one side of the microchannel along microelectrode geometry d, e Cells with smaller diameter (expressed with blue circle) are not affected by a dominant dielectrophoretic force

4. IMPEDANCE ANALYSIS

Impedance measurements at stations where cells were individually captured before and after cell entrapment are recorded. Experimental results are divided into cases where the conductivity of the medium is higher and lower than the cell conductance. Overall magnitude of impedance shift is significantly higher when the medium conductivity is lower than the cell condunctance. When all results are evaluated, it can be seen that depending on the target cell type, an optimum medium conductivity and frequency range can be selected so as to obtain the measurement result with the highest sensitivity.

4.1 Design and Simulations

By placing simple obstacles in the microchannel, it is also possible to capture individual cells / particles. In Jang's study (Jang et al., 2007), cells are caught between three obstacles placed in the microchannel center. As shown in Figure 4.1 (a), impedance measurement is also provided with electrodes placed just below the area where the cell is captured. When the fluid velocity profile of this design is examined, it is seen that Figure 4.1 (b) can follow the general flow profile of the particle and escape from the side lanes. In this study, the capture rate of the particle is given as 10%. In our study, a similar approach was produced in Figure 4.1 (c). Instead of three obstacles in Wang's work, the aim was to capture the cell in the center of two cylindrical obstacles. Although the capture yields were similar in our experimental results, too many air bubbles were observed among the obstacles that were not mentioned in Wang's publication. At low flow rates it was observed that the particles could not be captured in any way but at 10µl/min and above, the particle was caught between the obstacles. In this flow, however, the cells easily evade (stretch) and escape from the capture zone after a short time. Although this design has a very simple production method, it has not been preferred in our study due to its low efficiency.

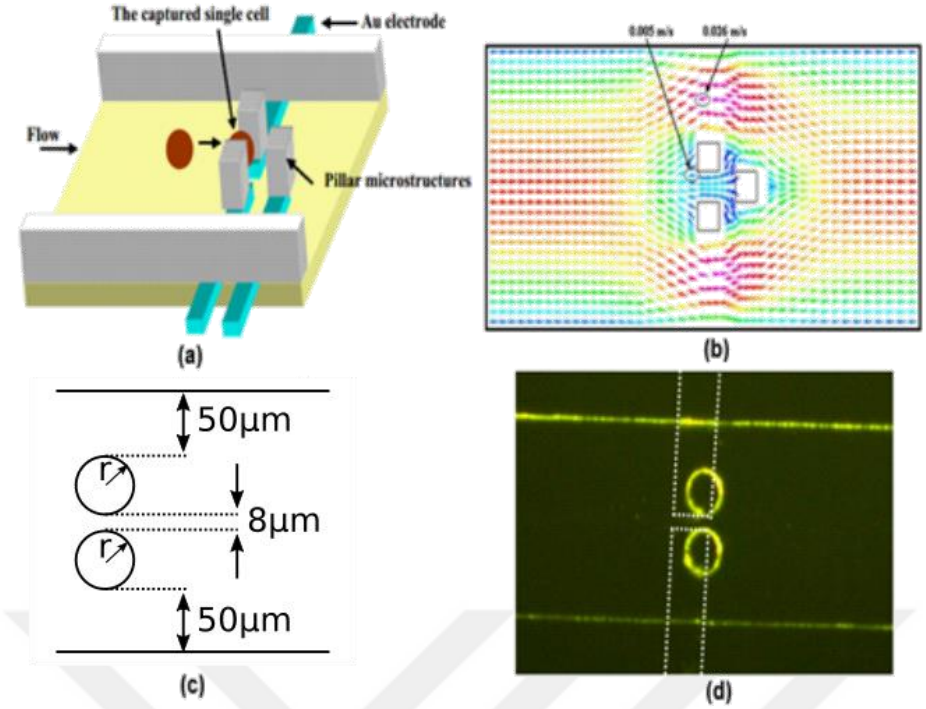

Figure 4.1 : a) Schematic drawing of the design in Wang's work; and b) fluid velocity profile. c) The geometric information of our design based on Wang's work, r = 50µm and d) the actual image of the system produced. A pair of electrodes placed under the obstacles is highlighted by dashed white lines.

Our simulations to improve the design are shown in Figure 4.2 with detailed geometric information. First, the obstacles placed in the microchannel, as shown in Figure 4.2(a), were extended to the outer edges and the fluid velocities divided into three lanes in this region were desired to be equalized. In order to decrease the flow pressure in the middle lane, the obstacle placed in the center were reduced further (Figure 4.2(b)) and the flow rate in the middle lane was increased. The fluid velocity profile obtained in the last case is more homogeneous in all three lanes than Wang's study. Thus, 10% capture efficiency is expected to increase to 30%.

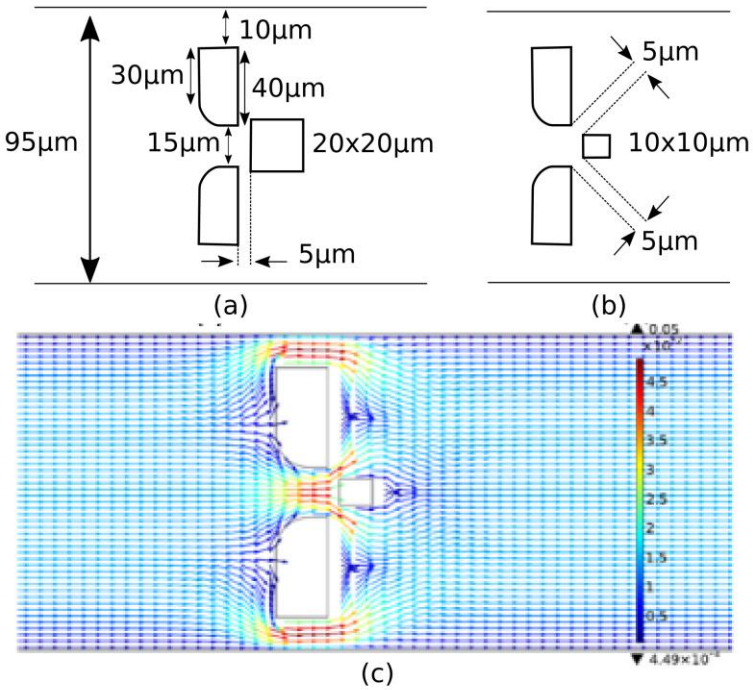

Figure 4.2 : Efforts to improve Wang's design a) An attempt was made to balance the flow profile by extending the obstacles in the middle of the microchannel towards the outer walls. b) The pressure in the middle lane is reduced by minimizing the obstacle placed in the center to the minimum possible size. c) Simulation output of the developed design. It is seen that the fluid velocities in the middle and outer lanes converge.

The design is not preferred in the final product because it is intended to capture a very small number of cells per unit area for single cell capture and is not foreseen to increase the yield above 30%.

Another example is the design in which Tan and Takeuchi (Tan et al., 2007) captures a single cell independent of fluid velocity. In the design of Figure 4.3, the microchannel geometry is expressed as path 1 (Path 1) in which the cell / particle is captured and path 2 (Path 2) in which it continues without being captured. When the flow rate Q1 of path 1 is greater than the flow rate Q2 of path 2, the cell/particle is captured in the reservoir in the path 1 and blocks this path. Thus, as Q1 falls to zero, the next cell/particle prefers path 2, successive capture of a large number of cells/particles is achieved with high efficiency. The critical factor in this design is that the microchannel width is at most 1.5 times larger than the targeted cell/particle size and as the length of path 2 is extended, the probability of trapping cells/particles increases in the path 1 (Tan, 2007).

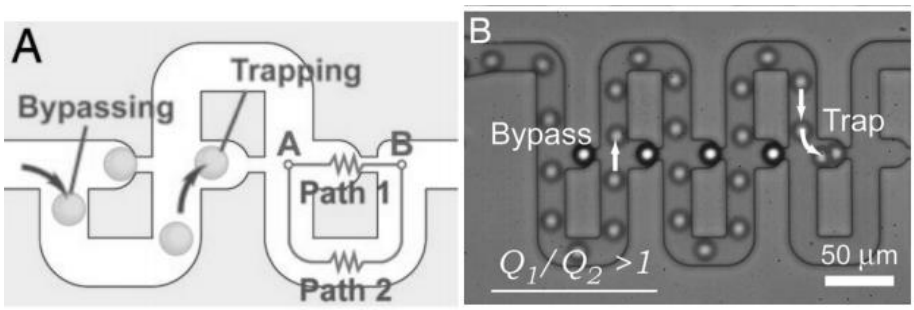

Figure 4.3 : Takeuchi's design for single-cell capture. A) After capturing single cells in path 1, it is ensured that other cells are sequentially captured individually by following path 2. B) The flow rate of path 1 should be greater than path 2 as a condition for single cell capture (Tan, 2007).

In this study, we aimed to develop this design. With the infrastructure we have, a design that can be produced and which yields high efficiency is studied. The following section includes simulations to improve design.

In the design of Tan and Takeuchi, there is a 5x5µm passage channel after the reservoir on path 1, but in our study, SU-8 was further extended as shown in Figure 4.4 (a, b) in order to facilitate the production of the narrow neck on path 1 with the infrastructure we have. It is aimed that the developer can better penetrate this part of the mold. When the simulation output in Figure 4.4 (c) is examined, it is seen that single cell capture is possible with this design as the flow rate in path 1 is higher.

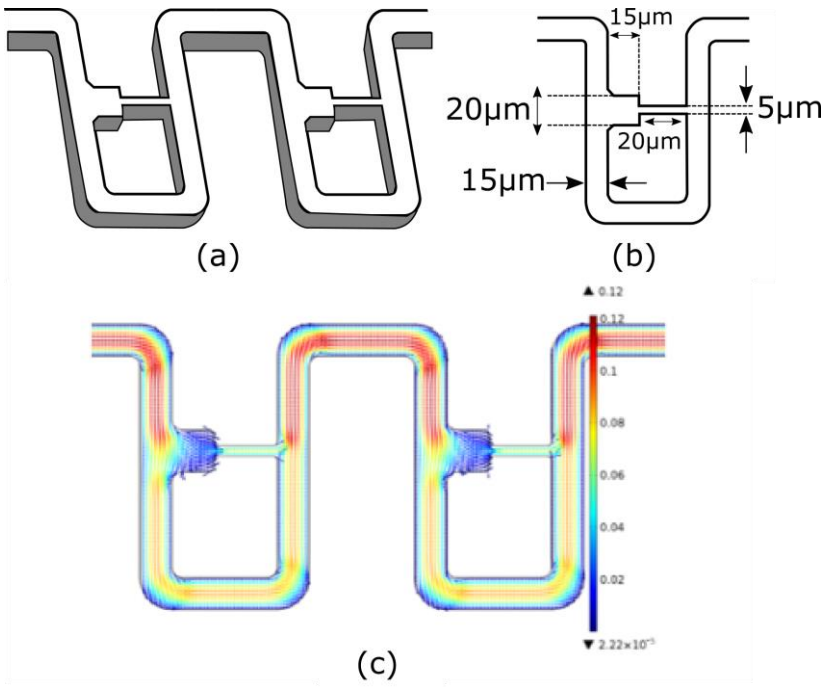

Figure 4.4 : The length of narrow neck on path 1 of Takeuchi's design is extended to better penetrate the SU-8 developer and to produce the desired geometry. a) Three-dimensional overview b) geometric information of the design c) Simulation output of the design.

We have approached 3-dimensional microchannel geometry to reduce the pressure in path 1. Instead of the narrow neck at the end of the chamber, an outlet of the same width as the chamber is formed, but the height of this path is reduced. The microchannel height is limited to 5μm to create a narrow neck and the height is 20μm in all other regions. Figure 4.5 (a, b) shows the geometric information of the system designed. Examining Fig. 4.5 (c), the flow profile obtained with this design is most suitable for single cell capture of the designs studied so far. Further, extending the path 2 to increase the yield for single cell / particle capture in path 1 also contributes as shown in Figure 4.5 (c). Increasing the width of the bottleneck after the reservoir and extending the length of path 2 made the design more favorable with the infrastructure we have and the geometric sharpness.

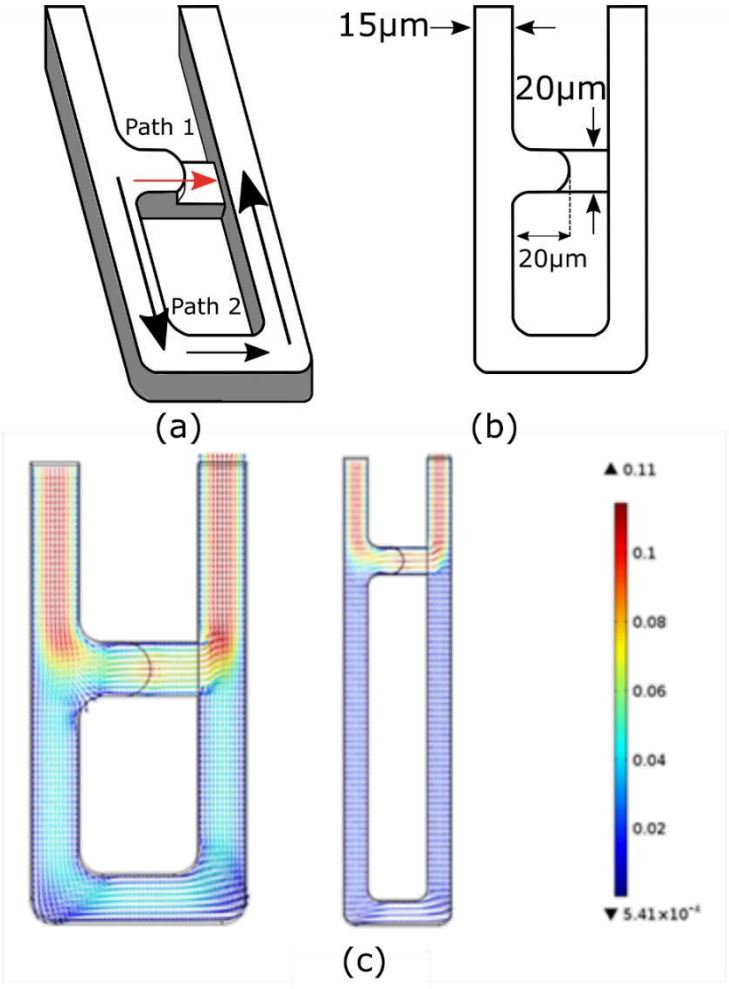

Figure 4.5 : A 3D approach to Takeuchi's design. a) The narrow neck width after the reservoir is increased but the height is limited to 5μm. Microchannel height is 20μm on all other surfaces. b) geometric information of the design c) simulation output of the design: It is seen that the cell / particle will be captured in high efficiency in path 1. By extending the length of path 2, the capture efficiency increases.

The effect of a triangular chamber placed on the path 1 to flow rate and capture efficiency was also investigated. Triangles with three different base angles were studied and detailed geometric information is given in Figure 4.6 (a, b). In this design, if a cell is already caught in the reservoir, the next cell is intended to be swept by flow and directed to path 2. Thus, it was aimed to prevent the capture of more than one cell at a trap-site. Similar to the flow profile of other designs, it is also possible to see in Fig. 4.6 (c, d) that it is possible to capture particle / cell in path 1 with this design.

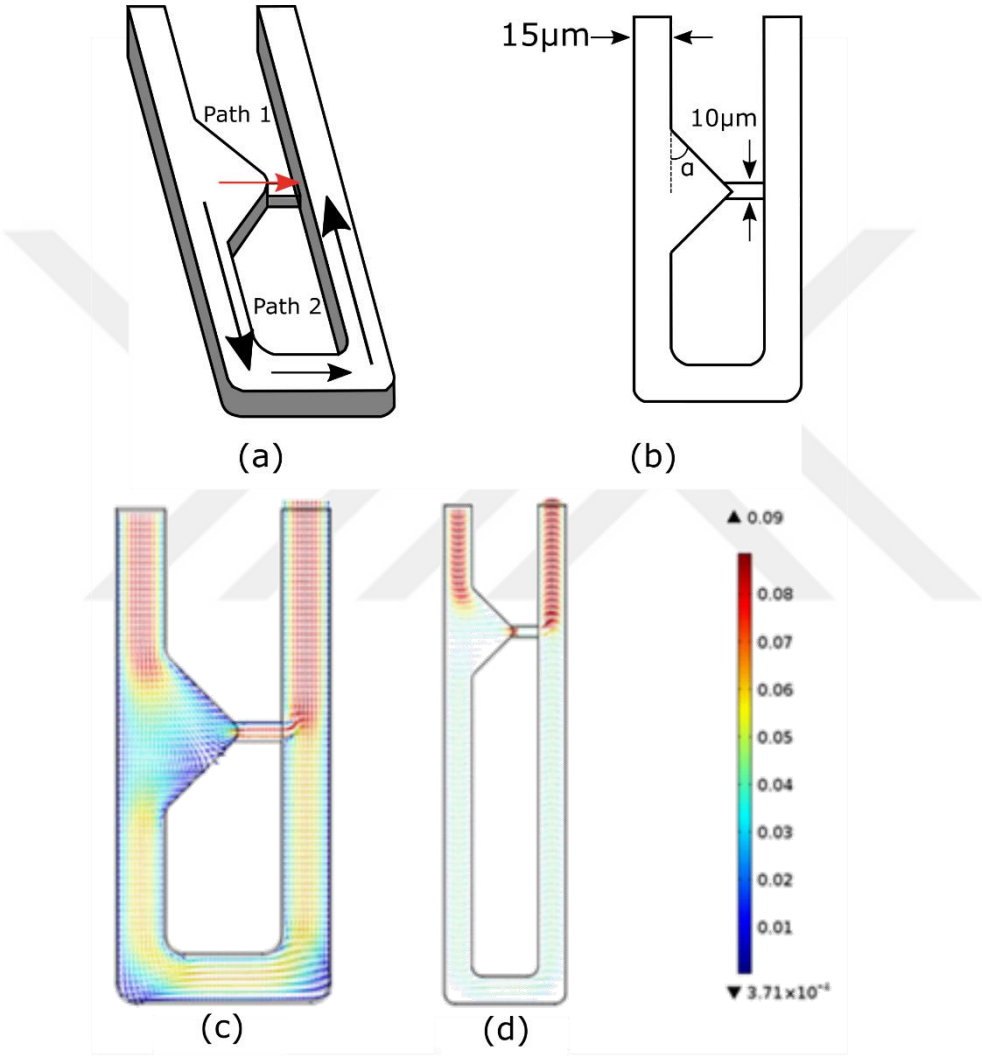

Figure 4.6 : (a) Triangular chamber placed in path 1 b) Flow was examined using three different base angles (α = 30 °, 45 °, 60 °). c) unchanged path 2 for α = 45 °; and d) examination of flow by extended length of path 2.

In order to increase the efficiency of single cell / particle capture, the effect of stepwise geometries in the chamber geometries as in Figure 4.7 was investigated. With these designs, it is aimed to capture the cell singularly and to remove a second cell which may come from the main stream lane by sweeping the flow under a wider angle. This

design is preferred for the capture region in the final product, as it allows individual cells to be captured individually.

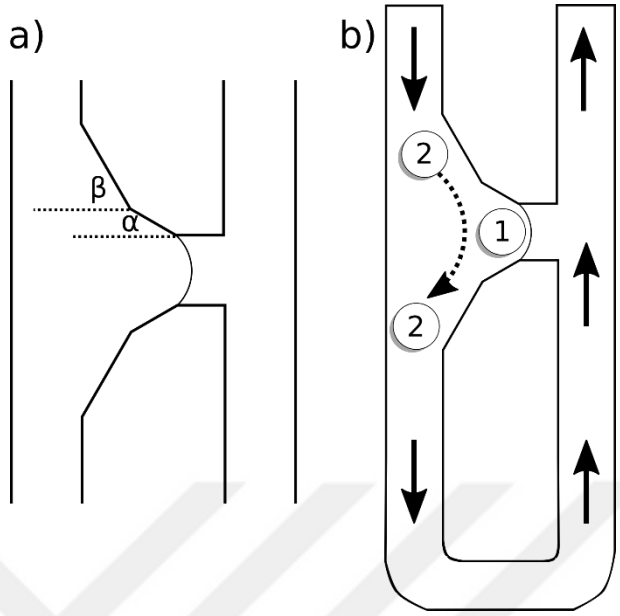

Figure 4.7 : Trapping of more than one cell in the triangular region with a stepped angle (α <β) was prevented. After cell number 1 has been captured, following cell (number 2) is dragged under the main stream to the next capture zone.

4.2 Fabrication

Fabrication steps given in detail in section 3.2 is applied for the production of designs presented in this section.

4.3 Experimental

Human colorectal carcinoma cell line (HCT116, ATCC® CCL 247TM), human epithelial embryonic kidney cell line (HEK-293, ATCC® CRL-1573 ™), human epithelial adenocarcinoma cell line (HeLa 229, ATCC® CCL-2.1 ™) human breast cancer cell line (MDA-MB-231; ATCC® HTB-26 ™), human chronic myelogenic lymphoblast K-562 (ATCC® CCL-243 ™); and human B lymphoblast HCC1143 BL (ATCC® CRL2362 ™) cell lines were used.

HCT116, HEK-293, HeLa 229 and MDA-MB-231 are adherent cells. K-562 and HCC1143 BL are suspension cells. Cells were cultured in McCoy's 5a Medium Modified (HCT116), Eagle's Minimum Essential Medium (HEK-293 and HeLa 229), RPMI-1640 (HCC1143 BL), DMEM-F12 (MDA-MB-231), and Iscove's Modified Dulbecco's Medium (K-562) containing 10% FCS and 1% glutamine. Cells were incubated in 75cm^2 flasks and 5% CO_2 atmosphere at 37˚C. The cultured suspension

cells, K562 and HCC1143 BL, were collected by centrifugation at 12000 rpm for 5 minutes. Cell counts were made with a Thoma slide. Cells were frozen in FCS containing 10% DMSO at a concentration of 250,000 cells / ml. HCT116, HEK-293, HeLa 229 and MDA-MB-231 cells were resuspended with 2ml of Trypsin-EDTA solution when the flask surface coated 80% and collected by centrifugation at 12000 rpm for 5 minutes. Cells were maintained in liquid nitrogen until working day. The cells to be studied were collected by centrifugation at 1200 rpm for 5 minutes and the experiments were carried out with 200mM sucrose solutions whose conductivity was controlled by PBS concentration.

As a result of the simulations made on many different designs, it was decided to fabricate systems with 3-dimensional channel geometry. Experiments were made between 1-50µl/min flow rates and polystyrene particles (9.8µm) were captured independently from the flow rate in trap-sites. In the experiments with the designs presented in Figures 4.5 and 4.6, particles captured in trap-sites are shown in Figure 4.8. Since it was seen that more than one particle was caught in some of the trap-sites, these designs were improved.

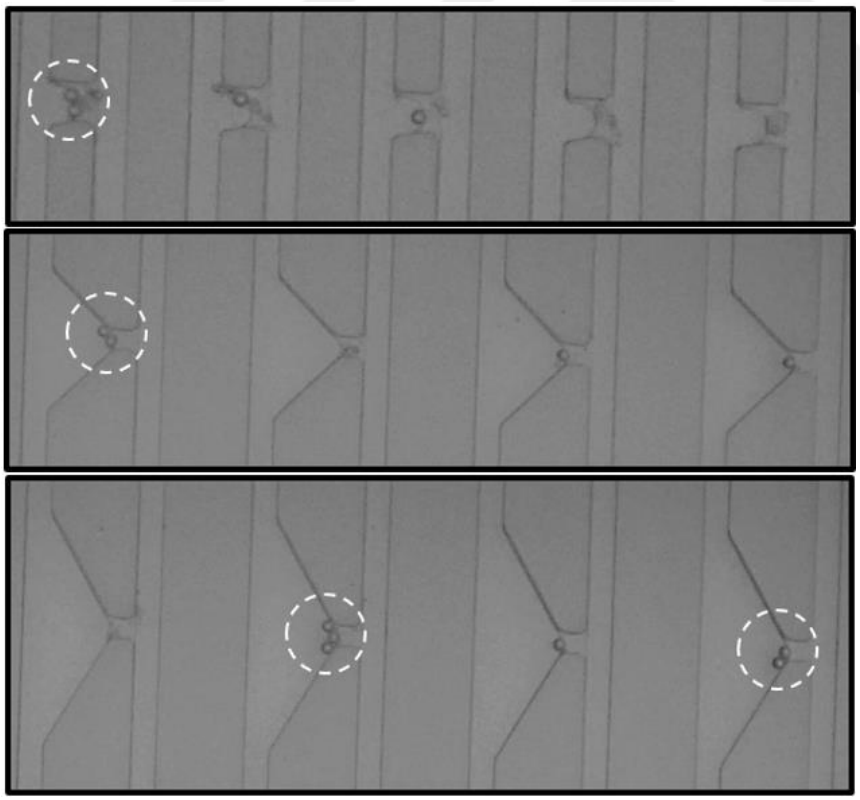

Figure 4.8 : The preliminary designs fabricated for the analysis zone. At a flow rate of 3µl/min, particles of 9.8µm diameter were captured in trap-sites. These designs have been improved since some of the sites seem to capture multiple particles.

In all designs for the analysis zone, individual cell capture can be achieved by updating the channel sizes depending on the targeted particle size. When the particle settles in the narrow neck region, it must be large enough to block the path and reduce the flow to zero in the chamber. Otherwise, if the flow continues, it is possible to capture more than one particle in the chamber as in the experimental results. In our research, an original and alternative design was tried to solve this situation. It is aimed to capture the cell singularly and to remove a second cell which may come from the main stream lane by sweeping the flow under a wider angle.

Microchannel geometry having gradual angle (α1 = 30 °, β1 = 45 °), 9.8 µm polystyrene particles in DI water were captured in 10 wells and impedance deviations were recorded with Agilent 4980A LCR meter (100Hz - 500KHz). The impedance values recorded for DI water and after capture of polystyrene particles, depending on the applied frequencies, are shown in Figure 4.9.

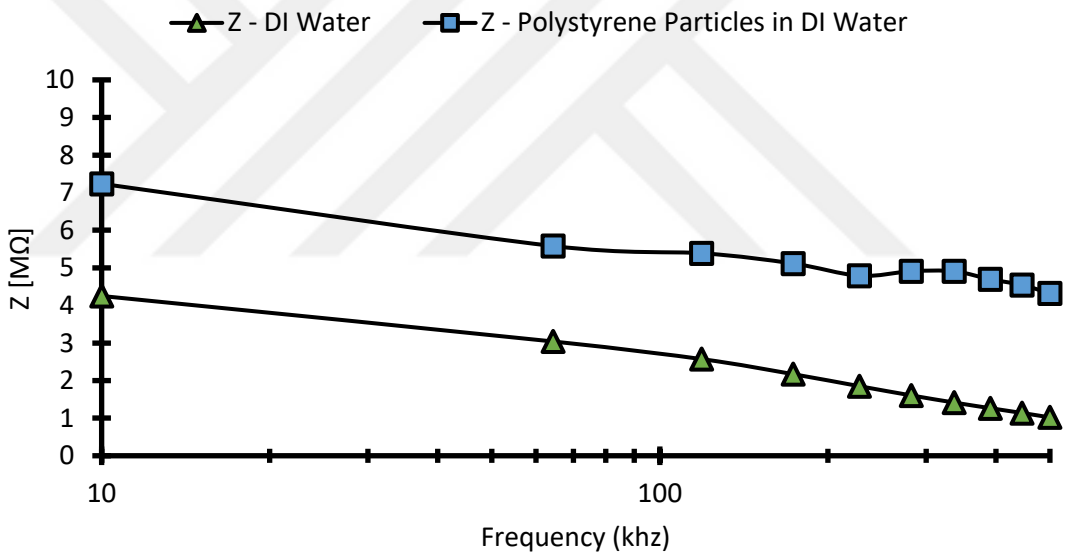

Figure 4.9 : Impedance values of polystyrene particles in DI water in the frequency range 10-500kHz.

The individual capture of live cells and the impedance measurements were also studied experimentally. Experimental results for MDA-MB-231 (breast cancer epithelial cells), HCT116 (colon cancer cell), HeLa (cervical cancer cells), HEK293 (renal epithelial cells), K562 (cancerous lymphocyte cells) and CLR (non-cancerous lymphocyte cells) were obtained. In these experiments with designs of stepped triangular trap-sites, the impedance values were recorded depending on the conductivity of the medium in which the cells were added. Thus, the effect of solution conductivity on impedance values were investigated. Table 4.1 shows the medium conductivities used in the experimental studies. The 200mM sucrose solution was

preferred as the isotonic solution for maintaining the osmotic pressure balance of the cells. The solution conductivity was increased in a controlled manner with the amount of PBS added.

Table 4.1 : Medium conductivities used in experimental studies.

Medium	DI Water	200mM Sucrose	0.05XPBS Sucrose + 5% PBS (v/v)	0.1XPBS Sucrose + 10% PBS (v/v)	1XPBS 100% PBS (v/v)
Conductivity	0.80µS/cm	1,47µS/cm	1015µS/cm	1869.00µS/cm	15.70mS/cm

Figure 4.10 shows that HCT116 (colon cancer cell) cells in PBS are captured individually in a microchannel with a stepped angle (α1 = 30°, β1 = 45°) triangular trap-sites. Other geometries with different step angles (α1 = 30°, β1 = 60° and α1 = 45°, β1 = 60°) were also studied and observed that single cell capture was achieved in trap-sites. Cells were captured individually in all sites, while in two sites highlighted in red, the cells have no contact with the electrodes. The impedance readings for PBS were monitored for 10 minutes before the cells were injected into the microchannel and no deviation was observed during that time. Impedance values were re-recorded after the cells were injected and stations were filled.

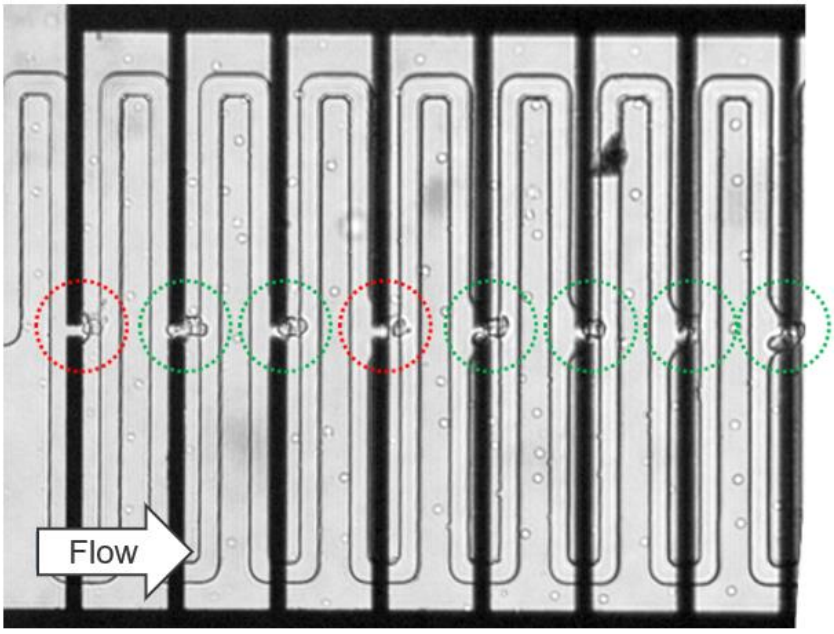

Figure 4.10 : Individual capture of HCT116 cells in PBS in a microchannel with a stepped angle (α1 = 30 °, β1 = 45 °) triangular trap-sites. The cells in the sites highlighted in red are not in contact with the microelectrodes.

Impedance data of HCT116 cells in 1XPBS and 0.1XPBS were recorded in the frequency range 1-500kHz, before and after capturing the cells at the stations. The impedance shift for HCT116 cells is shown in Figure 4.11.

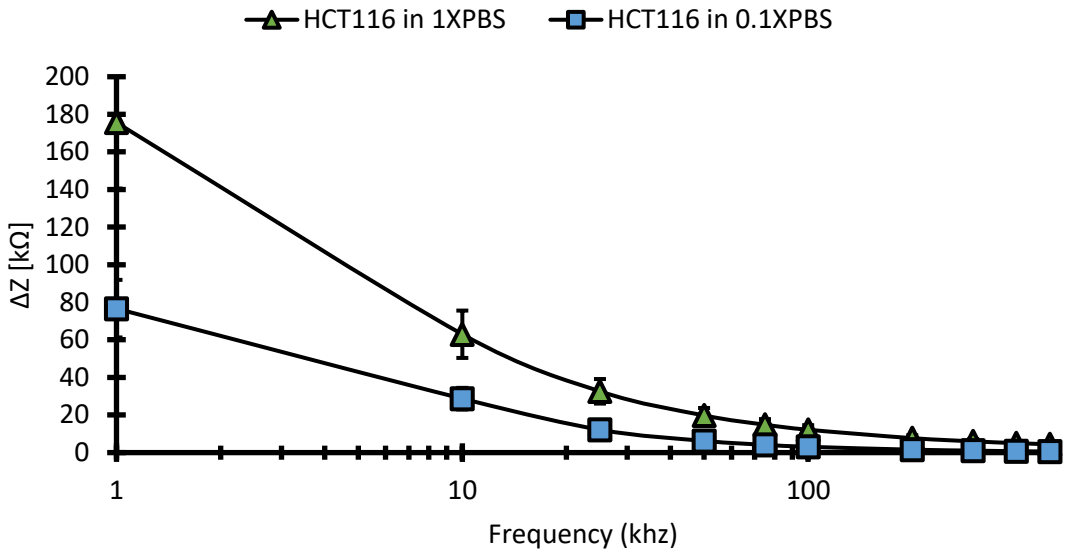

Figure 4.11 : Frequency-dependent impedance deviation (ΔZ) of HCT116 cells in 1XPBS and 0.1XPBS.

In experimental studies with MDA-MB-231 cells, cells could be captured individually and their impedance values were recorded. Figure 4.12 shows that individual breast cancer cells are caught in all trap sites.

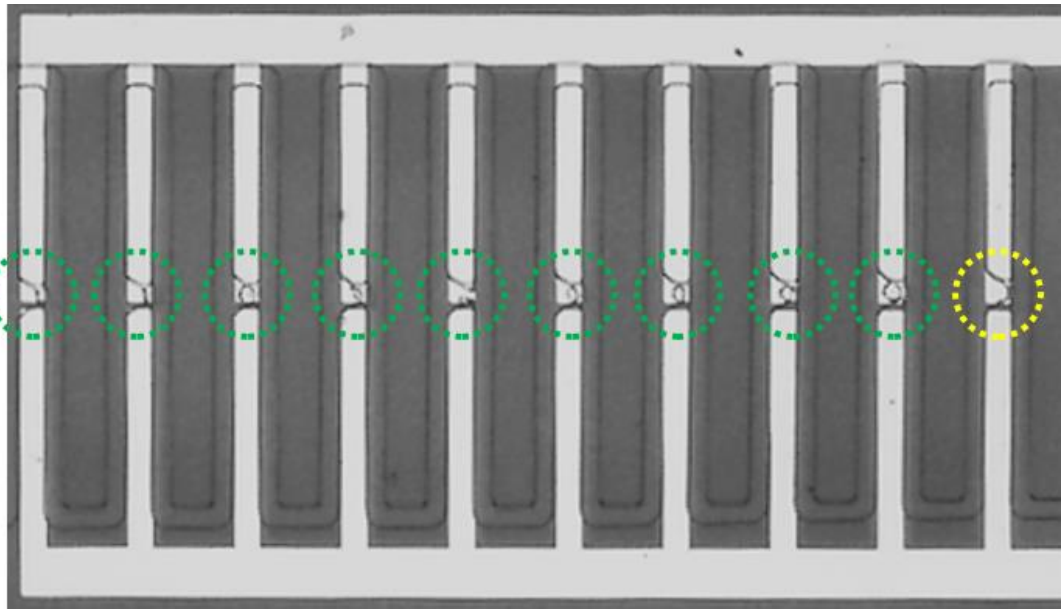

Figure 4.12 : MDA-MB-231 cells were individually captured at trap-sites. The cell is not in contact with the microelectrodes in the site highlighted in yellow.

Figure 4.13 shows the impedance deviations of breast cancer cells in 1XPBS and 0.1XPBS solutions.

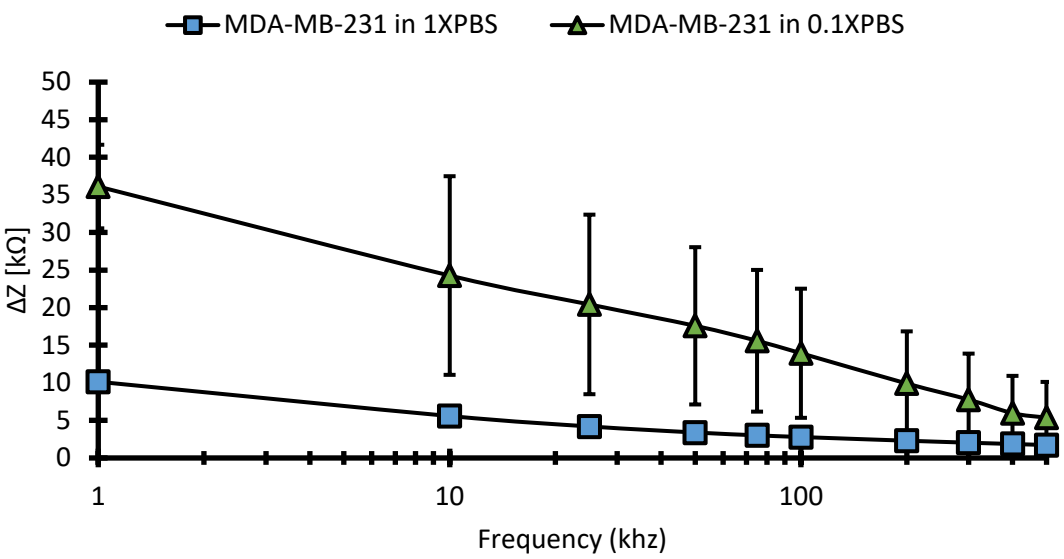

Figure 4.13 : Frequency-dependent impedance deviation (ΔZ) of MDA-MB-231 cells in 1XPBS and 0.1XPBS.

Similarly, in repeated experiments, HEK293 cells were individually captured and the impedance deviations in 1XPBS and 0.1XPBS solutions are given in Figure 4.14.

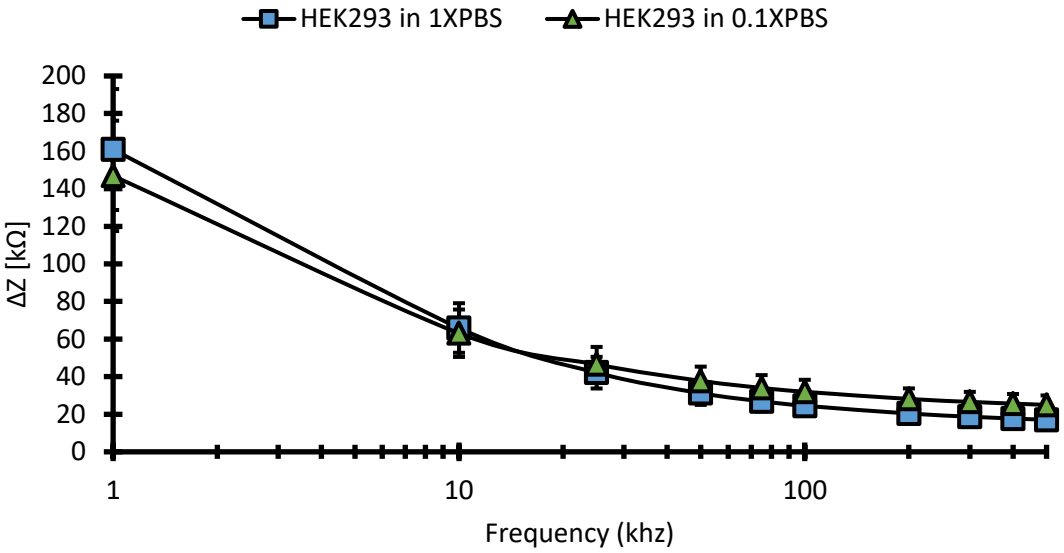

Figure 4.14 : Frequency-dependent impedance deviation (ΔZ) of HEK293 cells in 1XPBS and 0.1XPBS.

When cells are in contact with microelectrodes, a shift in impedance is observed depending on cell characteristics. Following the data of HeLa cells recorded in 1XPBS solution, the impedance values obtained in Figure 4.12, 4.13 and 4.14 are presented

together in Figure 4.15 and 4.16. According to these data, impedance shifts vary depending on the conductivity of the medium and cell type. The impedance deviation of each cell type is characteristic and the optimum solution conductivity and frequency range can be determined for identification of the target cell.

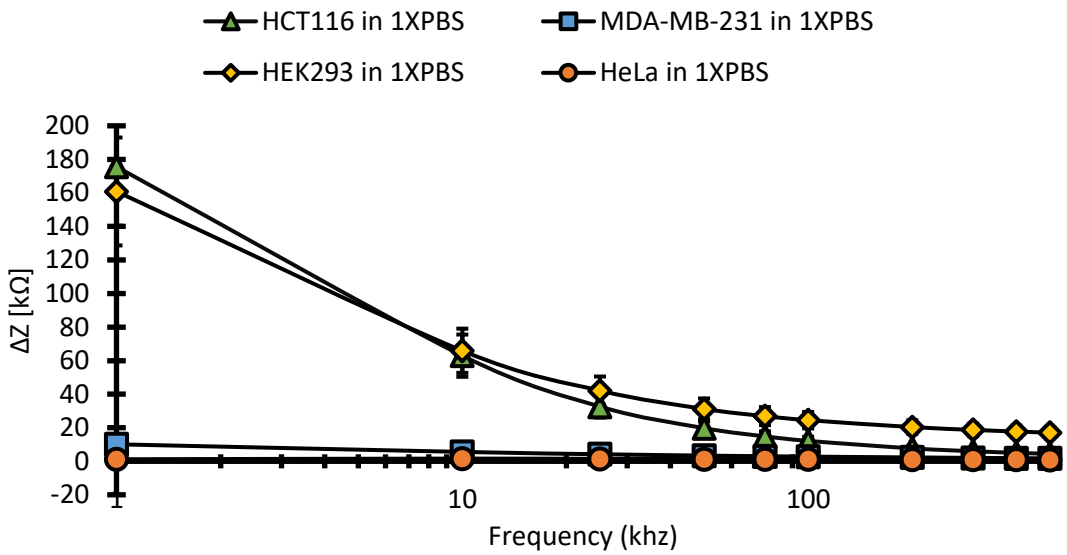

Figure 4.15 : Frequency-dependent impedance deviation (ΔZ) of various cells in 1XPBS solution.

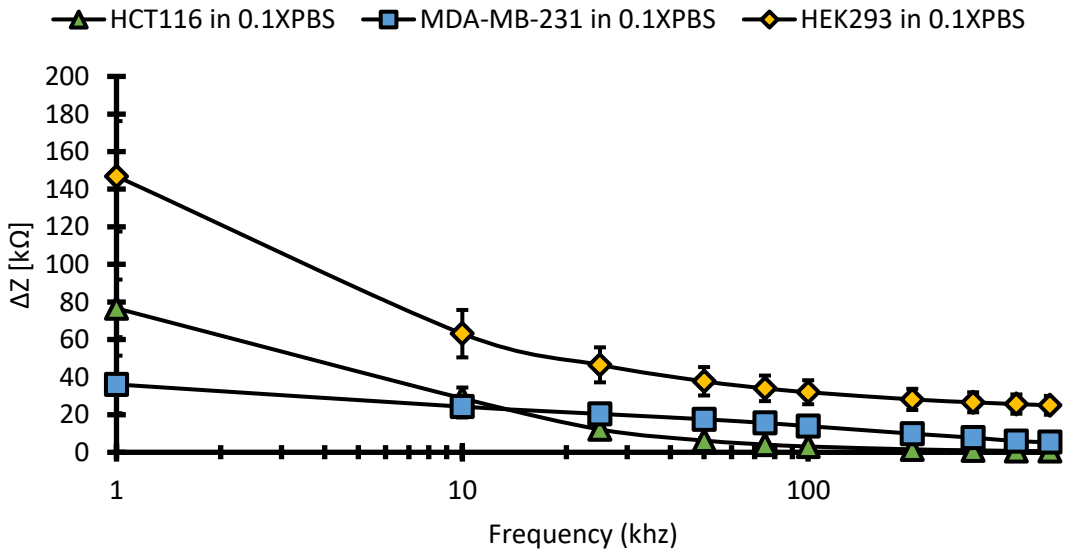

Figure 4.16: Frequency-dependent impedance deviation (ΔZ) of various cells in 0.1XPBS solution.

Impedance deviation for HCT116 cells decreases as solution conductivity decreases, while the impedance deviation obtained for MDA-MB-231 cells increases with solution conductivity. HEK293 cells showed similar impedance deviation at the two solution conductivity levels studied. When cell types are compared with each other, HCT116

and HEK293 cell lines produce similar impedance deviations in 1XPBS solution, while a distinct difference in impedance deviations with a low conductivity of 0.1XPBS occurs.

When the samples are examined in the literature, the signal strength, frequency range and solution conductivity applied when recording the impedance data from the cell placed between the two electrodes should be determined correctly in order to understand the deviation in the impedance. In the impedance data recorded at low signal strength, the noise is high, increasing the signal strength, decreases the impedance values taken from the cell, but the ion exchange between the isotonic solution and the cell increases and information is collected directly from the cell. Similarly, since the interaction of solution conductivity and cell conductivity with each other determines the direction of the electric field lines, collecting information inside or outside the cell can be accomplished by controlling the conductivity of the solution. If the cell has a higher conductivity than the solution, the electric field lines pass through the cell while the solution is more conductive than the cell, the electric field lines pass outside the cell. This is also observed with the direction of the impedance deviation after cell capture. In the experimental results presented above, the selected solution conductivity is higher than the cell conductivity and the impedance deviation is positive after cell capture. As the frequency increases, the amount of impedance deviation decreases, indicating that the cells are capacitive in this frequency range. In order to gather more accurate information about the cell, the solution conductivity was chosen to be lower than the cell conductivity and experimental studies were continued.

Experiments were performed with MDA-MB-231, K562 and CLR cells in 200mM sucrose solution. The results obtained in the frequency range of 100Hz-500kHz and signal strength of $2V_{pp}$ are shown in Figure 4.17.

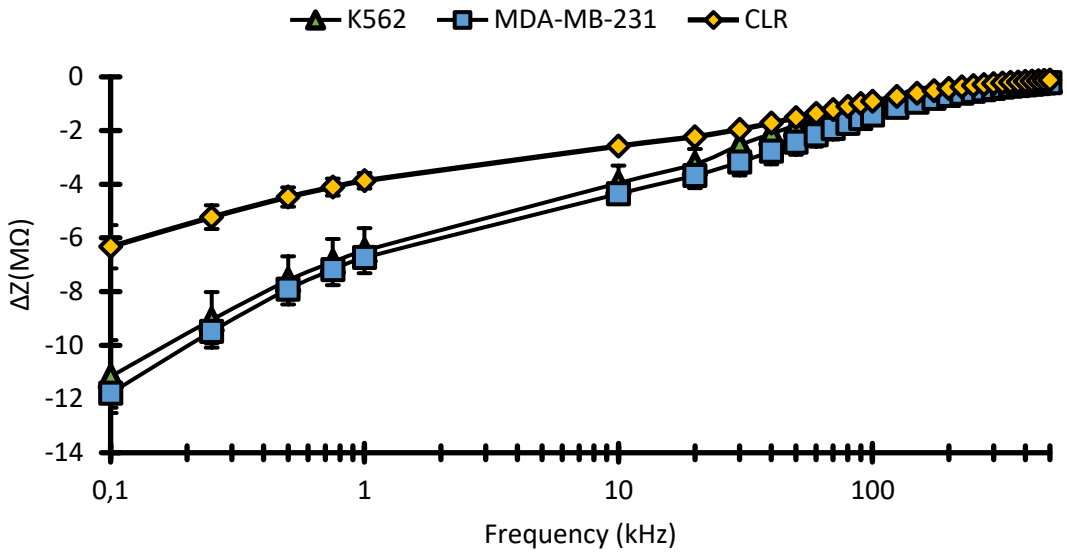

(a)

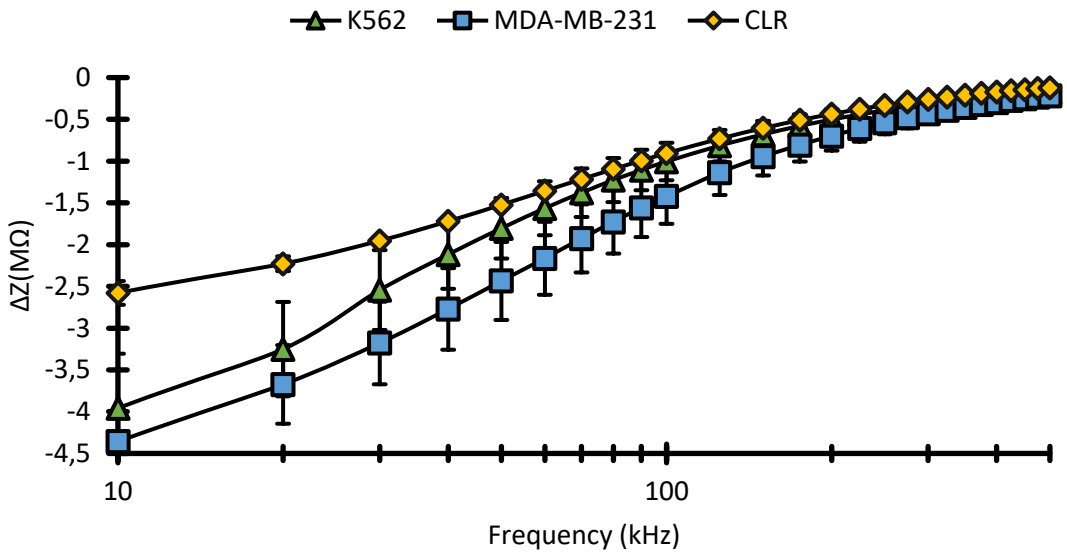

(b)

Figure 4.17 : a) Impedance shifts recorded in the frequency range of 0.1-500kHz for K562, MDA-MB-231 and CLR cells in 200mM sucrose solution. b) More detailed representation of the results for the frequency range 10-500kHz.

When the results in Figure 4.17 are examined, it is seen that there is a distinctive impedance deviation difference between cancerous lymphocyte cells and healthy blood cells. The range in which the produced system has the highest sensitivity to differentiate healthy blood cells is the frequency range of 0.1kHz and 10kHz.

5. DIELECTROPHORESIS AND IMPEDANCE ANALYSIS

The results obtained through the final design combining cell separation and analysis regions are presented in this section.

5.1 Design and Simulations

The final system designed and fabricated is shown in Figure 5.1. Impedance analysis is performed by directing the cell type of interest from the main lane to the channel where the trap-stations are located. Variations were made in the total number of stations where impedance information was recorded simultaneously in the impedance measurement area. While impedance data can be recorded from a total of 20 stations at the same time from a single branch, designs have been produced that can only receive information from a single station with changes in electrode design and station arrangement.

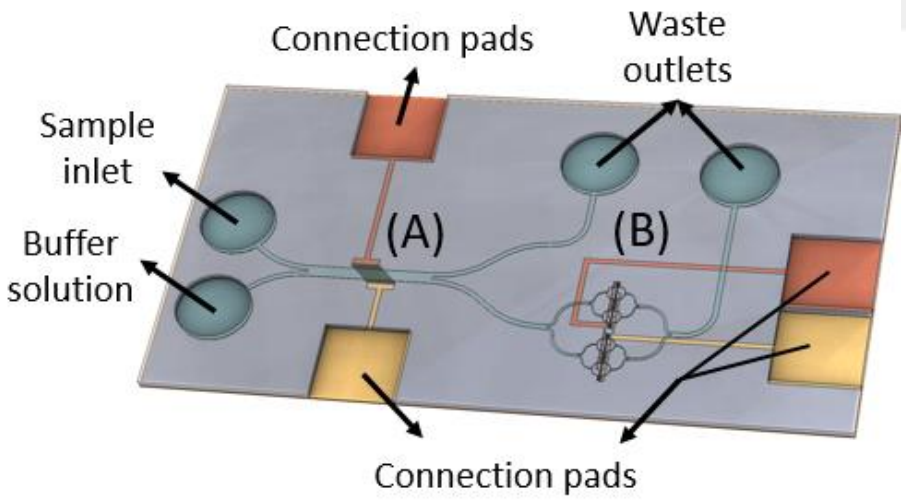

Figure 5.1 : Schematic view of the final design for the separation of the target cell by dielectrophoresis and for individual impedance analysis on trap-sites. A) Separation of target cells under nDEP B) A trap-station for impedance analysis of a captured cell by hydrodynamic methods.

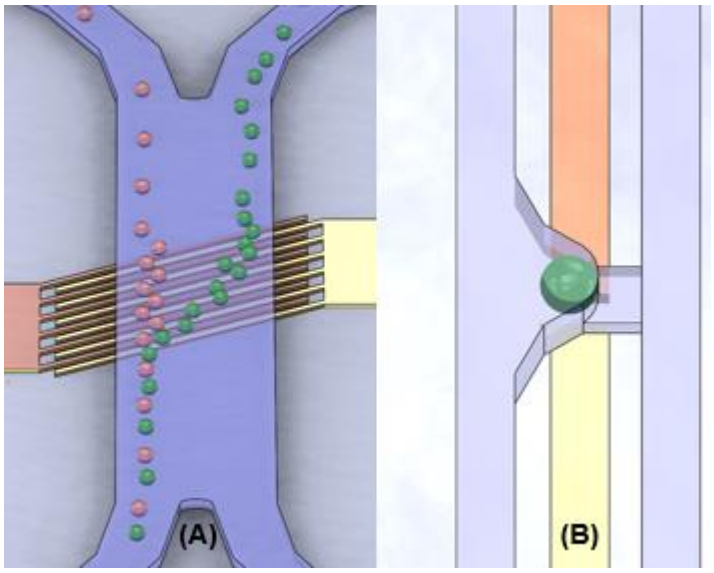

Figure 5.2 (continued) : Schematic view of the final design for the separation of the target cell by dielectrophoresis and for individual impedance analysis on trap-sites. A) Separation of target cells under nDEP B) A trap-station for impedance analysis of a captured cell by hydrodynamic methods.

Microelectrode geometries for each design were fabricated for the impedance measurements of the cells captured in trap-stations. The interdigitated electrode pairs are arranged sequentially and aligned to each trap site. Titanium microelectrodes with a thickness of 200nm are 15μm wide and the gap between the electrode pairs is 8μm.

5.2 Fabrication

Fabrication steps given in detail in section 3.2 is applied for the production of designs presented in this section.

5.3 Experimental

DEP + IA design was fabricated as a single LOC as seen in Figure 5.2 and preliminary experimental studies were made. In this system, there is one sample input and three outputs. After separation with DEP, the cell of interest is directed to the respective outlet to perform IA, while the other two outlets are designed as waste outlets.

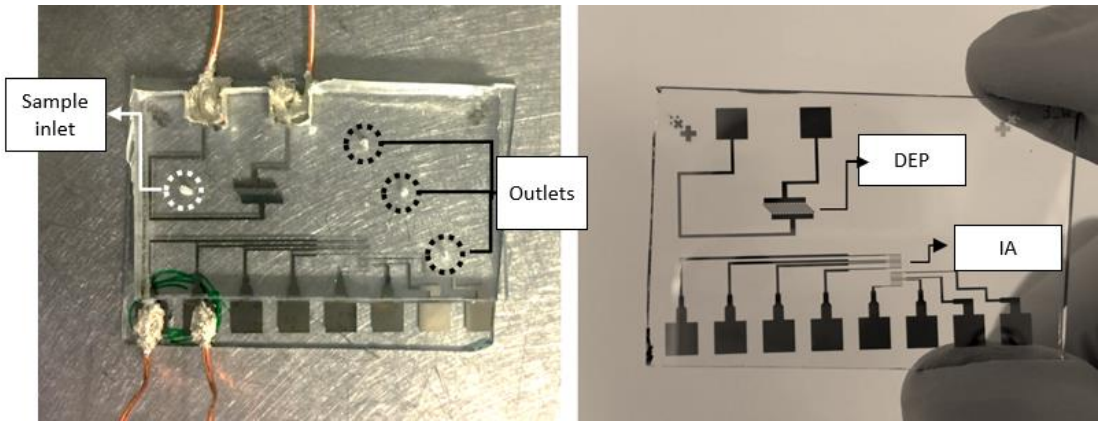

Figure 5.3 : DEP + IA LOC (right) obtained by aligning and bonding Ti microelectrodes (left) fabricated on a glass slide and PDMS microchannels. The microelectrodes are connected to copper cables with epoxy-based silver adhesive.

The preliminary experiments on DEP + IA based on-chip system were carried out with polystyrene particles of two different sizes, 9.8µm (green) and 3.2µm (red). Figure 5.3 shows that particles are directed under the effect of DEP force depending on the on / off state of the signal applied to the microelectrodes. When the signal is switched off, all the particles are collected from all three outlets. Since both particle types have the same dielectric properties, the red particles are also directed by DEP to some extent, and when the signal is on, the red particles can be directed to channel 2. Here it is critical to determine the optimal signal strength and flow rates that can push large particles into channel 3, but keep small particles in channel 1 and 2. In the experimental output in Figure 5.3, the signal applied to the microelectrodes is $6V_{pp}$ - 2MHz and the flow rate is 1µl / min.

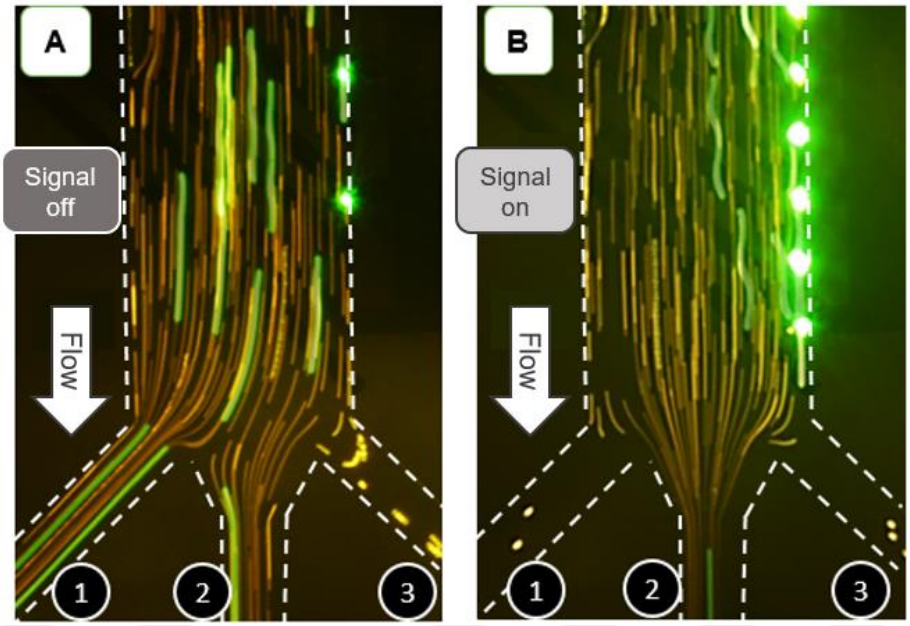

Figure 5.4 : When the signal A) applied to the microelectrodes is closed, the particles leave the channel at all outlets in free state. B) When the signal is turned on, 9.8μm (green) particles are directed to channel 3, while 3.2μm (red) particles are less directed and leave the system from channel 2.

The design improved and the systems produced by equalizing the flow resistances at the waste outlets are given in Figure 5.4. With the variety of electrode connections made in the final product, designs have been produced in which impedance data are recorded from 1,4 or 8 different stations simultaneously.

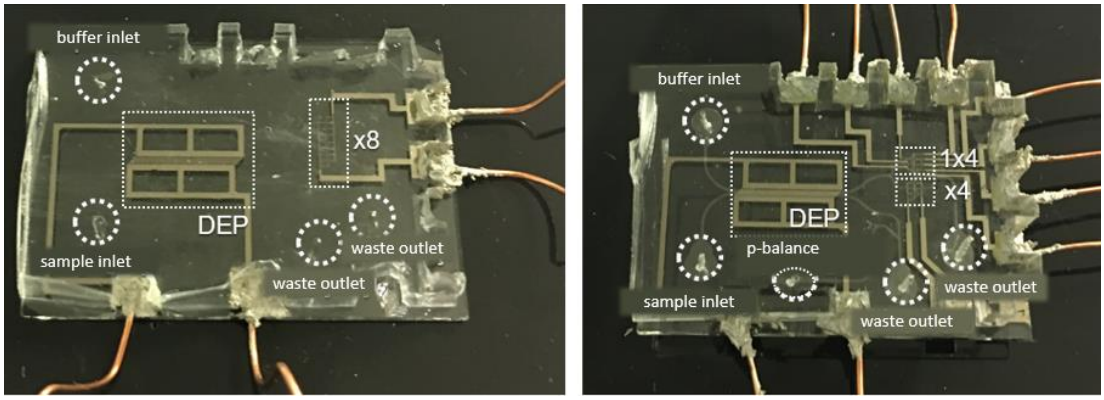

Figure 5.5 : Alternative designs of the final system were produced. Impedance data can be recorded from 8 stations (x8) at the same time, as well as variations that record impedance data from 4 stations (1x4) for recording individual impedance data and 4 stations (4) at the same time.

Experiments with K562 cells were performed on the final system. Following the orientation of K562 cells by DEP, individual capture of the cells at trap sites was performed. Figure 5.5 left side shows that the cells are directed under DEP at the

channel entrance, and on the right, the K562 cells are completely oriented towards the end of the microchannel and aligned by the channel side boundary.

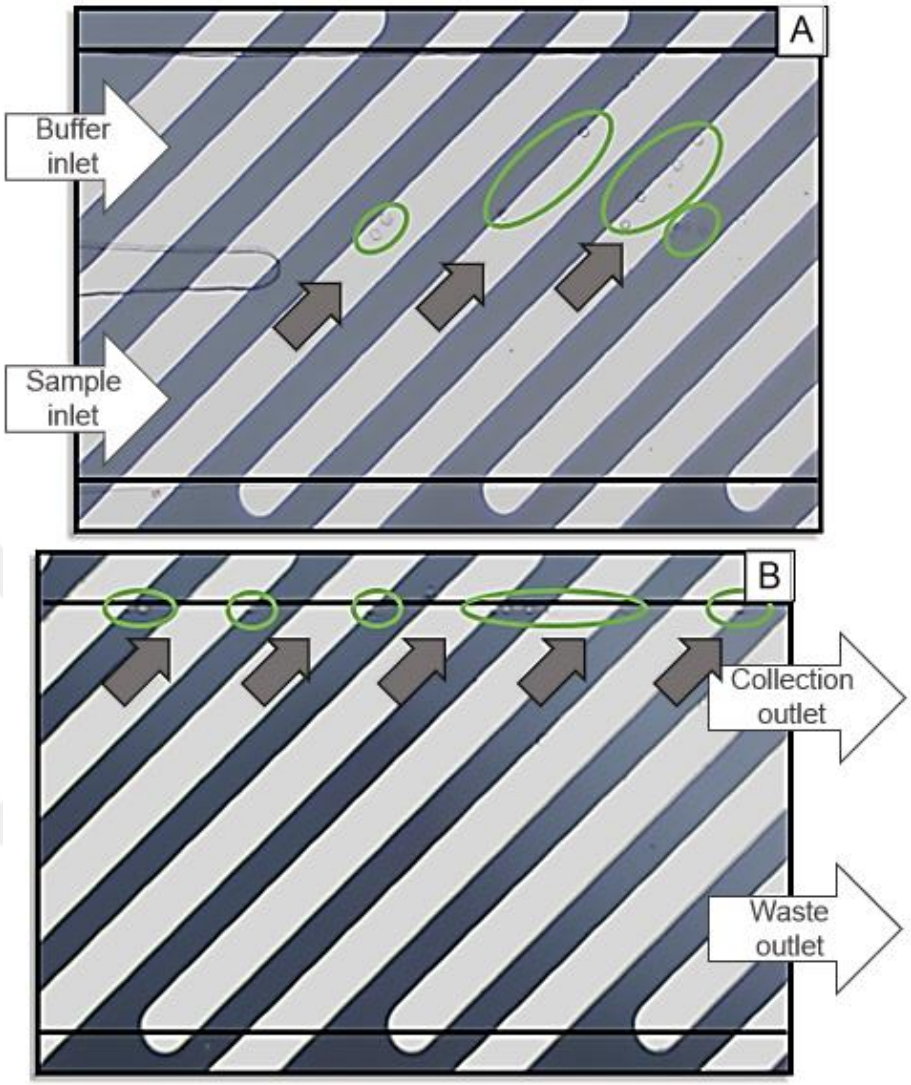

Figure 5.6 : K562 cells under nDEP were directed and collected at trap stations. A) K562 cells at the channel entrance were seen to be directed under nDEP, B) all cells were aligned along the microchannel border towards the end of the channel.

Impedance measurements with two-terminal microelectrodes are particularly sensitive to changes in the electrode-medium interface at low frequency. The equivalent circuit model of the two-terminal system (Figure 5.6) includes a charge transfer resistance, Rct, and a Warburg impedance, W, in parallel with double-layer capacitance, Cdl. In addition, a medium resistance, Rs, and a medium capacity, Cs, reflect the properties of the solution. The four-terminal impedance system is less sensitive to changes in the electrode-medium interface at low frequencies. The equivalent circuit model takes into account the volumetric solution resistance, Rs, solution capacitance, Cs and the parasitic capacitors, Cp, which are related to the

proximity of the electrodes to each other. Specific immobilization of cells or particles between electrodes will create a change in the impedance of the conductive path between the electrodes. In a two-terminal system, at low frequencies, electrode polarization associated with the double-layer capacitance may mask some changes associated with the presence of cells or particles in solution.

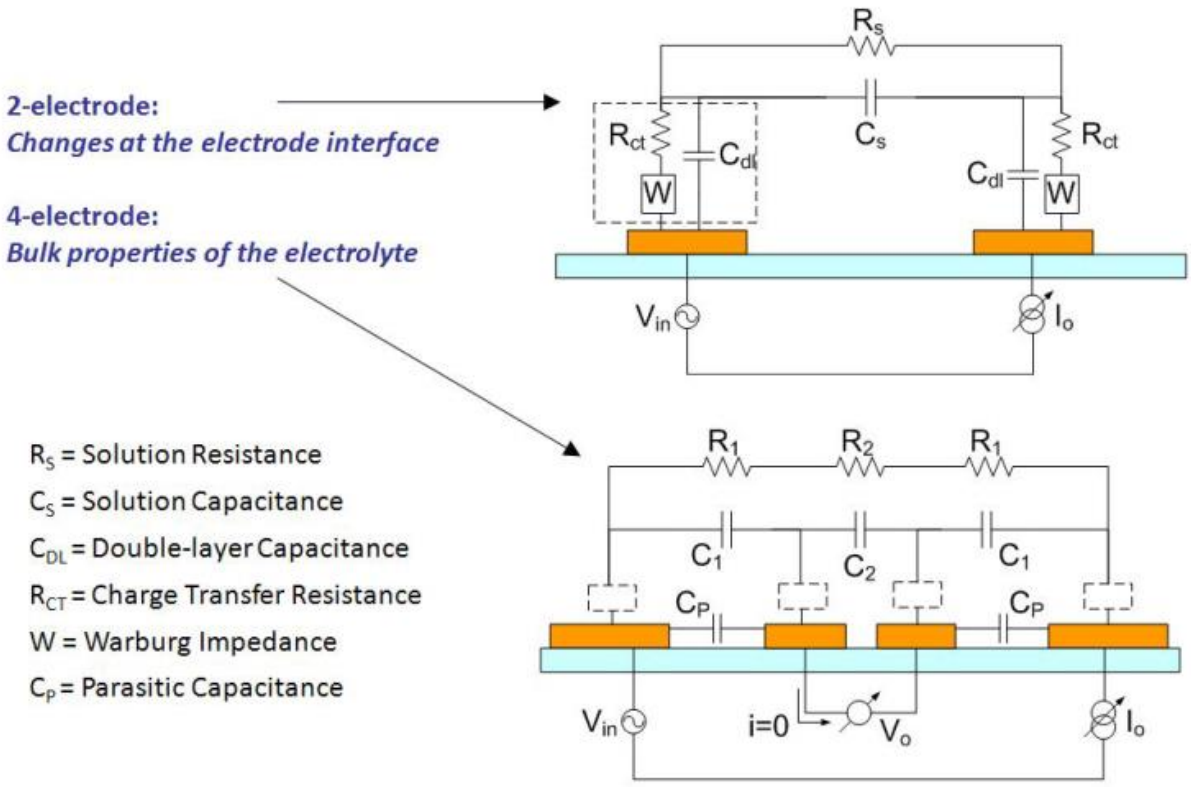

Figure 5.7 : Equivalent circuit models of 2- and 4-terminal configuration for impedance measurements. (Justin, et al 2011)

A schematic view of the four-terminal impedance measurement design for the second region of our system is given in Figures 5.7, 5.8 and 5.9. Current will be applied from external electrodes (Lcur, Hcur) and measurements will be taken from internal electrodes (Lpot, Hpot).

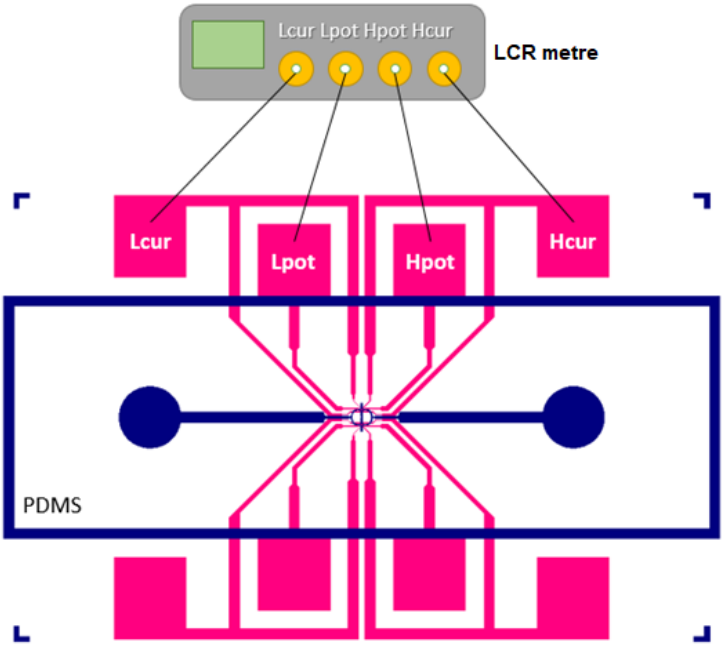

Figure 5.8 : Schematic view of four-terminal impedance measuring system for second region.

Detailed views of the same structure are given in Figures 5.8 and 5.9 below. There are also variations in electrode structures where the signal is collected from two stations at the same time (Figure 5.9, left) or only one station is present (Figure 5.9. right).

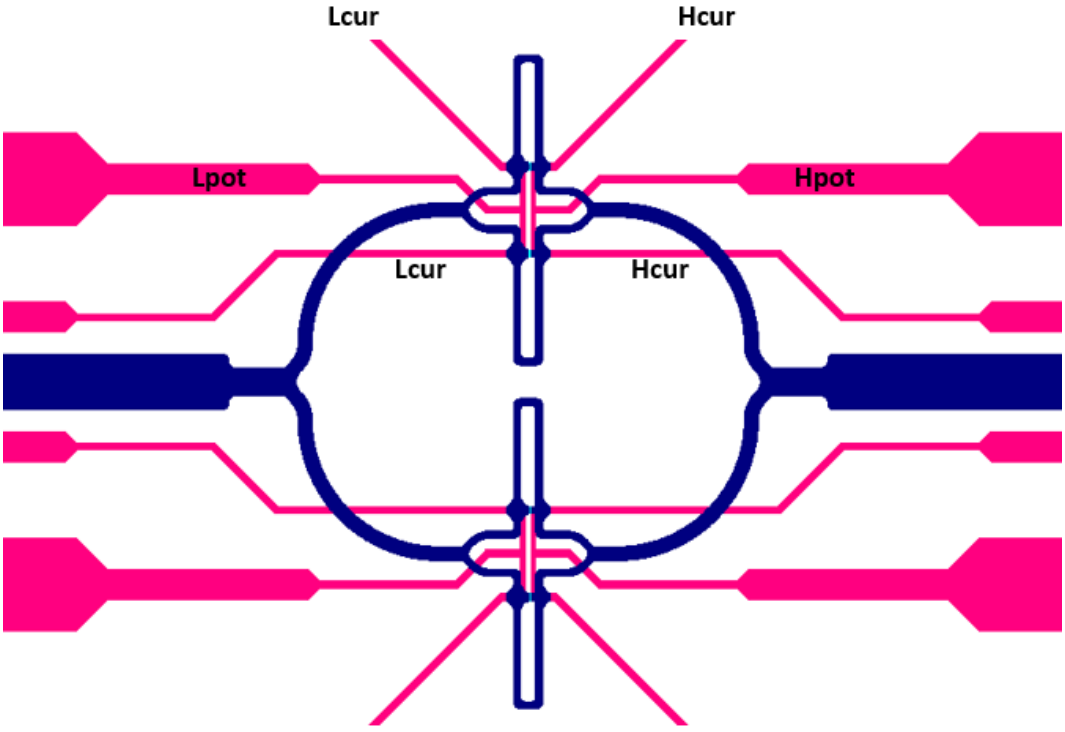

Figure 5.9 : Detailed view of the four-terminal impedance measurement system.

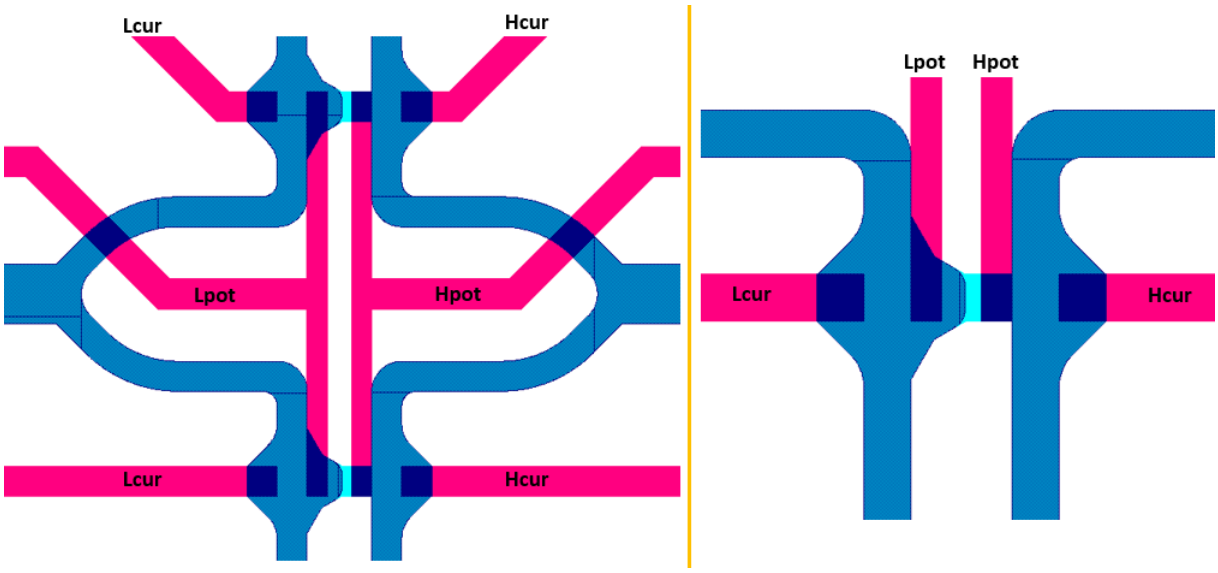

Figure 5.10 : The signal is collected from two stations simultaneously (left) or only from one station (right).

The four-terminal impedance measurement system shown in Figure 5.7 are fabricated as shown in Figure 5.10.

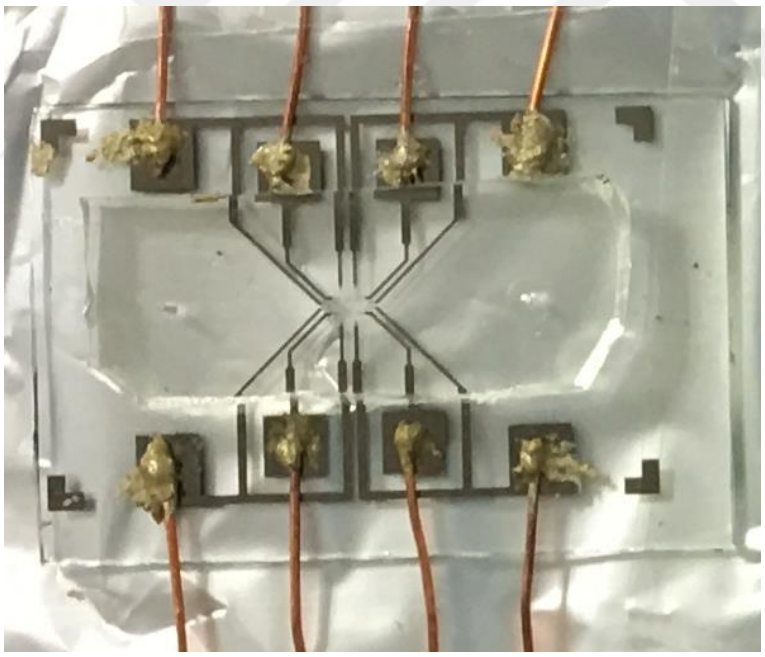

Figure 5.11 : Microfluidic chip with four-terminal electrode design.

In the first part of the study, Agilent 4980A LCR meter (Keysight Technologies, USA) was used in the 100 Hz - 500KHz frequency range. In the second part, Zurih Instruments HF2IS (Zurich Instruments AG, Switzerland) impedance spectrometer is used to perform 4-terminal measurements and to scan a wider frequency range. This spectrometer with a frequency range of 0.7μHz to 50MHz was also preferred because it allows working with 2-4 terminal electrodes.

Improvement has been made to connect microfluidic chips with less electrical noise to the impedance spectrometer to improve measurement accuracy.

In the first part of the study, as shown in Figure 5.10, after the copper wires were fixed to the electrode connection beds with silver-epoxy, the connection to the impedance spectrometer was made with crocodile ends. However, this method was abandoned because the silver-epoxy adhesive used caused different electrical noise for each connection.

In order to improve the accuracy of the measurement, a PCB circuit is designed to directly touch the metal electrodes. This circuit is designed in such a way that the entire surface area except the connection pads touching the metal electrodes is connected to ground of the impedance spectrometer. The connection of the PCB circuit to the impedance device is provided by BNC terminals and the microfluidic chip is sandwiched with the PCB circuit by a 3D printed body. Figures 5.11 and 5.12 show the system produced as a result of improvements.

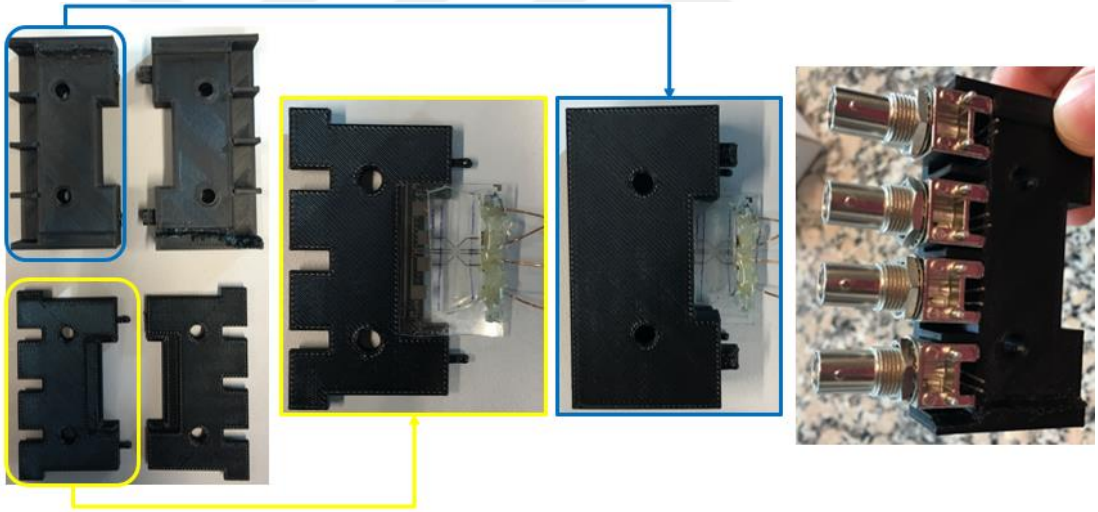

Figure 5.12 : The microfluidic chip with PCB circuit with and BNC connections on a 3D-printed body.

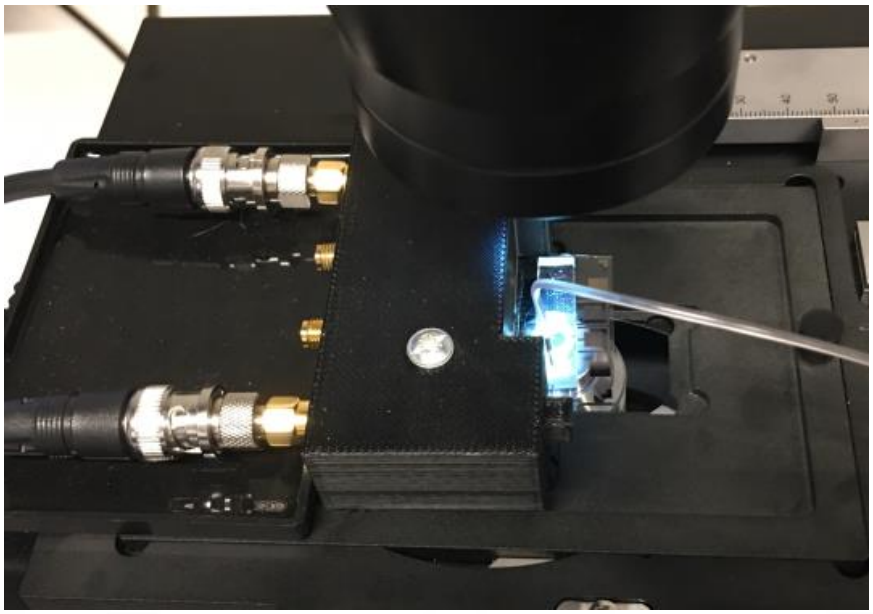

Figure 5.13 : The image taken during the experiments under the microscope after the completed production.

In the first part of the study, before reading the impedance values for the target cells, the cell-free sucrose solution (or medium) was injected into the microchannel and the impedance value was recorded. The target cells were then added to the same sucrose solution and injected into the microchannel, then the impedance value was again recorded when all individual cell entrapment stations were filled with the target cells. Microfluidic design has been improved to improve this two-stage measurement. In the system we designed, it is possible to capture single cells by means of a vertical narrow neck in the measuring station. In the design with two measuring stations, the narrow neck in one of the stations was removed, leaving the cells in the channel without being captured. Thus, while one of the stations continuously measures the impedance of the medium we inject into the microchannel, the cell continues to be captured individually at the other station. Thus, live differential measurement can be performed and it is aimed to obtain less incorrect measurement results in recording the

impedance information of the target cell. The change in design is schematically expressed in Figure 5.13.

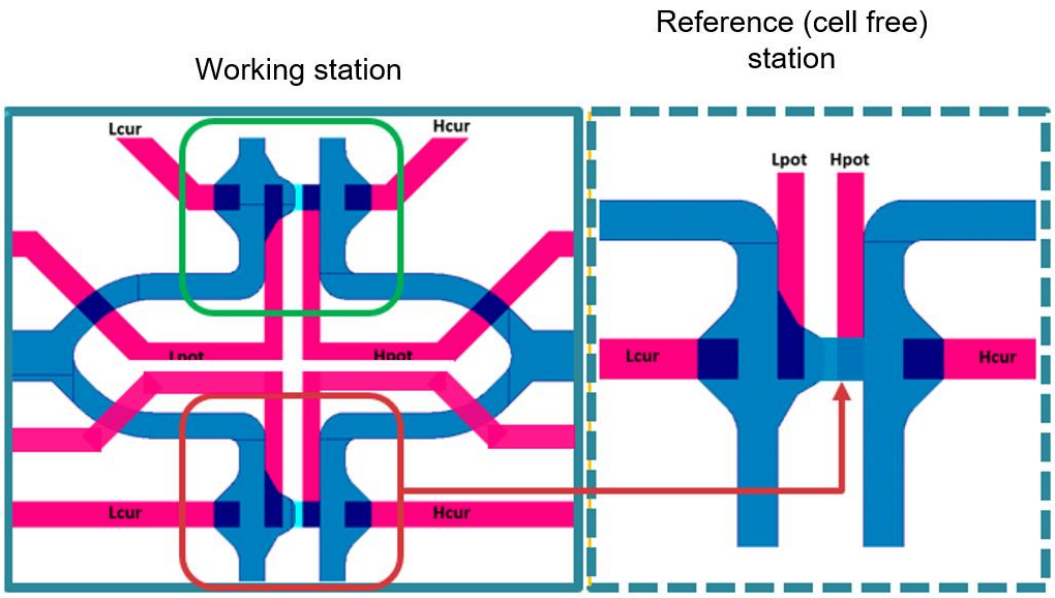

Figure 5.14 : One of the existing measuring stations was refabricated in such a way that the cell could not be captured and it was intended to be a reference to the cell-captured station by taking measurements from the medium only.

Experimental results with K562 cells in the 100Hz - 20MHz frequency range are presented here. While carrying out the impedance measurements, the measurements were divided into three frequency segments as 100Hz - 1kHz, 1kHz - 100kHz, 100kHz - 1Mhz, 1MHz - 20MHz. The signal quality was monitored from the oscilloscope on the spectrometer and the signal amplitude and amplification values were chosen for the most accurate reading. In addition, measurements were taken from a total of 100 points between each frequency segments and 32 readings were made from each point and the average was recorded. The results recorded are presented in Figures 5.14 - 5.16.

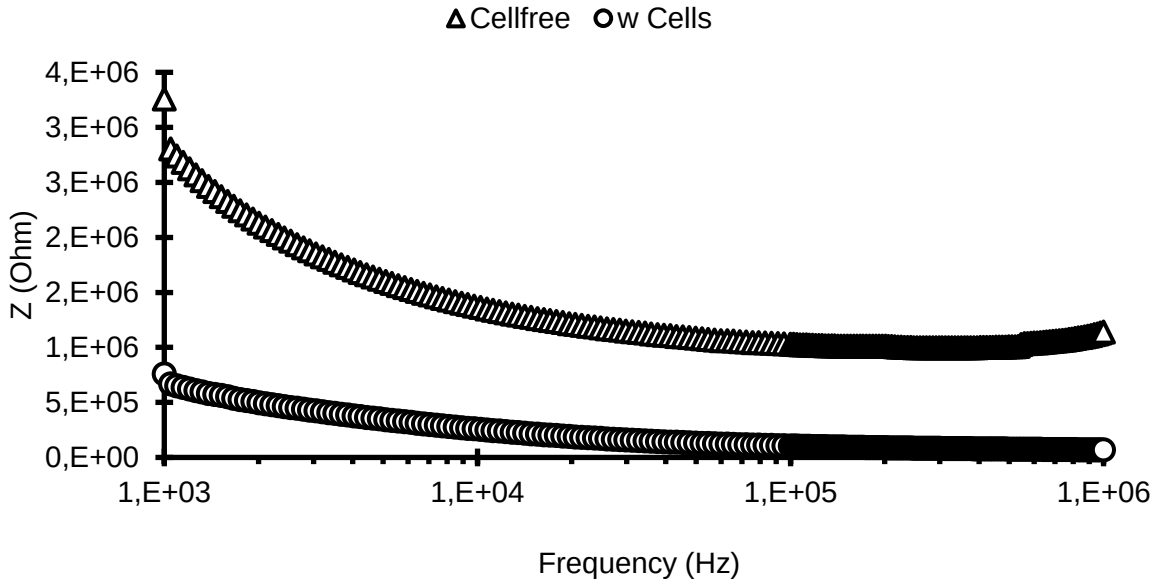

Figure 5.15 : Impedance results in the frequency range of 1kHz to 1MHz in 200mM sucrose solution (cellfree) and K562 cells (w Cells).

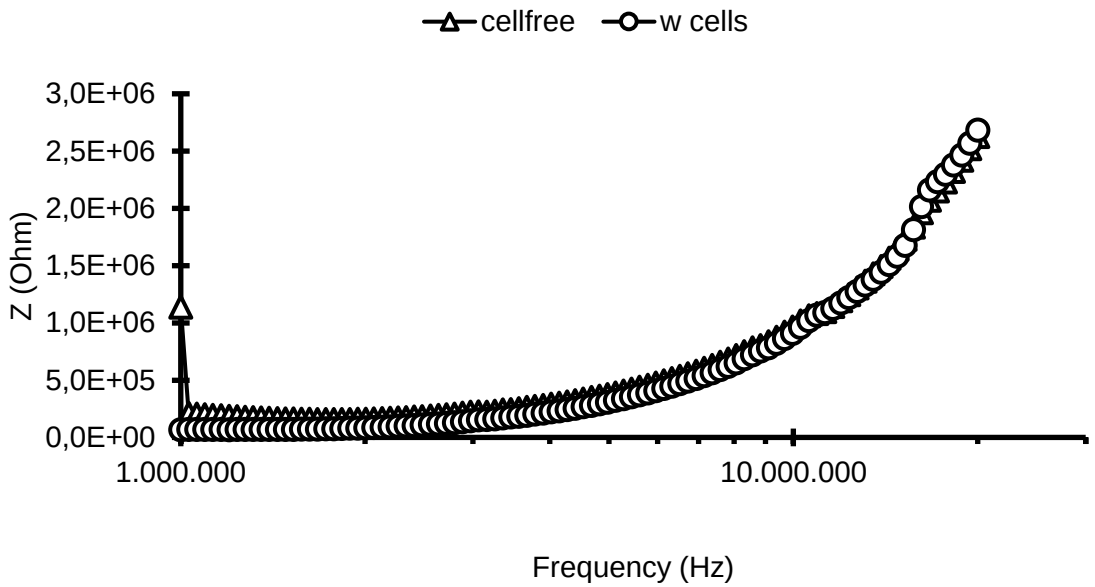

Figure 5.16 : Impedance results in the frequency range of 1MHz to 20MHz in 200mM sucrose solution (cellfree) and K562 cells (w Cells).

When we examine the results in Figure 5.14 and Figure 5.15, the total impedance change percentage graph is as shown in Figure 5.16. As can be seen from this figure, the optimal operating frequency of the tested system for K562 cells in 200mM sucrose solution is seen as 1MHz.

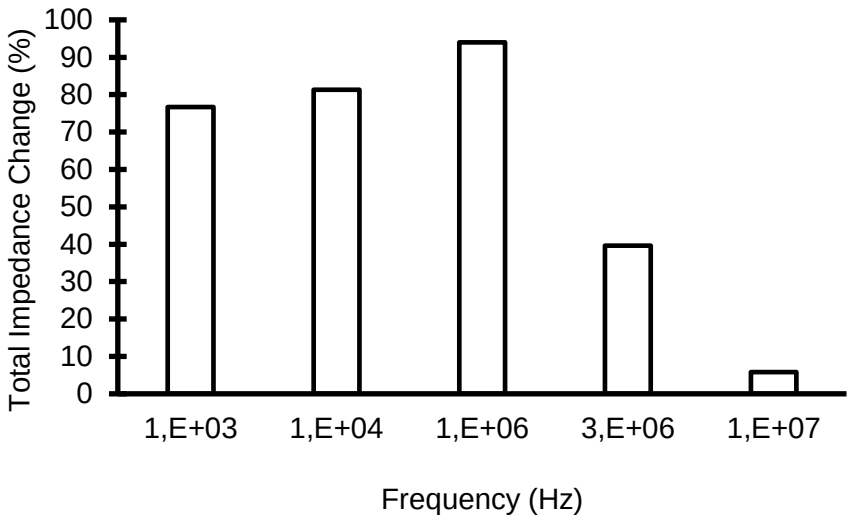

Figure 5.17 : Total impedance change of the system for K562 cells in 200mM sucrose solution.

6. ORGAN-ON-A-CHIP

In vivo, cells are in complex cell-cell and cell-matrix interactions. They are found in three-dimensional micro-environments where food and gas transmission is provided by complex transport systems. Cells in living tissue receive the nutrient and gas exchange they need to survive from the capillary structures surrounding the tissue, while at the same time being exposed to mechanical and other physiological effects such as respiratory movements in the lung and peristaltic movement in the intestine.

Cell culture is a process in which cells are grown in an artificial two-dimensional surface or three-dimensional structure under controlled conditions outside the living tissue (in vitro), conditions may vary for each cell type, and the regulation of physicochemical conditions by providing the necessary nutrients, growth factors, hormones and gases. However, it is not possible to mimic a living organ even if some elements of tissue-specific microenvironment can be provided in studies with a uniform cell culture. Studies with cell cultures lack tissue-tissue interactions within a very complex architectural structure. For example, there is interaction between parenchymal cells and connective tissue that provides vascular endothelium (vascular endothelial cells) and its environment in living tissue. Such interaction is critical to the functioning of all organs. Cells in cell cultures are not subjected to mechanical effects and shear stress of cells in living tissue. Cells in systems without a fluid flow cannot represent the actual living tissue environment as they are deprived of interaction with blood circulation and cells in the immune system. In addition to two-dimensional and three-dimensional cell cultures, it is possible to examine living tissues taken in biopsy or cross-section of live tissues in vitro. However, since these tissues lose their vitality within a few days, it is not possible to carry out a long-term and high-yield study.

6.1 Design

The design for the on-chip kidney includes a porous membrane between two microchannels aligned perpendicular to each other. The mask patterns for this design are detailed in Figure 6.1. Experimental studies were carried out by placing a membrane in the 2mm x 2mm area formed in the center of the microchannels with a width of 1mm and a length of 10mm. This design ensures that the membrane at the

center of the PDMS-PDMS interface is sealed leak-free. For TEER measurements, the electrode fingers with a width of 50μm, covering a 4mm^2 area in the center, are placed on upper and lower surface of the microsystem. Since periodic mechanical stress will be applied in the system to be produced for lung-on-a-chip system, vacuum channels are added on both sides of the main microchannel. With the periodic vacuum to be applied through the side channels, the alveolar environment of the lung will be simulated by making the middle channel elongate and re-shortening. Figure 6.2 shows detailed views of the masks of the design. Here the middle channel is 1mm wide and 10mm long. The side channels between the vacuum channels and the middle channel are designed in two different thicknesses (100μm and 200μm). For TEER measurements, electrode fingers with a width and gap of 50μm to cover the 10mm long middle microchannel are designed and placed on the upper and lower surface of the microchannels.

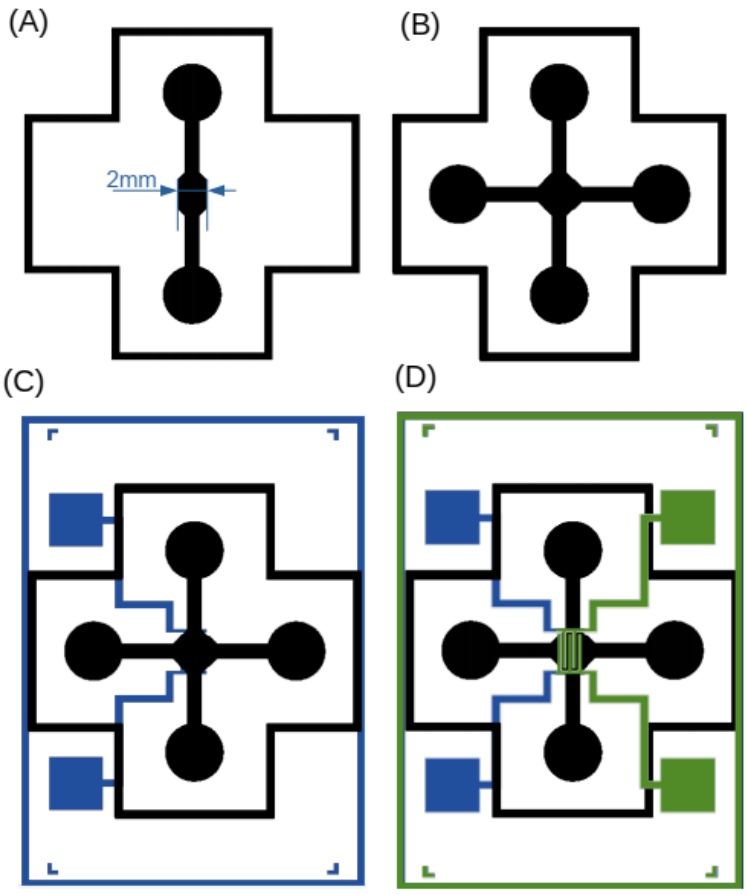

Figure 6.1 : Mask patterns for kidney-on-a-chip.

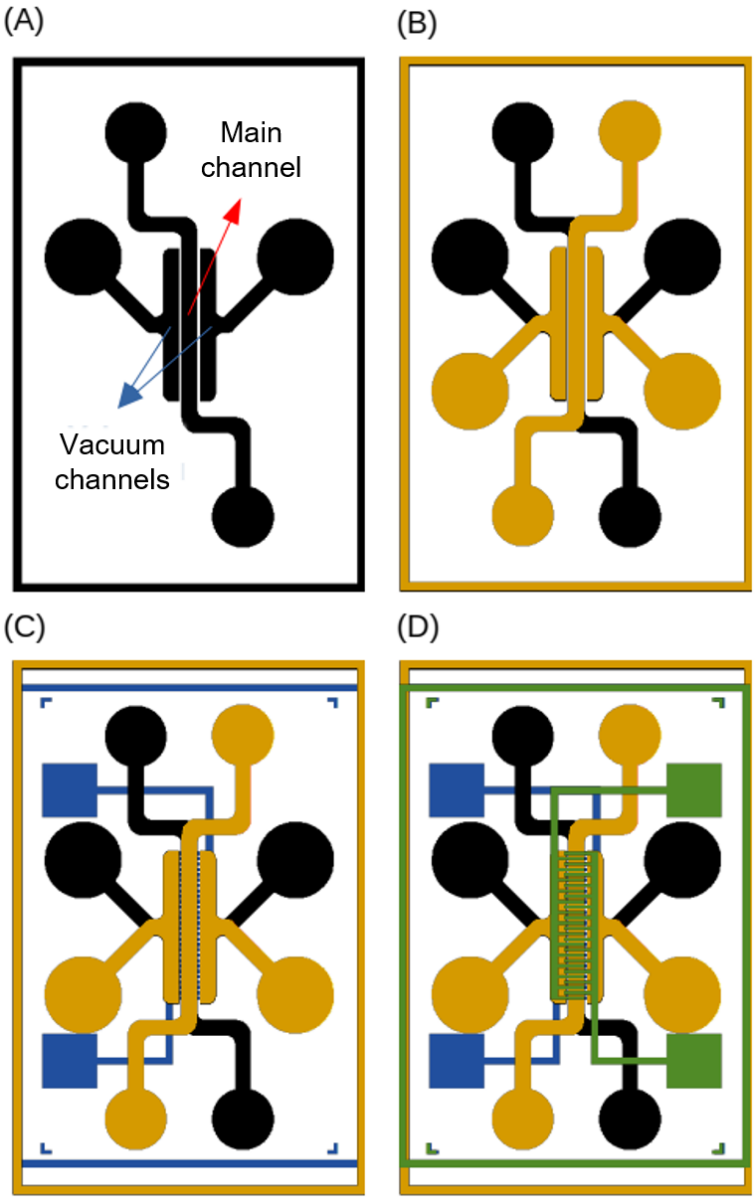

Figure 6.2 : Mask patterns for lung-on-a-chip.

Two types of polycarbonate (PC) membranes with different pore sizes were purchased for the on-chip organ platforms to be produced. Detailed information on preferred membranes is given in Table 6.1. These membranes have been shown to yield successful results for cell culture formation in various on-chip organ applications and have therefore been preferred. (Sciancalepore et al. 2014, Brown et al. 2015, van der Helm et al. 2016).

Table 6.1 : Polycarbonate membrane properties.

	Pore size (µm)	Thickness (µm)	Merck Catalog No.
Membrane #1	0.2	25	GTTP04700
Membrane #2	0.4	10	HTTP04700

6.2 Fabrication

Flexible masks for on-chip organ platforms were drawn and purchased from JT-Photo Data (Hitchin, UK) as an acetate mask layer. Similarly, drawings were made for electrode geometries to be used in TEER (trans epithelial electric resistance) measurements.

PDMS microchannel geometries are fabricated in a simple way by soft lithography. SU-8 3050 negative photoresist was used as a mold to form microchannels. This photoresist can achieve a maximum thickness of 100μm as a single layer. Two layers were fabricated on top of each other and a total film thickness of 200μm was obtained on 4" silicon wafer. Fabrication parameters are given in Table 6.2. Laurell WS-650 Spin Coater (Laurell Tech, USA) was used for spin coating of photoresists, and SÜSS MA6 Mask Aligner (SÜSS MicroTec SE, Germany) was used for soft-lithography.

Table 6.2 : SU-8 3050 with 200μm thickness mold fabrication parameters.

Process name and Layers	**First Layer**	**Second Layer**
Spin Coat	1000rpm - 35s	1000rpm - 35s
Soft Bake	95°C – 45m	95°C – 45m
UV Expose	200mJ	200mJ
Post Expose Bake	65°C – 1m and 95°C' – 5m	65°C – 1m and 95°C – 5m
Development	mr-DEV 600 – 15m	mr-DEV 600 – 15m
Hard Bake	not performed	150°C – 1h

The membranes to be placed between the microchannels have been reduced in size to provide a sealed bond with oxygen plasma on the surface where the PDMS microchannel surfaces touch each other. As shown in Figure 6.3, the PC membrane is sealed between two microchannels.

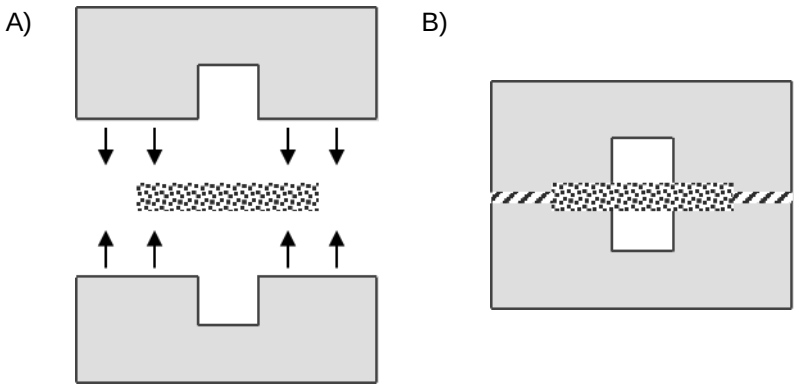

Figure 6.3 : Adhesion interfaces formed after oxygen plasma by reducing the dimensions of PC membrane.

An alternative membrane production has been tried to replace the PC membrane. Sucrose was added to the uncured PDMS (50% by weight) and spin coated (1000rpm-60s) on a silicon wafer to achieve a thickness of 50µm layer. PDMS layers, which were peeled off from the wafers, were cut into proper sizes and kept in a 20-minute ultrasonic bath at 60°C in DI-water. The sucrose particles were dissolved in water by this method and a porous PDMS structure was formed. Figure 6.4 shows the PDMS membrane produced and a kidney-on-chip system produced using this membrane.

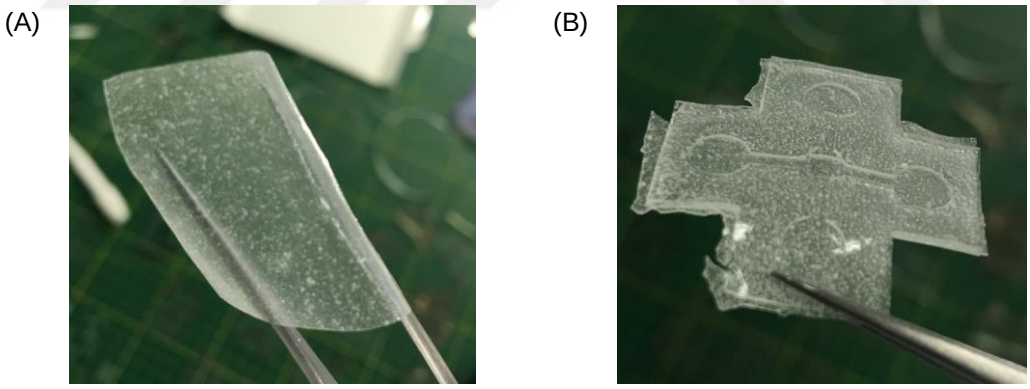

Figure 6.4 : A) Porous PDMS membrane and B) an example of a kidney-on-a-chip system.

In the production of PDMS microchannels, Dow Slygard 184 was mixed with 10% by weight of curing agent. The desired volume of the mixture placed under vacuum to remove air bubbles and then poured onto the SU-8 molds and allowed to solidify on a 90° C hot plate for 45 minutes. The PDMS microchannels, which were then peeled off from the mold, were cut one by one, punctured the microchannel inlets and outlets and prepared to be bonded with the membrane. The production steps vary according to the types of membranes used and on-chip organ systems. The simplest production

steps for kidney-on-a-chip system are shown in Figure 6.5. Here, a membrane covering a 4mm^2 area in the center is fixed between two microchannels. In the studies where TEER measurements would not be made, these on-chip systems without electrodes were used.

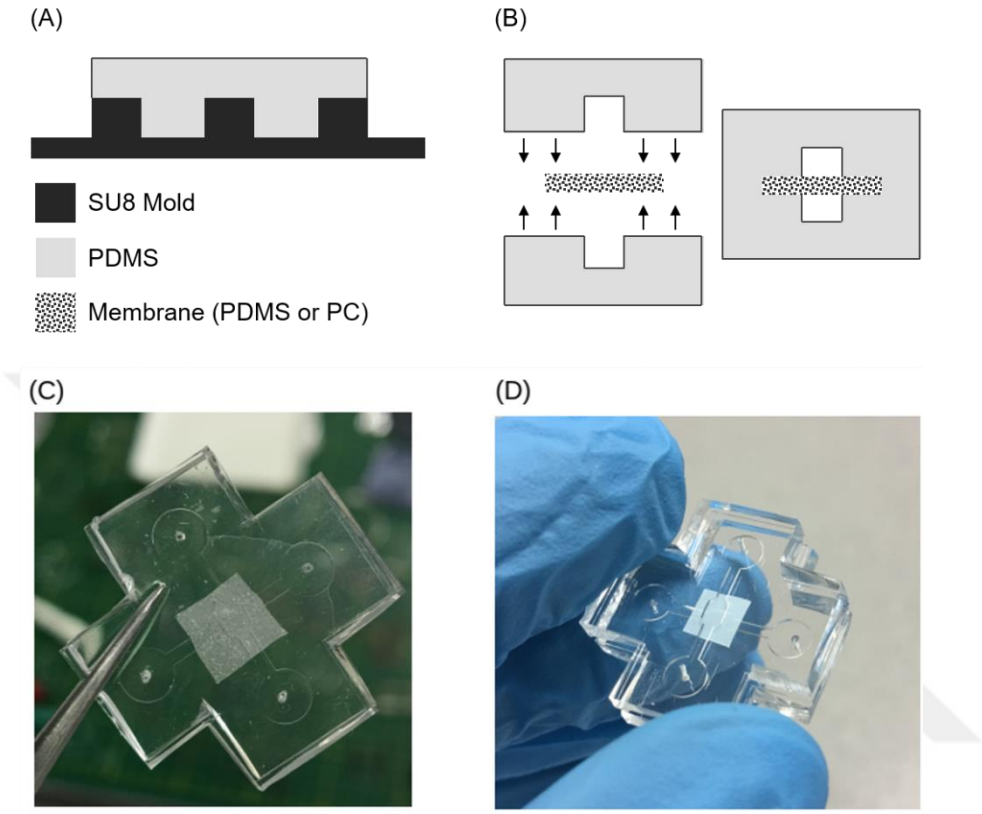

Figure 6.5 : Electrode-free on-chip kidney system A) fabrication steps C) with a PDMS membrane and D) with a PC membrane in the center.

Since the side walls separating the vacuum channels and the main channel in the lung-on-a-chip system will stretch outwards under applied vacuum, these side walls located in the upper and lower microchannels must be sealed to the membrane surface placed in the middle. The adhesion could not be achieved with the PC membrane and the PDMS surface. Therefore, the PDMS membrane we fabricated was placed between the two microchannels to cover the entire surface and was bonded with O_2 plasma.

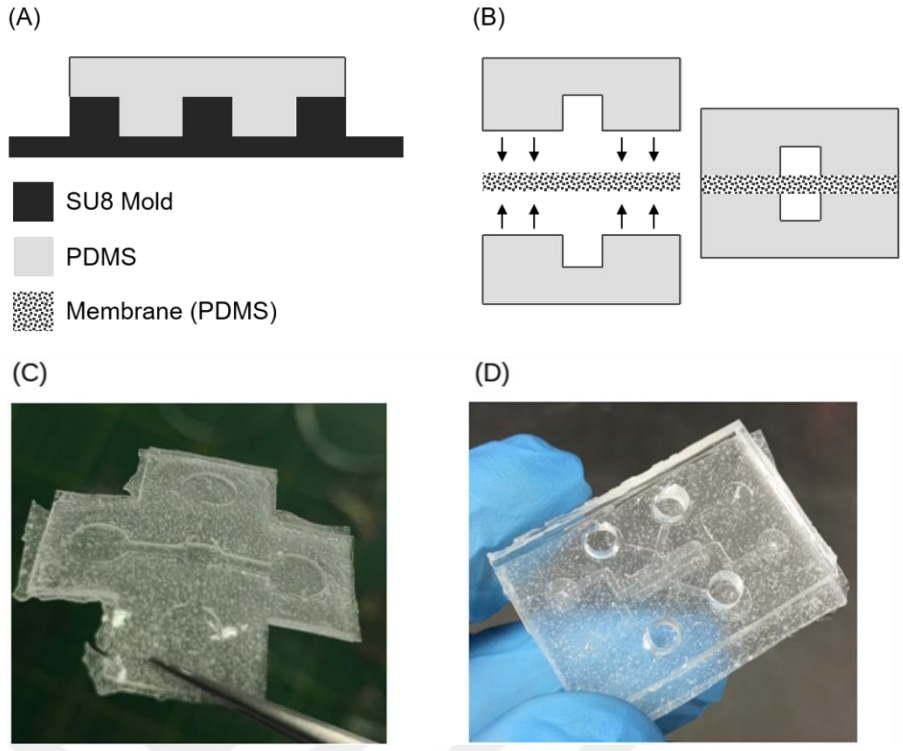

Figure 6.6 : (A-B) Fabrication steps of PDMS membrane covering the entire surface between two microchannels. C) Kidney-on-a-chip and D) Lung-on-a-chip are fabricated by this method.

To perform TEER measurements, the upper and lower channels of the microchannel must be combined with glasses with metal electrodes on them. In order to perform electrical measurements, a path must be made between the upper and lower electrode pairs, where only the cells attached on membrane surfaces located in the center. In order to meet this condition, the excess PDMS poured onto the SU8 mold in the first step of fabrication was removed by stripping with a cell scraper (Figure 6.7-B) and then allowed to solidify. A PDMS membrane is bonded on top by O_2 plasma (Figure 16 C) and microchannel is peeled off from the mold. Finally, Glass slides with Al/Ti electrodes were aligned to the upper and lower microchannels and bonded with O_2 plasma. For the fabrication of metal electrodes on glass slides, glass samples were placed in 1M KOH solution for 10 minutes in an ultrasonic bath, washed with DI-water and placed in acetone in an ultrasonic bath for another 10 minutes. After washing with isopropyl alcohol and DI water, glass slides dried with nitrogen and coated with AZ9260 positive photoresist. Following the soft-lithography process, patterned slides are placed in a physical vapor deposition system. Immediately after coating 100nm Al on photoresist coated glass samples with Vaksis Midas physical vapor deposition device, 200nm Ti was coated without disturbing the vacuum conditions. The Al coating is coated by thermal evaporation, while Ti is coated with DC Magnetron Plasma. Glass holes were drilled with a diamond drill for liquid and vacuum inlets.

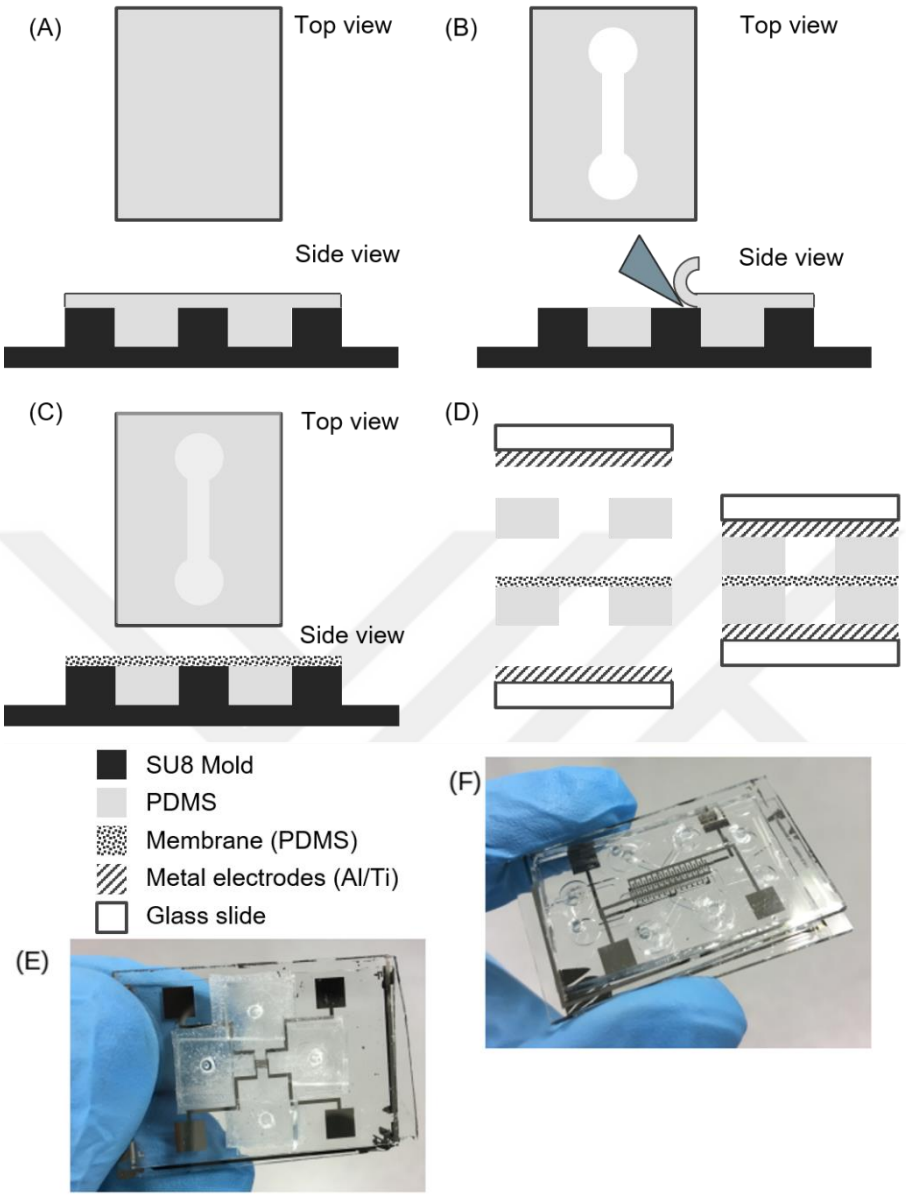

Figure 6.7 : (A-D) On-chip kidney and lung fabrication steps to be used in TEER measurements and (E-F) examples of the systems produced.

6.3 Experimental

Experimental studies on the organ-on-a-chip systems are presented here under related titles. The adhesion of the preferred cell types on the membrane produced was examined. Experimental studies have been concluded by measuring the viability and differentiation of the cells seeded in the on-chip organ systems following the verification of the membranes.

6.3.1 Cell adhesion on PC membranes

The HaCaT (human creteocytes) cell line was first tested for cell culture on polycarbonate membranes. HaCaT cell line was cultured in DMEM F-12 medium containing 10% FCS and 1% L-glutamine; Cells were incubated in 5% CO_2 atmosphere at 37° C. Cytotoxicity studies were performed in aseptic environment. Sterilization of the membranes was carried out by autoclaving at 121°C for 20 minutes. The membranes were then washed with PBS. Cell adhesion performance of membranes for 3 days was determined. The HaCaT cell line was planted with a concentration of 100,000 cells/ml in a 24-well plate containing a 0.2μm or 0.4μm diameter porous membranes. Plates were incubated at 37° C, 5% CO_2 atmosphere for 72 hours. MTT test was performed every 24 hours. After incubation, the extracts were discarded and the wells were pipetted with 1000μL of fresh medium containing 100μL of MTT solution (25mg / mL, with PBS). After 4 hours of incubation, the medium was discarded and 500μL of DMSO solution was added to the wells. The optical density of DMSO-soluble formazan dye was examined at 570 nm.

MTT cytotoxicity test was performed for 3 days to examine the cell adhesion profile on 0.2 and 0.4 μm porous membranes. Cell viability of the 0.2 μm porous membrane was 34.73% (std. Error ± 1.37%) on day 1, 51.58% (std. Error ± 1.83%) on day 2 and 75% on day 3, 47 (std. Error ± 3.73%). The results are shown in Figure 6.8. Table 6.3 shows the mean and standard deviation values obtained from 4 membranes at each 24 hours. The formazan absorbance value here should be considered as coherent with cell viability. As the absorbance value of formazan increases, it is understood that the live cell population on the membrane increases.

Table 6.3 : Readings of Formazan Absorbance on 4 samples from 0.2μm and 0.4μm porous membranes for 24 hours with HaCaT cells.

Day		**1**	**2**	**3**
Formazan Abs (Avg.)	*0,2μm*	0,3473	0,5158	0,7547
	0,4μm	0,2709	0,5792	0,8061
SD	*0,2μm*	0,0137	0,0183	0,0373
	0,4μm	0,0066	0,0321	0,0428

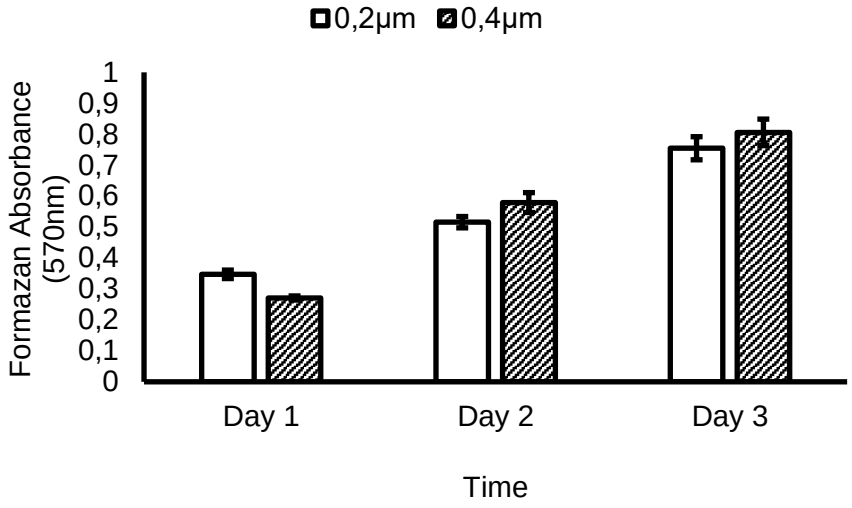

Figure 6.8 : The viability results measured for 3 days on both PC membrane types according to the MTT test results of the HacaT cell line.

When the 3 days cell adhesion profiles were examined on both membranes; The cell viability of the 0.2 µm porous membrane is significantly higher than the 0.4 µm porous membrane on the first day. On the 2nd day; The cell viability of the 0.4 µm porous membrane is significantly higher than the 0.2 µm porous membrane. On the third day, the cell viability difference between the two membranes is not a significant difference. Cell viability increased significantly in both membranes and reached 75% viability after 3 days. In the light of these results, it was determined that both membranes were a good environment for the cells to attach and develop.

Cell adhesion tests on PC membrane were repeated with RPTEC (Renal Proximal Tubule Epithelial Cell - ATCC CRL 4031) renal epithelial cells to be used in on-chip kidney applications with the same method and MTT tests were repeated for a period of 9 days. Figure 6.9 shows the results. Here, formazan absorbance readings were performed on 3 membranes for each time interval. Mean values and standard deviation values are given in Table 6.4.

Table 6.4 : Formazan absorbance values of renal cells on the PC membrane for the specified time intervals. 3 membranes were used for each time interval.

Days	**1**	**2**	**5**	**7**	**9**
Formazan Abs (Avg.)	0,15	0,07	0,22	0,45	0,70
SD	0,01	0,01	0,06	0,05	0,02

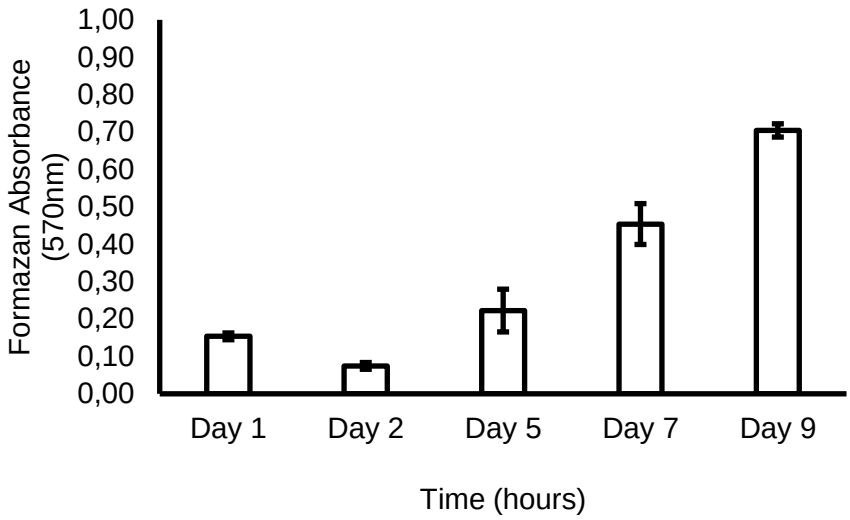

Figure 6.9 : The 9-day viability results of the RPTEC cell line on the PC membrane. 3 membranes were used for each time interval.

6.3.2 Kidney-on-a-chip

The RPTEC cell line for the on-chip kidney system was cultured in DMEM F-12 containing 10% FCS and 1% L-glutamine. Cells were incubated in 5% CO2 atmosphere at 37°C. Sterilization of the kidney-on-chip systems was performed by autoclaving for 20 minutes at 121°C. RPTEC cell lines were seeded with a concentration of 100,000 cells/ml in each set of experiments. The shear stress applied under dynamic conditions was 0.012 dyne / cm^2 (1µl / min). The experimental setup is shown in Figure 6.10.

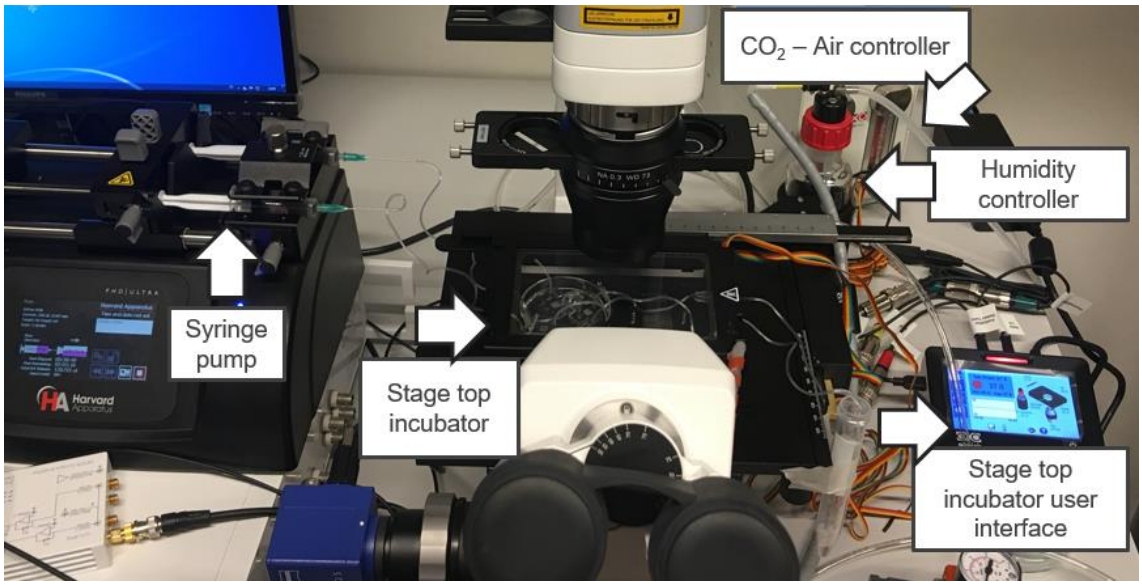

Figure 6.10 : Incubation chamber on microscope stage and syringe pump setup for dynamic conditions.

The effect of PC membrane and PDMS membranes on cell viability were also studied. Cells were cultured in microfluidic chips containing different types of membranes. RPTEC cells were cultured statically for 1 hour and adhered to membrane surfaces, then cells were cultured under static and dynamic conditions. Figure 6.11 shows the on-chip kidney systems under static and dynamic conditions within the microscope stage top incubator system.

Figure 6.11 : Kidney-on-chip systems under static and dynamic conditions within the microscope stage top incubator system.

Figure 6.12 shows the viability of kidney cells as a result of MTT test under static and dynamic conditions on different types of membranes.

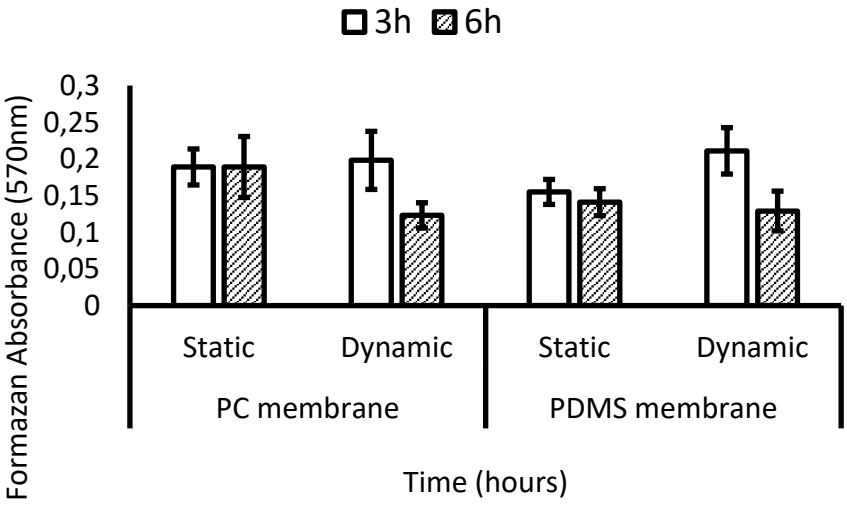

Figure 6.12 : Cell viability in PC and PDMS membrane based kidney-on-chip systems.

As shown in Figure 6.12, both membranes gave similar results and it was found that the PDMS membrane we produced was suitable for the organ-on-a-chip systems.

The studies with the kidney-on-chip systems were repeated for 0-48 hours and cell viability was monitored by MTT test. Figure 6.13 shows the cell viability results under static and dynamic conditions for the 0-48 hour interval.

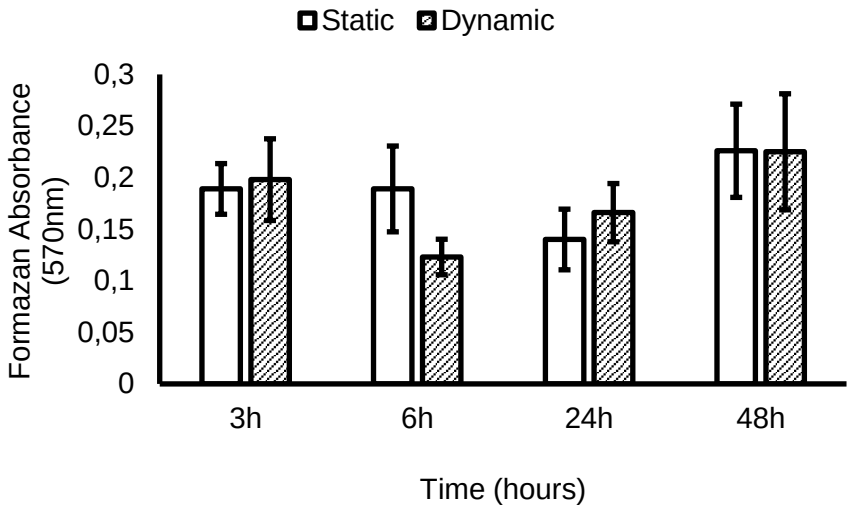

Figure 6.13 : Monitoring of cell viability by MTT test in kidney-on-chip systems for the 0-48 hour interval.

When the results obtained here are examined, it is seen that cell viability is rapidly recovered and increased, although some cell viability is lost initially under dynamic conditions. In the same set of experiments, resistance values of the cell barrier were recorded with the kidney-on-chip kidney systems with metal electrodes and are shown in Figure 6.14. Especially in the first 24 hours, the difference under static and dynamic conditions is significant. When Figure 6.13 and Figure 6.14 are examined together, although the cell populations are very close, the resistance value read from the cell barrier is more than 7 times for dynamic conditions shows that the density of tight-junctions between the cells is much higher than the static conditions and is consistent with the examples in the literature.

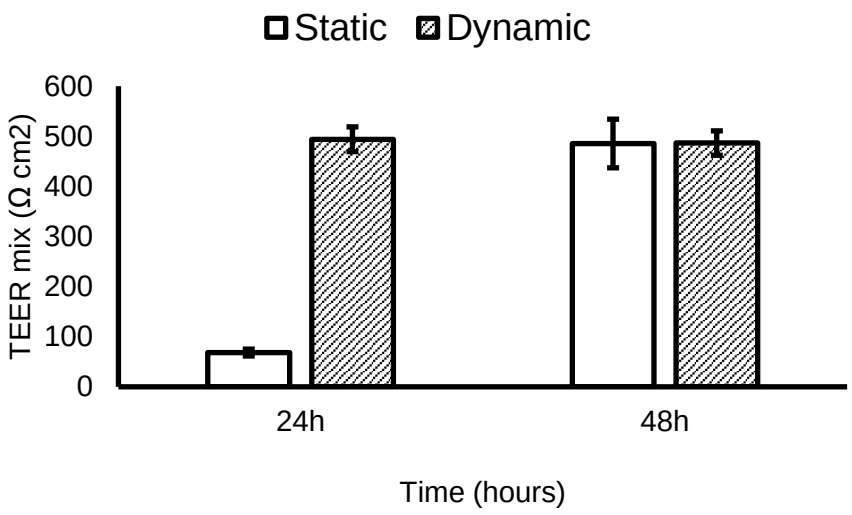

Figure 6.14 : Cell barrier resistance values recorded under static and dynamic conditions for kidney-on-chip systems in the range of 0-48 hours.

It is also expected that the resistance values under static and dynamic conditions will be close to each other after 48 hours. Similarly, in the literature, it is seen that rapidly increasing resistance values for dynamic conditions are fixed after a certain period of time.

In Figure 6.15, MTT test and TEER values are given together at the end of 24 hours.

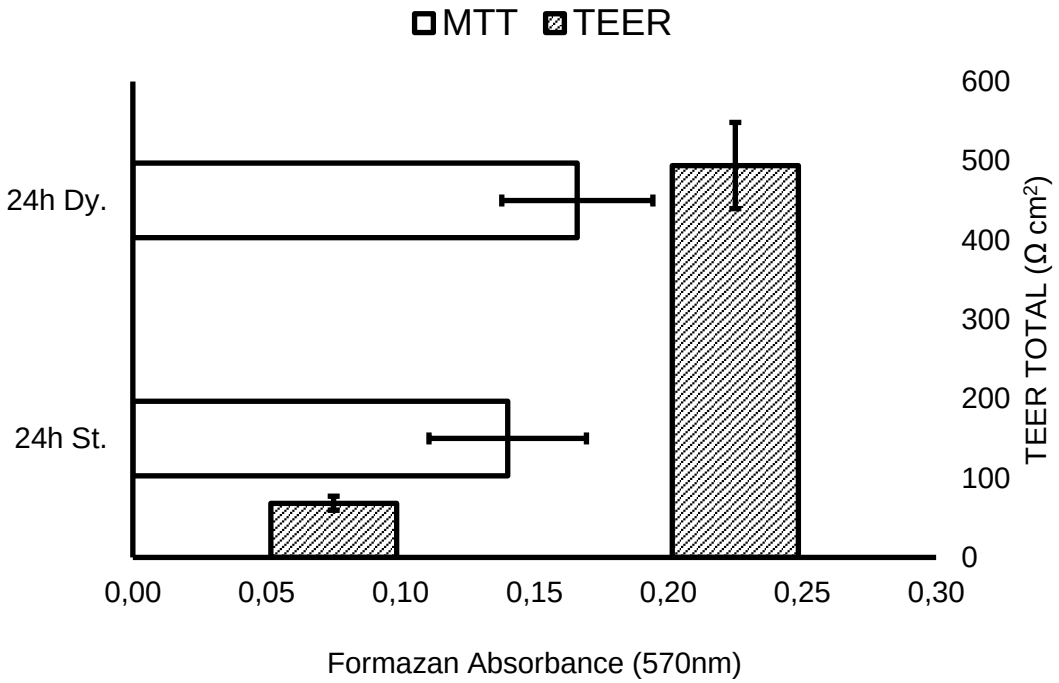

Figure 6.15 : MTT test and TEER values recorded under static and dynamic conditions for 0-24 hours.

6.3.3 Lung-on-a-Chip

NCI-82 (human lung carcinoma, ATCC HTB 175) and MRC-5 (human lung fibroblast, ATCC CCL-171) cell line for on-chip lung system is cultured in DMEM F-12 medium containing 10% FBS and 1% L-glutamine. The cells were cultured in 5% CO2 atmosphere at 37°C. Sterilization of the microfluidic chips was performed by autoclaving for 20 minutes at 121°C. In each experiment set, the MRC-5 cell line was seeded with a concentration of 100,000 cells/ml on one side of the membrane in the microfluidic chip and incubated for 2 hours. The microfluidic chip was then inverted and the NCI-82 cell line was seeded on the other surface of the membrane and incubated. Only PDMS membranes that we produce are used in lung-on-chip systems. MTT test cell viability results for chips where both cell types are cultured together under static and dynamic conditions (shear stress and periodic vacuum) for 0-48 hours interval are shown in Figure 6.16 and recorded TEER values are shown in Figure 6.17.

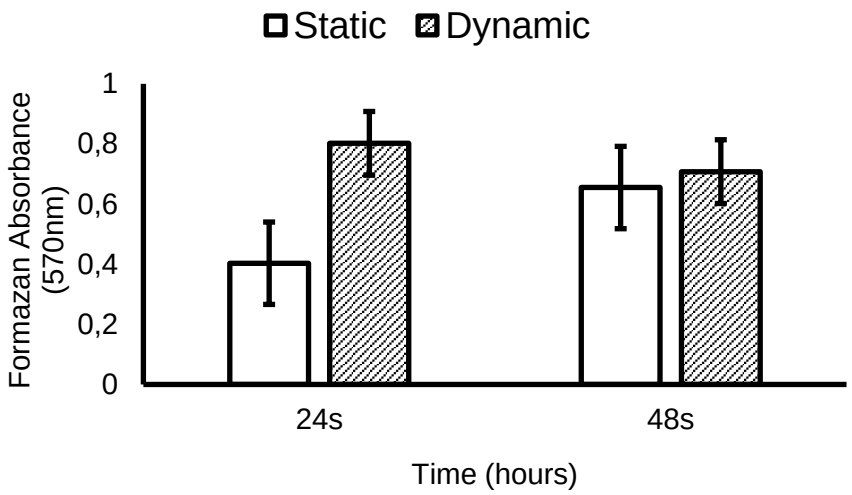

Figure 6.16 : Cell viability obtained after co-cultivation of the MRC-5 and NCI-82 cell line in lung-on-a-chip lung for 0-24 hour interval.

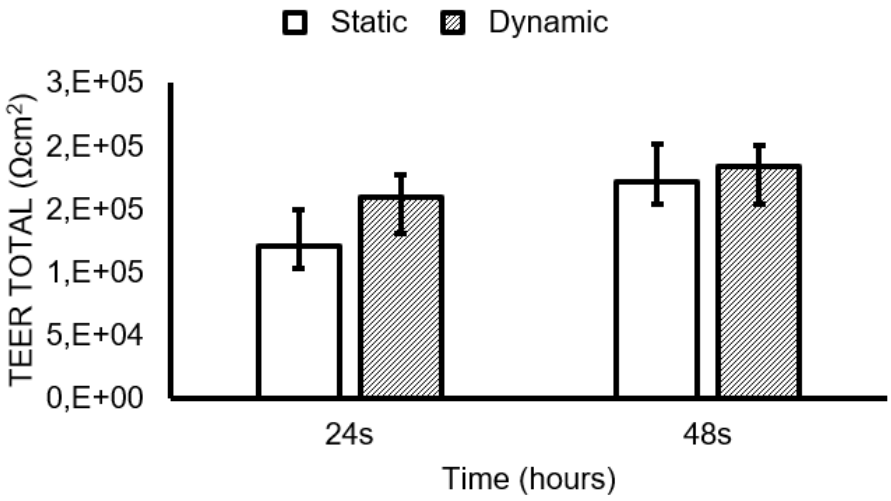

Figure 6.17 : TEER values recorded for the lung-on-a-chip system in the range of 0-48 hours.

There are several factors that influence the TEER values, including the physical support (membrane) used for cell cultures (Lo et al. 1999), the temperature of the measured medium (Light 1984; Blume et al. 2010), the material, quality and surface condition of the electrodes. TEER values differ significantly for various cell types. Moreover, even the TEER values for the same cell type differ greatly in different studies. In general, for studies where multiple cells are co-cultured, the reported values are higher than in monocultures (Griep et al. 2013). It is also stated that TEER values are much higher in microsystems with longer channel or lower channel height. Therefore, the TEER values in Figure 6.17 are significantly higher than the on-chip kidney systems. According to the recorded results, higher TEER values in dynamic conditions compared to static conditions indicate that the density of tight-junctions between the cells is higher and it is in line with the results obtained in the kidney-on-chip systems.

Although the PDMS membrane we produce provides a suitable environment for cell adhesion, problems have been experienced in the combination of the microfluidic system, especially the sealing of the side walls between the vacuum channels and the main channel with the PDMS membrane surface. This is due to the fact that the PDMS sidewalls, which are produced very thin (50μm), and the membrane are flexible, do not provide a complete contact with the PDMS microchannel surface, causing the membrane to cause micro / macro curl. Therefore, the design has been renewed and the thickness of the side walls has been increased by 2 times and a tight adhesion has been achieved. Experiments on the differentiation of lung cells under the effect of a specific shear stress and vacuum-based mechanical elongation / shortening were carried out as intended. The test set-up is shown in Figure 6.18.

Incubator compatible syringe pumps (ExiGo Pump - Cellix, Ireland) were used to flow media in microfluidic chips, while vacuum hoses connected to the on-chip lung systems were vacuumed periodically at a frequency of 5Hz with a vacuum pump and solenoid valve.

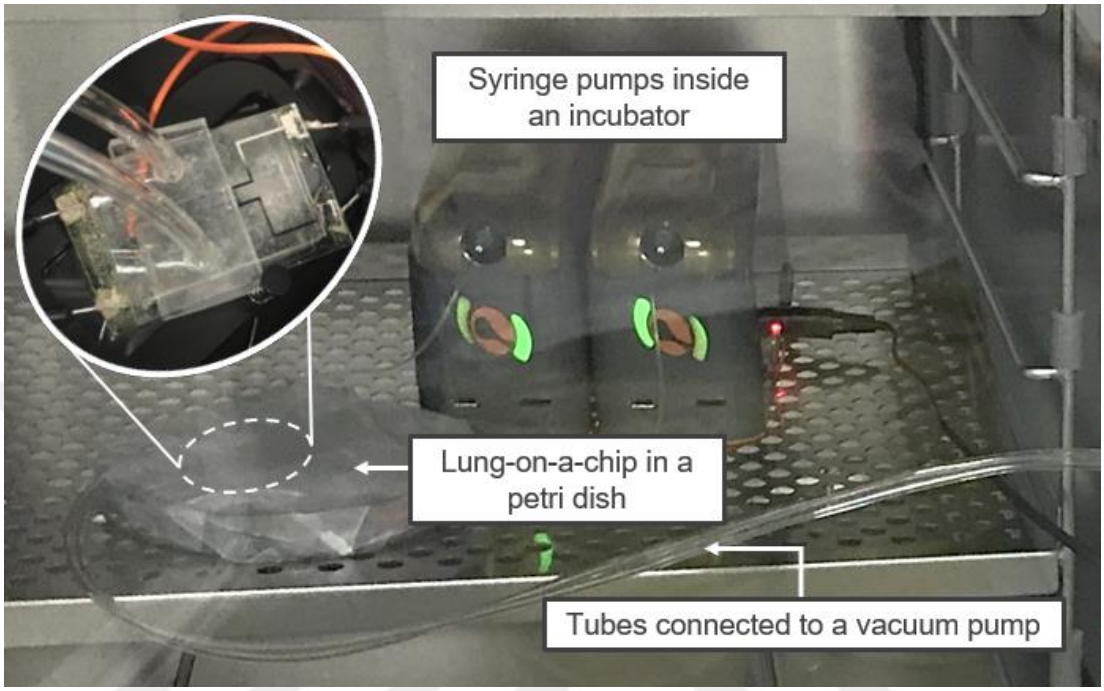

Figure 6.18 : Experimental setup for lung-on-a-chip system in an incubator.

7. CONCLUSION

A microfluidic system has been developed to isolate target cells from different types of cell populations by dielectrophoresis and to capture them individually at the stations where the impedance analysis will be performed continuously. In our study, the elements that are divided into two parts as “separation” and “capture / analysis” are examined separately, and the designs that give the best results are combined in the final product.

Experimental studies have shown that the impedance shift generated by each cell type is characteristic and an optimum medium conductivity and frequency value can be determined for diagnosing a cell type. While the impedance deviation for HCT116 cells decreases as the solution conductivity decreases, the impedance deviation for MDA-MB-231 cells increases with the solution conductivity. HEK293 cells, on the other hand, showed similar impedance deviations at the two solution conductivity levels studied. When the cell types are compared with each other, HCT116 and HEK293 cell lines generate similar impedance deviations in 1XPBS solution, while a distinctive difference in impedance deviations occurs in solutions with a concentration as low as 0.1XPBS.

When the medium conductivity is lower than the cell conduction, more current passes through the cell and the impedance shift is negative. Thus, more information about the cell type is collected and diagnostic sensitivity is increased. In 200mM sucrose solution, there is a distinctive impedance deviation difference between cancerous lymphocyte cells and healthy blood cells. The range in which the produced system has the highest sensitivity in distinguishing healthy blood cells is the frequency range of 0.1kHz and 10kHz.

Systems with separation and impedance analysis with dielectrophoresis have also been produced and it has been recorded in experimental studies that K562 cells are directed by this system and collected at the stations. In order to measure the separation efficiency of the final system, each cell type integrated into the system should be labeled with a different color fluorescent dye and monitored under a fluorescent microscope. Besides, the cells collected from the outlets after separation

with dielectrophoresis should be counted by flow cytometry and the separation efficiency should be demonstrated.

The impedance shift recorded at a certain frequency offers the possibility of diagnosis for the target cell type and stage. Characterization of cancer cells is critical in drug tests, the mechanism of the drug and understanding of cell biology. It is possible to monitor, diagnose and improve the effects of different chemical and drug concentrations on the cell with the system developed with this project.

In this study, it is also aimed to produce two different on-chip organ models. Some methods determined based on the literature (APTES and PC membrane adhesion to PDMS microchannels) were found to be inapplicable during our study and the methods applied in various steps were changed.

Microfluidic systems, which have metal electrodes on the lower and upper surfaces of the microchannel and which have a membrane in the center, are successfully produced for the organ-on-a-chip platforms. Satisfactory results were determined especially on the kidney-on-a-chip application, and the increase in the tight junctions of the cell cultures in the microfluidic system under dynamic conditions was recorded by electrical measurements. Although there is some loss of cell viability initially in dynamic conditions in kidney-on-chip, it is seen that cell viability is rapidly recovered and increased. Although the cell concentrations are the same, the resistance values obtained from the cells under dynamic conditions are 7 times higher than the static conditions. This indicates that cell differentiation takes place and tight junctions are formed.

In the lung-on-a-chip systems, two different cell types have been successfully cultured together. Viability and cell barrier resistance values were recorded under static and dynamic conditions. When MTT test results were examined, cell viability in static conditions remained lower for the first 24 hours compared to dynamic conditions, and cell viability showed close values for static and dynamic conditions at the end of 48 hours as seen in kidney application. In experiments performed with the renewed design on the lung-on-a-chip system, the TEER values taken for static and dynamic conditions indicate that the resistance value read from the cell barrier is higher than the dynamic conditions, and that the tight junctions between the cells is higher than the static conditions and shows that the cell differentiation has occurred.

The three-dimensional microfluidic tissue/organ on-a-chip culture system that we produced as a project output has been developed as a prototype product and is a technology platform that can be used in different fields such as tissue development,

organ physiology, drug screening and development research, molecular transport mechanisms, toxicity testing and biomarker identification. It will significantly contribute to the development of researchers and knowledge in the field, especially in terms of drug development, shortening the process of market launching of the final drug and personalized treatment, and will create new projects and collaborations for the product.

REFERENCES

Abhyankar, V. V., & Beebe, D. J. (2007). Spatiotemporal micropatterning of cells on arbitrary substrates. *Analytical Chemistry*, *79*(11), 4066-4073.

Alix-Panabières, C., & Pantel, K. (2014). Technologies for detection of circulating tumor cells: facts and vision. *Lab on a Chip, 14*(1)*,* 57-62.

Alshareef, M., Metrakos, N., Perez, E.J., Azer, F., Yang, F., Yang, X., ve Wang, G. (2013). "Separation of tumor cells with dielectrophoresis-based microfluidic chip". *Biomicrofluidics, 7(1),* 011803.

Ameri, S. K., Singh, P. K., Dokmeci, M. R., Khademhosseini, A., Xu, Q., & Sonkusale, S. R. (2014). All electronic approach for high-throughput cell trapping and lysis with electrical impedance monitoring. *Biosensors and Bioelectronics, 54,* 462-467.

Anh-Nguyen, T., Tiberius, B., Pliquett, U., & Urban, G. A. (2016). An impedance biosensor for monitoring cancer cell attachment, spreading and drug-induced apoptosis. *Sensors and Actuators A: Physical, 241,* 231-237.

Asphahani, F., Wang, K., Thein, M., Veiseh, O., Yung, S., Xu, J., & Zhang, M. (2011). Single-cell bioelectrical impedance platform for monitoring cellular response to drug treatment. *Physical Biology, 8*(1)*,* 015006.

Bashir, R. (2004). BioMEMS: state-of-the-art in detection, opportunities and prospects. *Advanced Drug Delivery Reviews, 56*(11)*,* 1565-1586.

Bhatia, S. N., & Ingber, D. E. (2014). Microfluidic organs-on-chips. *Nature*, 2014.

Bhushan, B. (2009). Biomimetics: lessons from nature–an overview. *Philosophical Transactions of the Royal Society of London A: Mathematical, Physical and Engineering Sciences, 367*(1893)*,* 1445-1486.

Blume, L. F., Denker, M., Gieseler, F., & Kunze, T. (2010). Temperature corrected transepithelial electrical resistance (TEER) measurement to quantify rapid changes in paracellular permeability. *Die Pharmazie-An International Journal of Pharmaceutical Sciences, 65*(1)*,* 19-24.

Boughton, A. P., Yang, P., Tesmer, V. M., Ding, B., Tesmer, J. J., & Chen, Z. (2011). Heterotrimeric G protein β1γ2 subunits change orientation upon complex formation with G protein-coupled receptor kinase 2 (GRK2) on a model membrane. *Proceedings of the National Academy of Sciences, 108*(37)*,* E667-E673.

Brown, J. A., Pensabene, V., Markov, D. A., Allwardt, V., Neely, M. D., Shi, M., ... & Samson, P. C. (2015). Recreating blood-brain barrier physiology and structure on chip: A novel neurovascular microfluidic bioreactor. *Biomicrofluidics, 9*(5)*,* 054124.

Castellanos, A., Ramos, A., Gonzales A., Green, N.G., and Morgan, H. (2003). "Electrodynamics and Dielectrophoresis in Microsystems: Scaling Laws", *Journal of Physics D: Applied Physics, 36*, p. 2584-2597.

Caviglia, C., Zor, K., Canepa, S., Carminati, M., Larsen, L. B., Raiteri, R., ... & Emnéus, J. (2015). Interdependence of initial cell density, drug

concentration and exposure time revealed by real-time impedance spectroscopic cytotoxicity assay. *Analyst, 140*(10), 3623-3629.

Čemažar, J., Miklavčič, D., & Kotnik, T. (2013). Microfluidic devices for manipulation, modification and characterization of biological cells in electric fields–a review. *Electronic Components and Materials, 43*(3), 143-161.

Chang, Y., Bu, J., & Cho, Y. H. (2017). Frequency-Dependent Impedance Analysis for Discriminating Cancer and Normal Cells Using Microchamber Array. *Sensors and Materials, 29*(3), 293-301.

Chen, J., Li, J., & Sun, Y. (2012). Microfluidic approaches for cancer cell detection, characterization, and separation. *Lab on a Chip, 12*(10), 1753-1767.

Dastider, S. G., Barizuddin, S., Yuksek, N., Dweik, M., & Almasri, M. (2016, January). Impedance biosensor for rapid detection of low concentration of E. coli 0157: H7. In 2016 IEEE 29th International Conference on Micro Electro Mechanical Systems (MEMS) (pp. 302-306). IEEE.

Demircan, Y., Koyuncuoğlu, A., Erdem, M., Özgür, E., Gündüz, U., & Külah, H. (2015). Label-free detection of multidrug resistance in K562 cells through isolated 3D-electrode dielectrophoresis. *Electrophoresis, 36*(9-10), 1149-1157.

Discher, D. E., Janmey, P., & Wang, Y. L. (2005). Tissue cells feel and respond to the stiffness of their substrate. *Science, 310*(5751), 1139-1143.

El Hasni, A., Schmitz, C., Bui-Göbbels, K., Bräunig, P., Jahnen-Dechent, W., & Schnakenberg, U. (2017). Electrical impedance spectroscopy of single cells in hydrodynamic traps. *Sensors and Actuators B: Chemical, 248*, 419-429.

Engler, A. J., Sen, S., Sweeney, H. L., & Discher, D. E. (2006). Matrix elasticity directs stem cell lineage specification. *Cell, 126*(4), 677-689.

Esch, M. B., King, T. L., & Shuler, M. L. (2011). The role of body-on-a-chip devices in drug and toxicity studies. *Annual Review of Biomedical Engineering, 13*, 55-72.

Folch, A., & Toner, M. (2000). Microengineering of cellular interactions. *Annual Review of Biomedical Engineering, 2*(1), 227-256.

Fernandez, P., Bourget, C., Bareille, R., Daculsi, R., & Bordenave, L. (2007). Gene response in endothelial cells cultured on engineered surfaces is regulated by shear stress. *Tissue Engineering, 13*(7), 1607-1614.

Galbraith, C. G., Skalak, R., & Chien, S. (1998). Shear stress induces spatial reorganization of the endothelial cell cytoskeleton. *Cell Motility and the Cytoskeleton, 40*(4), 317-330.

Gascoyne, P. R., Noshari, J., Anderson, T. J., & Becker, F. F. (2009). Isolation of rare cells from cell mixtures by dielectrophoresis. *Electrophoresis, 30*(8), 1388-1398.

Gascoyne, P. R., & Shim, S. (2014). Isolation of circulating tumor cells by dielectrophoresis. *Cancers, 6*(1), 545-579.

Griep, L. M., Wolbers, F., De Wagenaar, B., ter Braak, P. M., Weksler, B. B., Romero, I. A., ... & van den Berg, A. (2013). BBB on chip: microfluidic platform to mechanically and biochemically modulate blood-brain barrier function. *Biomedical Microdevices, 15*(1), 145-150.

Gurski, L. A., Jha, A. K., Zhang, C., Jia, X., & Farach-Carson, M. C. (2009). Hyaluronic acid-based hydrogels as 3D matrices for in vitro evaluation of chemotherapeutic drugs using poorly adherent prostate cancer cells. *Biomaterials, 30*(30), 6076-6085.

Haber, D. A., Gray, N. S., & Baselga, J. (2011). The evolving war on cancer. *Cell, 145*(1), 19-24.

Hajba, L., & Guttman, A. (2014). Circulating tumor-cell detection and capture using microfluidic devices. *TrAC Trends in Analytical Chemistry, 59,* 9-16.

Hamada, R., Takayama, H., Shonishi, Y., Mao, L., Nakano, M., & Suehiro, J. (2013). A rapid bacteria detection technique utilizing impedance measurement combined with positive and negative dielectrophoresis. *Sensors and Actuators B: Chemical, 181,* 439-445.

Harouaka, R. A., Nisic, M., & Zheng, S. Y. (2013). Circulating tumor cell enrichment based on physical properties. *Journal of Laboratory Automation, 18(6),* 455-468.

van der Helm, M. W., van der Meer, A. D., Eijkel, J. C., van den Berg, A., & Segerink, L. I. (2016). Microfluidic organ-on-chip technology for blood-brain barrier research. *Tissue Barriers, 4*(1), e1142493.

Hong, J. L., Lan, K. C., & Jang, L. S. (2012). Electrical characteristics analysis of various cancer cells using a microfluidic device based on single-cell impedance measurement. *Sensors and Actuators B: Chemical, 173,* 927-934.

Huebsch, N., Arany, P. R., Mao, A. S., Shvartsman, D., Ali, O. A., Bencherif, S. A., & Mooney, D. J. (2010). Harnessing traction-mediated manipulation of the cell/matrix interface to control stem-cell fate. *Nature Materials, 9*(6), 518-526.

Huh, D., Matthews, B. D., Mammoto, A., Montoya-Zavala, M., Hsin, H. Y., & Ingber, D. E. (2010). Reconstituting organ-level lung functions on a chip. *Science, 328*(5986), 1662-1668.

Huh, D., Hamilton, G. A., & Ingber, D. E. (2011). From 3D cell culture to organs-on-chips. *Trends in Cell Biology, 21*(12), 745-754.

Huh, D., Leslie, D. C., Matthews, B. D., Fraser, J. P., Jurek, S., Hamilton, G. A., ... & Ingber, D. E. (2012). A human disease model of drug toxicity–induced pulmonary edema in a lung-on-a-chip microdevice. *Science Translational Medicine, 4*(159), 159ra147-159ra147.

Hutmacher, D. W. (2010). Biomaterials offer cancer research the third dimension. *Nature Materials, 9*(2), 90-93.

Hyman, D. M., Taylor, B. S., & Baselga, J. (2017). Implementing genome-driven oncology. *Cell, 168*(4), 584-599.

Ingber, D. (2003). Mechanobiology and diseases of mechanotransduction. *Annals of Medicine, 35*(8), 564-577.

Jang, L. S., & Wang, M. H. (2007). "Microfluidic device for cell capture and impedance measurement", *Biomedical Microdevices, 9*(5), 737-743.

Jang, K. J., & Suh, K. Y. (2010). A multi-layer microfluidic device for efficient culture and analysis of renal tubular cells. *Lab on a Chip, 10*(1), 36-42.

Jang, K. J., Mehr, A. P., Hamilton, G. A., McPartlin, L. A., Chung, S., Suh, K. Y., & Ingber, D. E. (2013). Human kidney proximal tubule-on-a-chip for

drug transport and nephrotoxicity assessment. *Integrative Biology, 5*(9), 1119-1129.

Jin, C., McFaul, S. M., Duffy, S. P., Deng, X., Tavassoli, P., Black, P. C., & Ma, H. (2014). Technologies for label-free separation of circulating tumor cells: from historical foundations to recent developments. *Lab on a Chip, 14*(1), 32-44.

Justin, G., Nasir, M., & Ligler, F. S. (2011). Hydrodynamic and electrical considerations in the design of a four-electrode impedance-based microfluidic device. *Analytical and Bioanalytical Chemistry, 400*(5), 1347-1358.

Kaji, H., Kawashima, T., & Nishizawa, M. (2006). Patterning cellular motility using an electrochemical technique and a geometrically confined environment. *Langmuir, 22*(25), 10784-10787.

Karabacak, N. M., Spuhler, P. S., Fachin, F., Lim, E. J., Pai, V., Ozkumur, E., ... & Yang, J. (2014). Microfluidic, marker-free isolation of circulating tumor cells from blood samples. *Nature Protocols, 9*(3), 694.

Kievit, F. M., Florczyk, S. J., Leung, M. C., Veiseh, O., Park, J. O., Disis, M. L., & Zhang, M. (2010). Chitosan–alginate 3D scaffolds as a mimic of the glioma tumor microenvironment. *Biomaterials, 31*(22), 5903-5910.

Kim, H. J., Huh, D., Hamilton, G., & Ingber, D. E. (2012). Human gut-on-a-chip inhabited by microbial flora that experiences intestinal peristalsis-like motions and flow. *Lab on a Chip, 12*(12), 2165-2174.

Kim, M., Jung, T., Kim, Y., Lee, C., Woo, K., Seol, J. H., & Yang, S. (2015). "A microfluidic device for label-free detection of Escherichia coli in drinking water using positive dielectrophoretic focusing, capturing, and impedance measurement". *Biosensors and Bioelectronics, 74,* 1011-1015.

Knight, E., & Przyborski, S. (2015). Advances in 3D cell culture technologies enabling tissue-like structures to be created in vitro. *Journal of Anatomy, 227*(6), 746-756.

Lee, K. S., & Ram, R. J. (2009). Plastic–PDMS bonding for high pressure hydrolytically stable active microfluidics. *Lab on a Chip, 9*(11), 1618-1624.

Leite, S. B., Wilk-Zasadna, I., Zaldivar, J. M., Airola, E., Reis-Fernandes, M. A., Mennecozzi, M., & Coecke, S. (2012). Three-dimensional HepaRG model as an attractive tool for toxicity testing. *Toxicological sciences, 130*(1), 106-116.

Light, T. S. (1984). Temperature dependence and measurement of resistivity of pure water. *Analytical Chemistry, 56*(7), 1138-1142.

Liu, Q., Wu, C., Cai, H., Hu, N., Zhou, J., & Wang, P. (2014). Cell-based biosensors and their application in biomedicine. *Chemical Reviews, 114*(12), 6423-6461.

Lo, C. M., Keese, C. R., & Giaever, I. (1999). Cell–substrate contact: another factor may influence transepithelial electrical resistance of cell layers cultured on permeable filters. *Experimental Cell Research, 250*(2), 576-580.

Mammoto, T., Mammoto, A., & Ingber, D. E. (2013). Mechanobiology and developmental control. *Annual Review of Cell and Developmental Biology, 29,* 27-61.

Manczak, R., Fouet, M., Courson, R., Fabre, P. L., Montrose, A., Sudor, J., ... & Reybier, K. (2016). Improved on-chip impedimetric immuno-detection of subpopulations of cells toward single-cell resolution. *Sensors and Actuators B: Chemical, 230,* 825-831.

Mateo, J., Gerlinger, M., Rodrigues, D. N., & de Bono, J. S. (2014). The promise of circulating tumor cell analysis in cancer management. *Genome Biology, 15*(8), 448.

van der Meer, A. D., & van den Berg, A. (2012). Organs-on-chips: breaking the in vitro impasse. *Integrative Biology, 4*(5), 461-470.

Meinhart, C., Wang, D., Turner, K. (2003). "Measurement of AC Electrokinetic Flows*", Biomedical Microdevices, 5*(2), 141-147.

van Midwoud, P. M., Merema, M. T., Verpoorte, E., & Groothuis, G. M. (2010). A microfluidic approach for in vitro assessment of interorgan interactions in drug metabolism using intestinal and liver slices. *Lab on a Chip, 10*(20), 2778-2786.

Moll, S., Ebeling, M., Weibel, F., Farina, A., Del Rosario, A. A., Hoflack, J. C., ... & Prunotto, M. (2013). Epithelial cells as active player in fibrosis: findings from an in vitro model. *PloS One, 8*(2), e56575.

Montrose, A., Cargou, S., Nepveu, F., Manczak, R., Gué, A. M., & Reybier, K. (2013). Impedimetric immunosensor for the detection of circulating pro-inflammatory monocytes as infection markers. *Biosensors and Bioelectronics, 49,* 305-311.

Neužil, P., Giselbrecht, S., Länge, K., Huang, T. J., & Manz, A. (2012). Revisiting lab-on-a-chip technology for drug discovery. *Nature Reviews Drug Discovery, 11*(8), 620.

Oh, J., Hart, R., Capurro, J. & Noh, H. (2009). "Comprehensive analysis of particle motion under non-uniform AC electric fields in a microchannel", *Lab on a Chip, 9,* 62-78.

Park, H., Kim, D., & Yun, K. S. (2010). Single-cell manipulation on microfluidic chip by dielectrophoretic actuation and impedance detection. *Sensors and Actuators B: Chemical, 150*(1), 167-173.

Pethig, R. (2013). Dielectrophoresis: An assessment of its potential to aid the research and practice of drug discovery and delivery. *Advanced Drug Delivery Reviews, 65(11-12),* 1589-1599.

Ríos, Á., Zougagh, M., & Avila, M. (2012). Miniaturization through lab-on-a-chip: Utopia or reality for routine laboratories? A review. *Analytica Chimica Acta, 740,* 1-11.

Reybier, K., Ribaut, C., Coste, A., Launay, J., Fabre, P. L., & Nepveu, F. (2010). Characterization of oxidative stress in Leishmaniasis-infected or LPS-stimulated macrophages using electrochemical impedance spectroscopy. *Biosensors and Bioelectronics, 25*(12), 2566-2572.

Sano, M. B., Henslee, E. A., Schmelz, E., & Davalos, R. V. (2011). Contactless dielectrophoretic spectroscopy: examination of the dielectric properties of cells found in blood. *Electrophoresis, 32*(22), 3164-3171.

Sciancalepore, A. G., Sallustio, F., Girardo, S., Passione, L. G., Camposeo, A., Mele, E., & Pisignano, D. (2014). A bioartificial renal tubule device embedding human renal stem/progenitor cells. *PloS one, 9*(1), e87496.

Shafiee, H., Sano, M. B., Henslee, E. A., Caldwell, J. L., & Davalos, R. V. (2010). Selective isolation of live/dead cells using contactless dielectrophoresis (cDEP). *Lab on a Chip, 10*(4), 438-445.

Shields IV, C. W., Reyes, C. D., and López, G. P. (2015). "Microfluidic cell sorting: a review of the advances in the separation of cells from debulking to rare cell isolation", *Lab on a Chip, 15*(5), 1230-1249.

Sun, J., Li, M., Liu, C., Zhang, Y., Liu, D., Liu, W., ... & Jiang, X. (2012). Double spiral microchannel for label-free tumor cell separation and enrichment. *Lab on a chip, 12*(20), 3952-3960.

Sun, J., Liu, C., Li, M., Wang, J., Xianyu, Y., Hu, G., & Jiang, X. (2013). Size-based hydrodynamic rare tumor cell separation in curved microfluidic channels. *Biomicrofluidics, 7*(1), 011802.

Sun, T., & Morgan, H. (2010). Single-cell microfluidic impedance cytometry: a review. *Microfluidics and Nanofluidics, 8*(4), 423-443.

Swinney, D. C., & Anthony, J. (2011). How were new medicines discovered? *Nature Reviews Drug Discovery, 10*(7), 507-519.

Tan, W. H., & Takeuchi, S. (2007). "A trap-and-release integrated microfluidic system for dynamic microarray applications", *Proceedings of the National Academy of Sciences, 104*(4), 1146-1151.

Tostoes, R. M., Leite, S. B., Serra, M., Jensen, J., Björquist, P., Carrondo, M. J., & Alves, P. M. (2012). Human liver cell spheroids in extended perfusion bioreactor culture for repeated-dose drug testing. *Hepatology, 55*(4), 1227-1236.

Trietsch, S. J., Hankemeier, T., & Van der Linden, H. J. (2011). Lab-on-a-chip technologies for massive parallel data generation in the life sciences: A review. *Chemometrics and Intelligent Laboratory Systems, 108*(1), 64-75.

De Wagenaar, B., Dekker, S., de Boer, H. L., Bomer, J. G., Olthuis, W., van den Berg, A., & Segerink, L. I. (2016). Towards microfluidic sperm refinement: impedance-based analysis and sorting of sperm cells. *Lab on a Chip, 16*(8), 1514-1522.

Wu, J. (2008). "Interactions of electrical fields with fluids: laboratory-on-a-chip applications", *IET Nanobiotechnology, 2,* 14-27.

Yasukawa, T., Hatanaka, H., & Mizutani, F. (2012). Simple detection of surface antigens on living cells by applying distinct cell positioning with negative dielectrophoresis. *Analytical Chemistry, 84*(20), 8830-8836.

Yasukawa, T., Yamada, J., Shiku, H., Mizutani, F., & Matsue, T. (2013). Positioning of cells flowing in a fluidic channel by negative dielectrophoresis. *Sensors and Actuators B: Chemical, 186*, 9-16.

Yip, D., & Cho, C. H. (2013). A multicellular 3D heterospheroid model of liver tumor and stromal cells in collagen gel for anti-cancer drug testing. *Biochemical and Biophysical Research Communications, 433*(3), 327-332.

Wei, Z., Amponsah, P. K., Al-Shatti, M., Nie, Z., & Bandyopadhyay, B. C. (2012). Engineering of polarized tubular structures in a microfluidic device to study calcium phosphate stone formation. *Lab on a Chip, 12*(20), 4037-4040.

Weinberg, E., Kaazempur-Mofrad, M., & Borenstein, J. (2008). Concept and computational design for a bioartificial nephron-on-a-chip. *International Journal of Artificial Organs, 31*(6)*,* 508-514.

Weitz, J., Kienle, P., Lacroix, J., Willeke, F., Benner, A., Lehnert, T., ... & von Knebel Doeberitz, M. (1998). Dissemination of tumor cells in patients undergoing surgery for colorectal cancer. *Clinical Cancer Research, 4*(2)*,* 343-348.

Wheater, P. R., Burkitt, H. G., & Daniels, V. G. (1979). *Functional Histology. A Text and Colour Atlas*. Churchill Livingstone, 23 Ravelston Terrace, Edinburgh, EH4 3TL.

Wu, M. H., Huang, S. B., & Lee, G. B. (2010). Microfluidic cell culture systems for drug research. *Lab on a Chip, 10*(8)*,* 939-956.

Yang, F., Yang, X., Jiang, H., Butler, W. M., & Wang, G. (2013). Dielectrophoretic separation of prostate cancer cells. *Technology in Cancer Research & Treatment, 12*(1)*,* 61-70.

Zhang, C., Zhao, Z., Rahim, N. A. A., van Noort, D., & Yu, H. (2009). Towards a human-on-chip: culturing multiple cell types on a chip with compartmentalized microenvironments. *Lab on a Chip, 9*(22)*,* 3185-3192.

Zhou, Jun (Ed.). (2010). *Multi-Drug Resistance in Cancer*, Humana Press, New York, ABD.

Zhou, Y., Basu, S., Laue, E., & Seshia, A. A. (2016). Single cell studies of mouse embryonic stem cell (mESC) differentiation by electrical impedance measurements in a microfluidic device. *Biosensors and Bioelectronics, 81,* 249-258.

Zhou, Y., Basu, S., Laue, E. D., & Seshia, A. A. (2016). Dynamic monitoring of single cell lysis in an impedance-based microfluidic device. *Biomedical Microdevices, 18*(4)*,* 56.

APPENDICES

APPENDIX A: Characteristic properties of cell lines used in thesis

APPENDIX A: Characteristic Properties Of Cell Lines Used in Thesis

Table A 1 : HL-60.

Organism	Homo sapiens, human
Tissue	peripheral blood
Cell Type	promyeloblast
Morphology	lymphoblast-like
Culture Properties	suspension
Biosafety Level	1
Disease	acute promyelocytic leukemia
Karyotype	The stemline chromosome number is pseudodiploid with the 2S component occurring at 6.2%. Five markers (M2 through M6) were common to most S metaphases. DM's, which varied in numbers per cell, occurred in all metaphases karyotyped. HSR chromosomes were not detected.
Receptor Expression	complement, expressed Fc, expressed
Oncogene	myc +
Tumorigenic	Yes
Images	ATCC Number: **CCL-240** Designation: **HL-60** 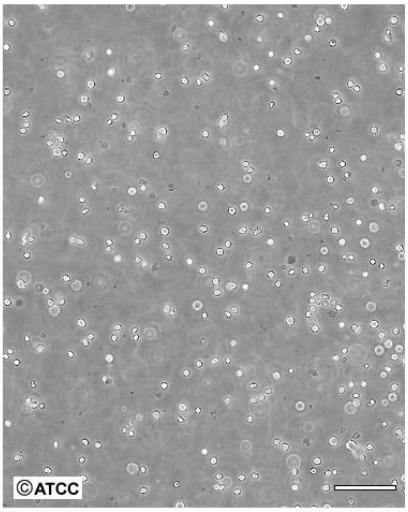 Low Density Scale Bar = 100µm 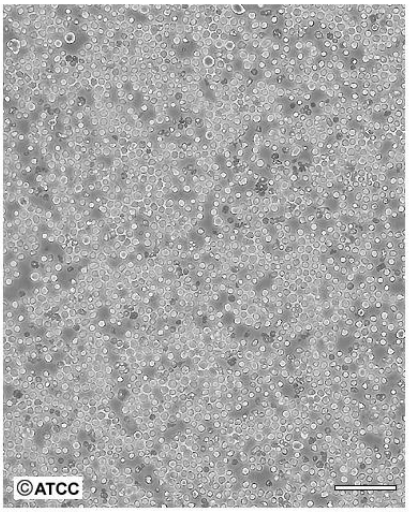 High Density Scale Bar = 100µm

Table A 2 : Jurkat (Clone E6-1).

Organism	Homo sapiens, human
Tissue	peripheral blood
Cell Type	T lymphocyte
Morphology	lymphoblast
Culture Properties	suspension
Biosafety Level	1
Disease	acute T cell leukemia
Karyotype	This is a pseudodiploid human cell line. The modal chromosome number is 46, occurring in 74% with polyploidy at 5.3%. The karyotype is 46,XY,-2,-18,del(2) (p21p23),del(18) (p11.2). Most cells had normal X and Y chromosomes.
Receptor Expression	T cell antigen receptor, expressed
Antigen Expression	CD3; Homo sapiens, expressed
Images	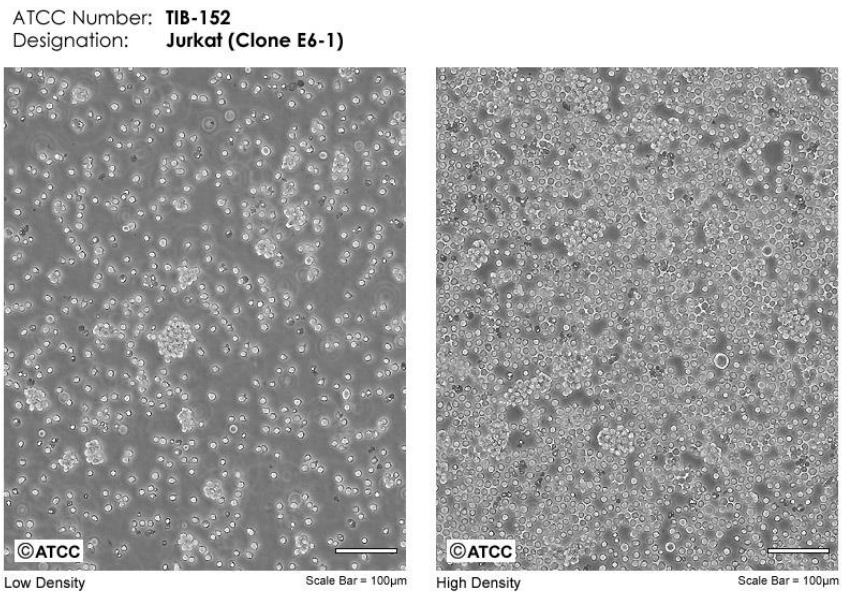

Table A 3 : Daudi.

Organism	Homo sapiens, human
Tissue	peripheral blood
Cell Type	B lymphoblast
Morphology	lymphoblast
Culture Properties	suspension
Biosafety Level	2 [Cells contain Herpesvirus]
Disease	Burkitt's lymphoma
Karyotype	Male human karyotype with stemline number of 46. The karyotype is diploid in 66% of the cells and is stable within the stemline. Note: Cytogenetic information is based on initial seed stock at ATCC. Cytogenetic instability has been reported in the literature for some cell lines.
Receptor Expression	complement, expressed Fc, expressed
Tumorigenic	Yes, in nude mice; forms colonies in agarose

Table A 4: THP-1

Organism	Homo sapiens, human
Tissue	peripheral blood
Cell Type	monocyte
Morphology	monocyte
Culture Properties	suspension
Biosafety Level	1
Disease	acute monocytic leukemia
Receptor Expression	complement (C3), expressed Fc, expressed
Antigen Expression	HLA A2, A9, B5, DRw1, DRw2
Genes Expressed	lysozyme,HLA A2, A9, B5, DRw1, DRw2
Images	ATCC Number: **TIB-202** Designation: **THP-1** 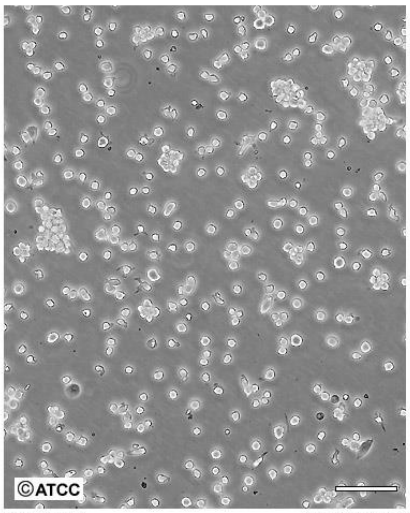 Low Density Scale Bar = 100µm 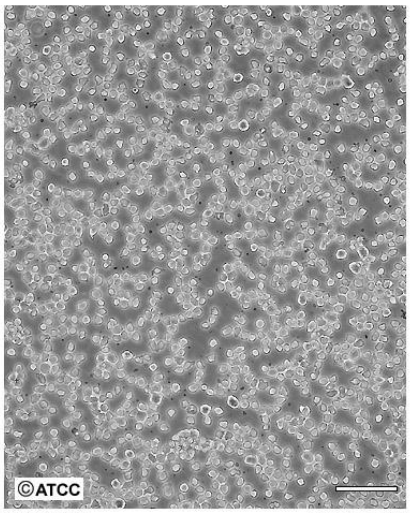 High Density Scale Bar = 100µm

Table A 5 : HCT-116.

Organism	Homo sapiens, human
Tissue	colon
Morphology	epithelial
Culture Properties	adherent
Biosafety Level	1
Disease	colorectal carcinoma
Karyotype	The stemline chromosome number is near diploid with the modal number at 45 (62%) and polyploids occurring at 6.8%. The markers 10q+ and t(?8p;18q) are present in all metaphases and t(9q;?16p-), in 80% of the cells karyotyped. N16 is monosomic in the presence of, but disomic in the absence of t(9q;?16p-). N10 and N18 are monosomic and other chromosomes from those mentioned above are disomic. Q-band observations revealed the presence of the Y chromosome, but not in all cells (50% of cells lacked the Y in G-band karyotypes).
Genes Expressed	carcinoembryonic antigen (CEA) 1 ng per 10^6 cells per 10 days.
Tumorigenic	Yes
Images	ATCC Number: **CCL-247** Designation: **HCT 116** 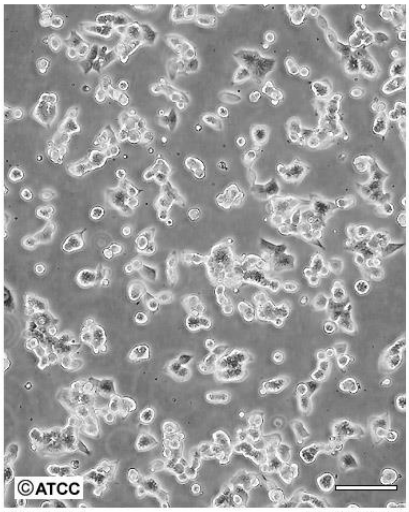 Low Density Scale Bar = 100µm 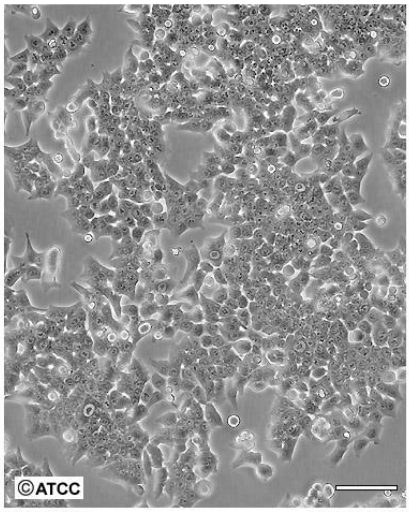 High Density Scale Bar = 100µm

Table A 6 : HeLa.

Organism	Homo sapiens, human
Tissue	cervix
Morphology	epithelial
Culture Properties	adherent
Biosafety Level	2 [Cells contain human papilloma virus]
Disease	adenocarcinoma
Karyotype	Modal number = 82; range = 70 to 164. There is a small telocentric chromosome in 98% of the cells. 100% aneuploidy in 1385 cells examined. Four typical HeLa marker chromosomes have been reported in the literature. HeLa Marker Chromosomes: One copy of Ml, one copy of M2, four-five copies of M3, and two copies of M4 as revealed by G-banding patterns. M1 is a rearranged long arm and centromere of chromosome 1 and the long arm of chromosome 3. M2 is a combination of short arm of chromosome 3 and long arm of chromosome 5. M3 is an isochromosome of the short arm of chromosome 5. M4 consists of the long arm of chromosome 11 and an arm of chromosome 19. Note: Cytogenetic information is based on initial seed stock at ATCC. Cytogenetic instability has been reported in the literature for some cell lines.
Gene Expressed	Lysophosphatidylcholine (lyso-PC) induces AP-1 activity and c-jun N-terminal kinase activity (JNK1) by a protein kinase C-independent pathway. The cells are positive for keratin by immunoperoxidase staining.
Virus Susceptibility	Human adenovirus 3 Encephalomyocarditis virus Human poliovirus 1 Human poliovirus 2 Human poliovirus 3
Images	ATCC Number: **CCL-2** Designation: **HeLa** 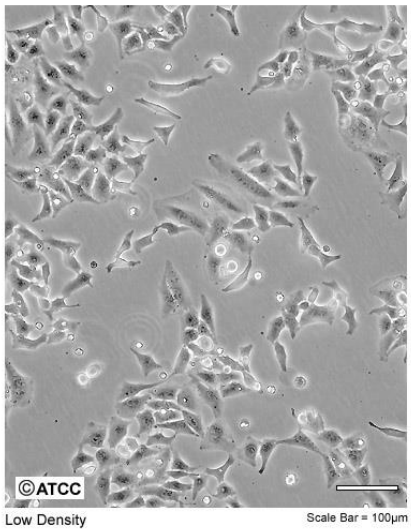 Low Density Scale Bar = 100µm 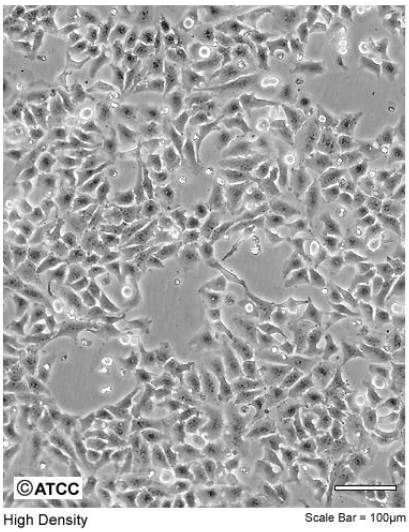 High Density Scale Bar = 100µm

Table A 7 : HEK293.

Organism	Homo sapiens, human
Tissue	embryonic kidney
Morphology	epithelial
Culture Properties	adherent
Biosafety Level	2 [Cells contain adenovirus]
Karyotype	This is a hypotriploid human cell line. The modal chromosome number was 64, occurring in 30% of cells. The rate of cells with higher ploidies was 4.2 %. The der(1)t(1;15) (q42;q13), der(19)t(3;19) (q12;q13), der(12)t(8;12) (q22;p13), and four other marker chromosomes were common to most cells. Five other markers occurred in some cells only. The marker der(1) and M8 (or Xq+) were often paired. There were four copies of N17 and N22. Noticeably in addition to three copies of X chromosomes, there were paired Xq+, and a single Xp+ in most cells.
Receptor Expression	vitronectin, expressed
Tumorigenic	Yes
Images	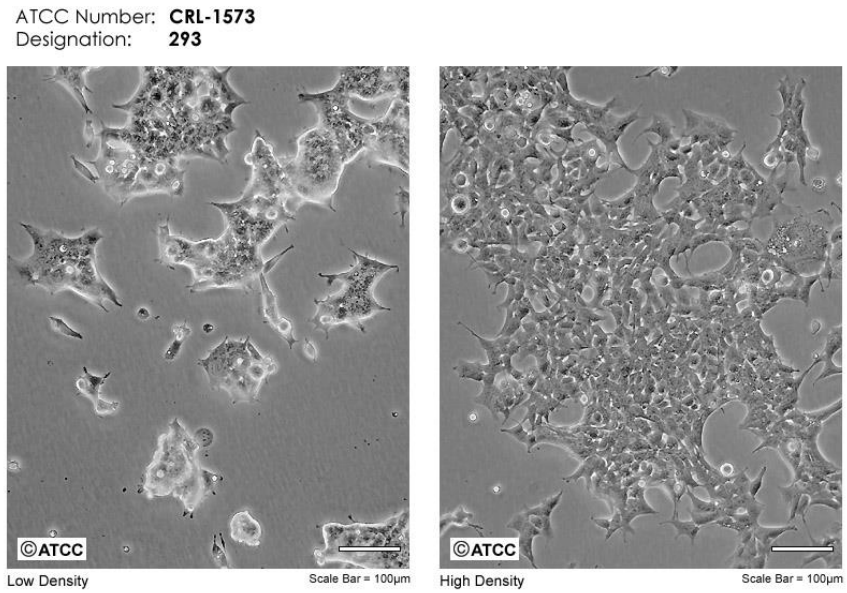

Table A 8 : MDA-MB-231.

Organism	Homo sapiens, human
Tissue	bone marrow
Morphology	lymphoblast
Culture Properties	suspension
Biosafety Level	1
Disease	chronic myelogenous leukemia (CML)
Karyotype	The stemline chromosome number is triploid with the 2S component occurring at 4.2%. Fifteen markers (M1 and M(15)) occurred in nearly all S metaphases. Spontaneous non-specific dicentrics occurred, but rarely. Unstable markers were also rarely seen. The X was disomic, and N9 was nullisomic.
Antigen Expression	CD7 (25%)
Tumorigenic	Yes
Images	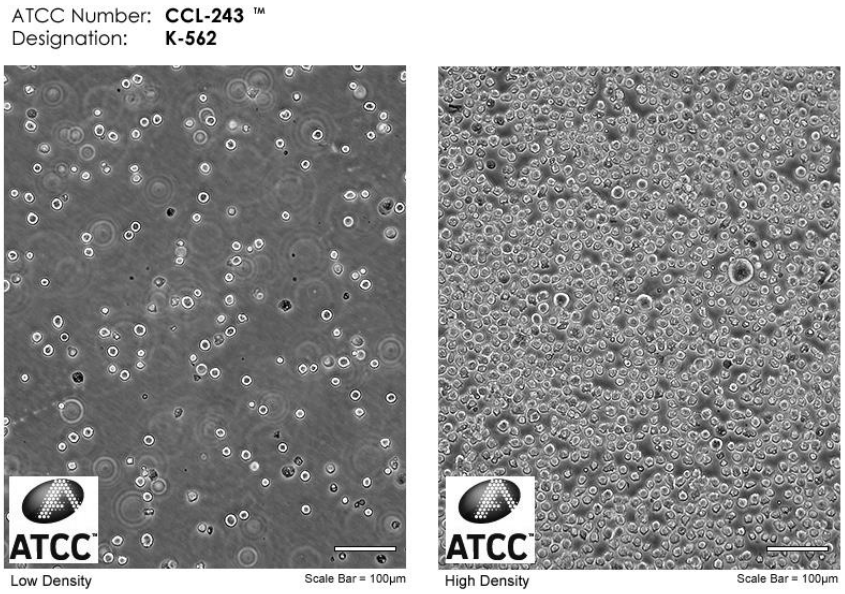

Table A 9 : Hacat.

Organism	Homo sapiens, human
Tissue	skin (epidermis)
Cell type	keratinocyte
Morphology	Cobblestone appearance; cells are rounded, not flat; cells display a high mitotic index; at near 80% confluence, the cells will be associated with each other in colonies.
Culture Properties	adherent
Biosafety Level	1
Disease	normal

Table A 10 : RPTEC.

Organism	**Homo sapiens, human**
Tissue	Renal cortex; proximal tubules, epithelium
Cell type	Epithelial cells immortalized with pLXSN-hTERT retroviral transfection
Morphology	Epithelial-like
Culture Properties	adherent
Biosafety Level	2 [Cells contain SV40 viral DNA sequences]
Karyotype	The stemline chromosome number is triploid with the 2S component occurring at 4.2%. Fifteen markers (M1 and M(15)) occurred in nearly all S metaphases. Spontaneous non-specific dicentrics occurred, but rarely. Unstable markers were also rarely seen. The X was disomic, and N9 was nullisomic.
Antigen Expression	The RPTEC/TERT1 cells express both Aminopeptidase N (verified at ATCC) and γ-Glutamyl Transferase (GGT) that are located in the brush border of the renal proximal tubular epithelium.
Images	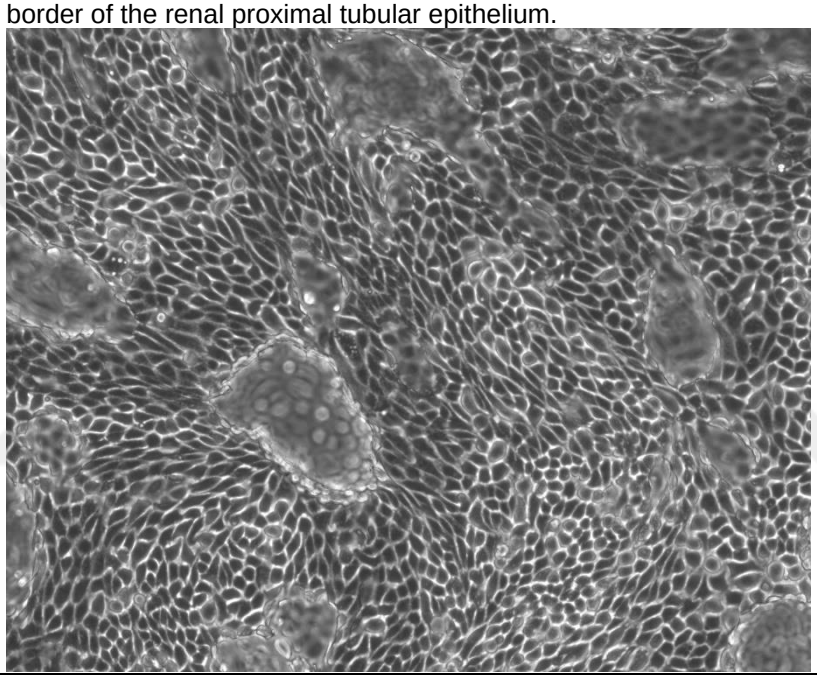

Table A 11 : NCI-82.

Organism	**Homo sapiens, human**
Tissue	lung; derived from metastatic site: pleural effusion
Morphology	epithelial
Culture Properties	aggregates in suspension; the cells grow in very large aggregates, and the aggregates are the only viable cell population
Biosafety Level	1
Disease	carcinoma; small cell lung cancer
Karyotype	This is a near triploid human cell line. The modal chromosome number is 58, occurring at 44% with polyploidy at 3%. Marker chromosomes der(1)t(1;709p13;p11), t(13q;?HSR;15q) and der(190t(19;?)(q13.4;?) were common to most cells., There were two distinct subpopulations readily distinguished by karyotype. Besides uniform changes in the numbers of copies of some normal chromosomes, one population had der(3)t(3;20)(p11;p11?), t(3q19p), i(7q) and a minute chromosome of unknown origin., The other had t(1q17p), del(1)(q21), der(3)t(3;7)(p12;q11) plus two other markers. Each cell had two copies of a normal X chromosome. The Y chromosome was not detected in Q banded preparations.
Receptor Expression	Insulin-like growth factor II (IGF II); atrial natriuretic peptide (ANP)
Oncogene	myc +; myb -; raf +; ras +; fms +; fes +
Tumorigenic	Yes

Table A 12 : MRC-5.

Organism	**Homo sapiens, human**
Tissue	lung
Cell type	fibroblast
Morphology	fibroblast
Culture Properties	adherent
Biosafety Level	1
Disease	Normal
Karyotype	Chromosome Frequency Distribution 50 Cells: 2n = 46. This is a normal diploid human cell line with 46,XY karyotype. The modal chromosome number was 46, occurring in 70% of cells. The rate of polyploidy was 3.6%. Both X and Y chromosomes were normal. Note: Cytogenetic information is based on initial seed stock at ATCC. Cytogenetic instability has been reported in the literature for some cell lines.
Antigen Expression	CD7 (25%)
Virus Susceptibility	Human poliovirus 1 Herpes simplex virus Vesicular stomatitis, Glasgow (Indiana) Vesicular stomatitis, Orsay (Indiana)
Images	ATCC Number: **CCL-171** Designation: **MRC-5** 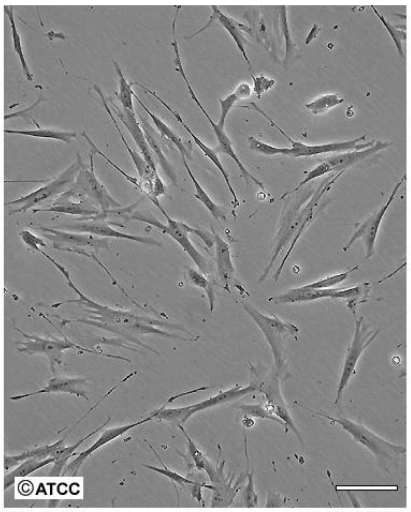 Low Density Scale Bar = 100µm 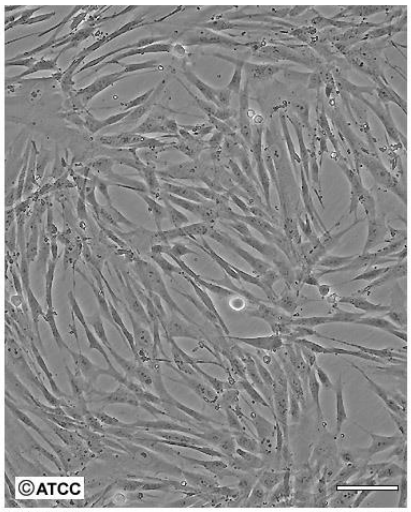 High Density Scale Bar = 100µm

CURRICULUM VITAE

Name Surname **:** Emre Altınağaç

Place and Date of Birth **:** 23.05.0989

E-Mail **:** altinagac@itu.edu.tr

EDUCATION **:**

- **B.Sc.:** 2011, Yıldız Technical University, Faculty of Chemical and Metallurgical Engineering, Department of Metallurgical and Materials Engineering
- **M.Sc.:** 2013, Istanbul Technical University, Department of Nanoscience and Nanoengineering, Nanoscience and Nanoengineering Programme

PUBLICATIONS, PRESENTATIONS AND PATENTS ON THE THESIS:

- KIZIL, H., **ALTINAGAC, Emre**., Microfluidic system for cancer cell separation, capturing and drug screening assays. U.S. Patent Application No 16/623,777, 2020.
- **Altinagac, E.,** Yalman, V., Demirbilek, M., & Kizil, H. A. 2019: Microfluidic 3D Cell Culture System for Drug Discovery Studies.
- **Altinagac, E.,** Taskin, S., & Kizil, H. 2017: Single Cell Array Impedance Analysis for Cell Detection and Classification in a Microfluidic Device. In *Biodevices* (pp. 49-53).
- **Altinagac, E.,** Taskin, S., & Kizil, H. 2016: Single cell array impedance analysis in a microfluidic device. *JPCS, 757*, 012010.
- **Altinagac, E.,** Kizil, H., & Trabzon, L. 2015. Biological particle manipulation: An example of Jurkat enrichment. *Micro & Nano Letters, 10(10),* 550-553.
- **Altinagac, E.,** Genc, Y., Kizil, H., Trabzon, L., & Beskok, A. 2014. Microdevices for continuous sized based sorting by AC dielectrophoresis.